(HAC-REF-E3256-VOL-2) CONCEPTUAL DESIGN STUDY OF CONCENTRATOR ENHANCED SOLAR ARRAYS FOR SPACE APPLICATIONS VOLUME 2: TECHNICAL Interim Final Report (Hughes Aircraft Co.) 115 p HC A06/MF A01 CSCL 10A G3/44

N79-32639

Unclas 35865

CONCEPTUAL DESIGN STUDY OF CONCENTRATOR ENHANCED SOLAR ARRAYS FOR SPACE APPLICATIONS

INTERIM FINAL REPORT
15 MAY 1979

VOLUME II
TECHNICAL

JPL CONTRACT NO. 955194
HUGHES REF NO. E3256

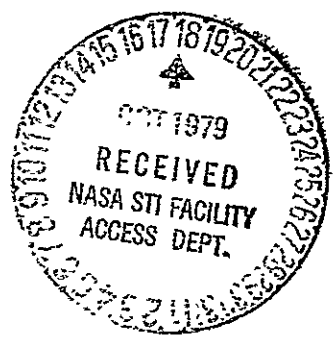

HUGHES
HUGHES AIRCRAFT COMPANY

HUGHES AIRCRAFT COMPANY
Technology Division
Space and Communications Group
El Segundo, California

CONCEPTUAL DESIGN STUDY OF CONCENTRATOR ENHANCED SOLAR ARRAYS FOR SPACE APPLICATIONS

INTERIM FINAL REPORT

15 MAY 1979

VOLUME II TECHNICAL

JPL Contract No. 955194

HAC Ref. No. E3256

Approved: I. Baker

I. Baker
Program Manager
15 May 1979

This work was performed for the Jet Propulsion Laboratory, California Institute of Technology, sponsored by the National Aeronautics and Space Administration under Contract NAS-7-100

VOLUME II TECHNICAL

VOL. II TABLE OF CONTENTS

TABLE OF CONTENTS (CONTINUED)

1.0 INTRODUCTION TO VOLUME II

This volume contains a detailed technical description of the various tasks that were performed during the course of the initial concentrator study contract. Additional work performed as part of a subsequent extension to the contract will be described in a final report to be released at a later date.

In addition to a description of each of the tasks performed, this volume also discusses the assumptions that were employed and the results obtained.

The study reported in this volume was divided into two phases. In Phase I, the various concentrator concepts were compared relative to cost related parameters and performance. Then the best design for each solar distance application was selected. In Phase II, one recommended "best" concept was further developed.

All concepts considered were required to employ very thin silicon solar cells. The cell temperature was not to exceed $150^{\circ}C$. The concentrators were required to produce illumination of the array within 15% of being perfectly uniform. The concentrators were also required to operate while misaligned as much as 5° with the solar axis. Finally, a reasonable expectation of implementation with existing materials and technology had to be assured.

In Phase I, all concentrated systems utilized a baseline solar array which generated 25 kW at 1 AU when unconcentrated. In Phase II, the size of the array was reduced to 2.08 kW at 1 AU.

2.0 PHASE I TECHNICAL EFFORT DESCRIPTION

2.1 Concept Selection Rationale

All concentrator concepts which have been proposed can be divided into those which utilize lenses, those which use mirrors and others which combine these optical elements. From a mass standpoint, the selection of coated thin film Kapton, about 8 μM thick, for use as a mirror material effectively eliminated from consideration all concepts employing lenses. Even ultra-thin Fresnel lenses cannot compete on a mass basis with the selected Kapton mirror material which by comparison is virtually zero mass. Thus, only mirror type concentrators were considered in this study.

All mirror type concentrators may be divided into two basic optical configuration categories; front-lit configurations (Figure 2.1-1) in which the solar array faces the sun and receives direct impingement in addition to the light reflected from concentrator mirrors, and back-lit configurations (Figure 2.1-2) in which the solar array faces away from the sun such that only reflected light is received by the solar cells. In Figures 2.1-1 and 2.1-2, the geometric concentration ratio, C_g is defined. In both configuration types, a parameter of particular interest is the area ratio, R, also defined in the figures. This is a measure of the relative mirror size required to achieve a given C_g. Although as previously mentioned the mirrors in all concepts studied have almost insignificant mass, structure with significant mass is required to deploy, shape and support the mirrors. Logically, mirror structure mass will be related to mirror size and hence proportional to R. Since high C_g is clearly desirable, one measure of relative effectiveness of a concentrator design is the ratio, C_g/R. Concepts which exhibit the highest value of this ratio would tend to be more mass efficient and hence more effective in increasing specific power.

$$Cg = \frac{L + W}{L}$$

$$R = \frac{S}{L}$$

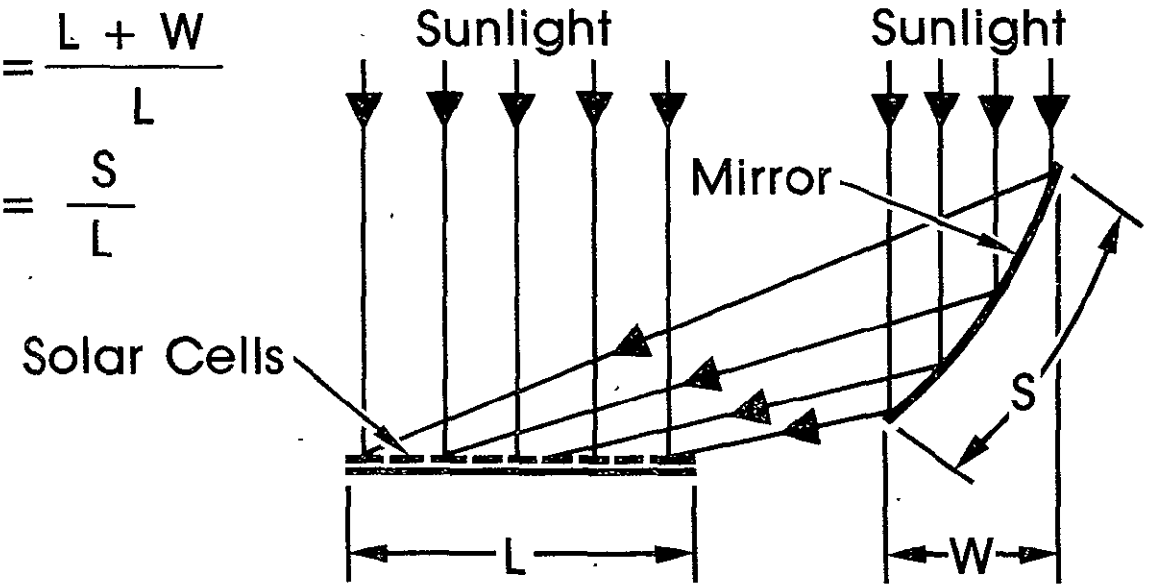

Fig. 2.1-1 - Front-lit concentrator

$$Cg = \frac{W}{L}$$

$$R = \frac{S}{L}$$

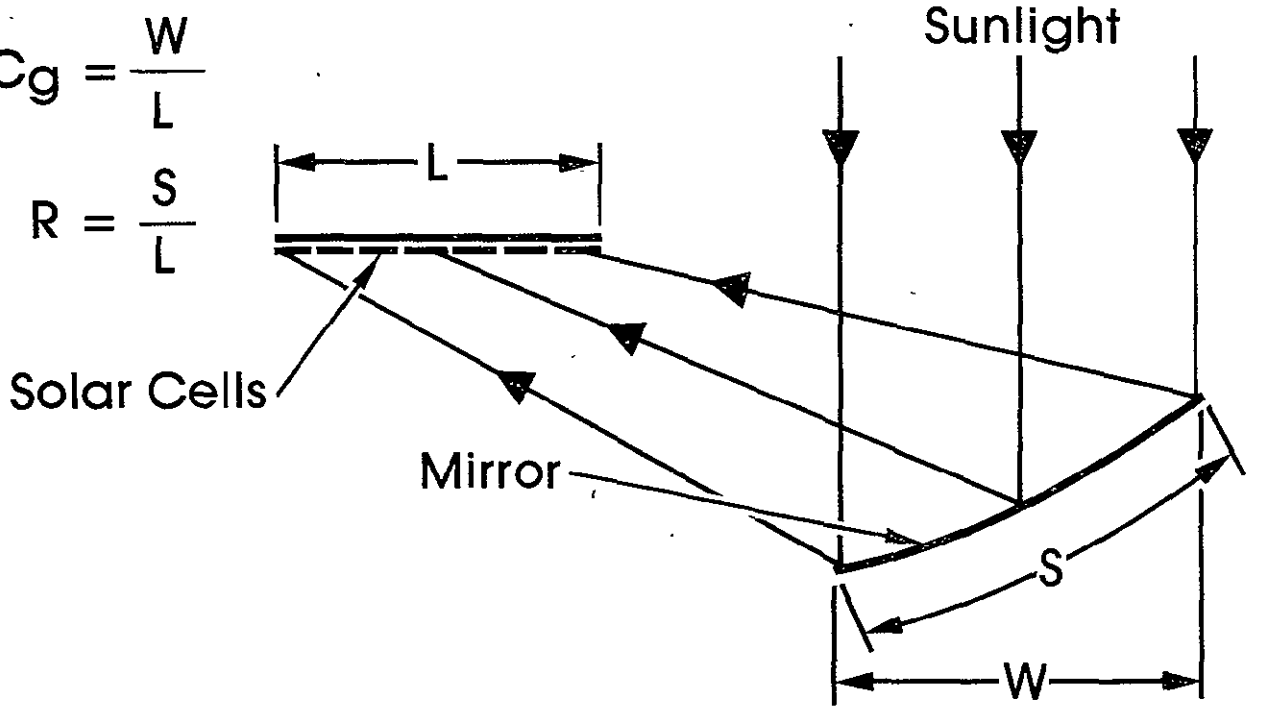

Fig. 2.1-2 - Back-lit concentrator

It was observed during the study that, in every case, much higher values of C_g/R could be achieved with back-lit designs than with front-lit designs. An explanation for this observation is found from the following mathematical proof that back-lit designs will always require smaller mirrors to reflect the same quantity of light than will front-lit designs.

Figure 2.1-3 shows two mirrors equidistant from a small solar cell in space, the one at A in the front-lit position, and the one at B in the back-lit position. The solar cell, which is normal to the sun's axis, faces the sun when using mirror A, and faces away from the sun when using mirror B. Both mirrors were positioned and sized to intercept the same column of sunlight of width dF, and to reflect it to the cell. Not only are the mirrors equidistant from the solar cell, but they are also equidistant from the plane of the solar cell. From the geometry shown in the figure, X_A, the width of the front-lit mirror at A, and X_B, the width of the back-lit mirror at B, are related to each other as follows:

$$X_A = \frac{dF}{\cos \phi_A} \; ; \qquad X_B = \frac{dF}{\cos \phi_B}$$

$$\phi_A = 45^\circ + \frac{\theta}{2} \; ; \qquad \phi_B = 45 - \frac{\theta}{2}$$

$$\frac{X_A}{X_B} = \frac{\cos \phi_B}{\cos \phi_A} = \frac{\cos (45 - \frac{\theta}{2})}{\cos (45 + \frac{\theta}{2})}$$

$$\therefore \frac{X_A}{X_B} = \frac{1 + \tan \frac{\theta}{2}}{1 - \tan \frac{\theta}{2}}$$

Since this ratio is always greater than 1, the statement is proved. Clearly, back-lit concepts configured to achieve high C_g would tend to have the highest ratio of C_g/R.

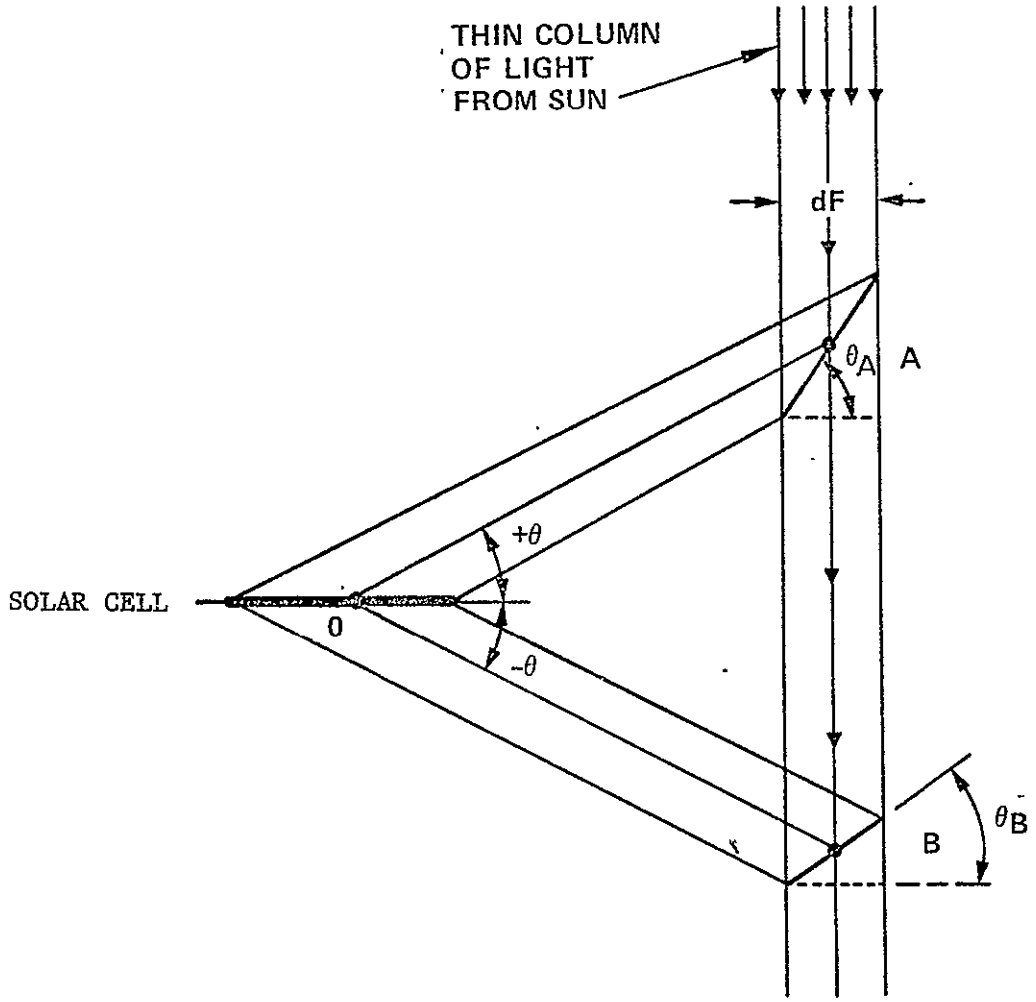

FIGURE 2.1-3. BACK-LIT VS. FRONT-LIT MIRROR SIZE

On the other hand, this advantage of back-lit over front-lit designs tends to disappear when the designs are required to be configured for low C_g. This is the case with silicon solar cells operating in earth orbit (1 AU) where array temperature limits prohibit the use of high C_g. At low C_g, the additional power generated by the direct illumination of the array in the front-lit design tends to compensate for its larger mirrors.

Thus, candidate concentrator concepts for comparative evaluation were selected from among all known and newly proposed mirror type concentrators; front-lit as well as back-lit. It was only necessary that each concept be judged capable of meeting the minimum requirements specified by the contract and summarized in Section 1.0.

2.2 Concepts Rejected

From the broad class of all concepts which were seriously considered in the study, several were found to be incapable of meeting the minimum design requirements of the contract and were rejected. (The major requirements are listed in Section 1.0.) The most interesting of these are summarized here for completeness.

One rejected concept was a front-lit conical light pipe shown in Figure 2.2-1. From an optical ray trace study it was determined that this concept could not be configured to meet the uniformity of illumination requirement.

Another rejected concept was a two dimensional back-lit simple parabolic concentrator, the SPC, shown in Figure 2.2-2 in cross-section. It was ultimately rejected because it cannot accept a $\pm 5^{\circ}$ misalignment with the sun's axis while maintaining the required illumination uniformity. This concept is of particular interest because, with perfect sun axis alignment, it is believed to be a theoretical upper limit for two dimensional

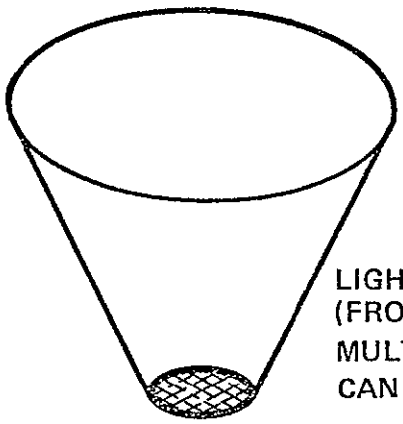

LIGHT PIPE CONCENTRATOR LPC
(FRONT-LIT)
MULTIPLE REFLECTING (2)
CAN BE CONFIGURED TO ACCEPT ± 5° FOV

REJECTED BECAUSE OF EXTREME NONUNIFORM ILLUMINATION

96067-13

FIGURE 2.2-1. LIGHT PIPE CONCENTRATOR

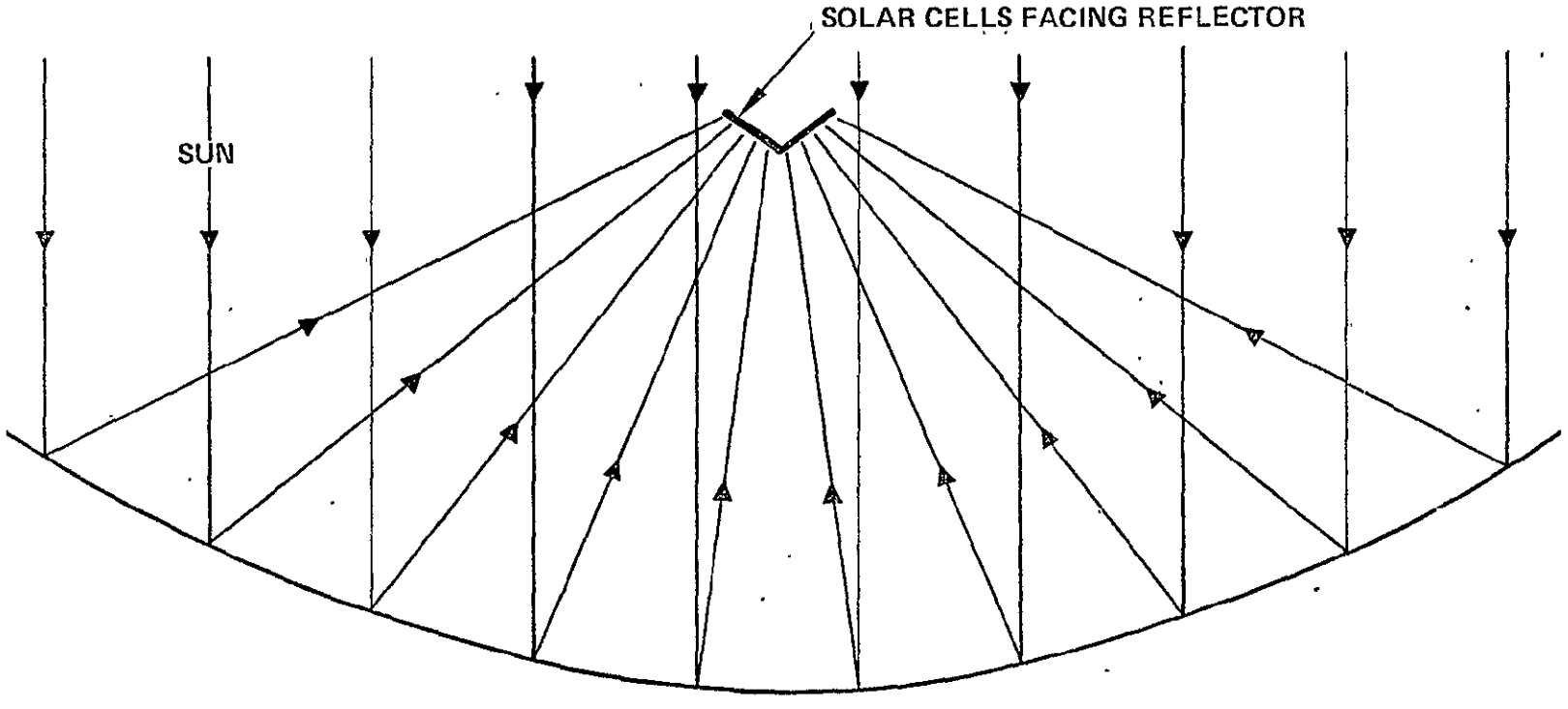

FIGURE 2.2-2. BACK-LIT SIMPLE PARABOLIC CONCENTRATOR (SPC)

trough concentrators. Although this contention has not been rigorously proven, no mirror type concentrator can be found to yield ratios of C_g/R even approaching that of the SPC for any C_g however high. With perfect pointing of the sun's axis along the axis of symmetry of the parabolic reflector, all reflected light converges to a line at the focal point of the parabola, the line running parallel to the longitudinal axis of the mirror trough. The array is placed to intercept the reflected light near the focal line. The deficiency of this otherwise ideal concept is illustrated in Figure 2.2-3. With a 5° sun axis misalignment, the reflected light is drastically shifted and grossly defocused and aberrated.

Figure 2.2-4 illustrates still another unique and interesting concept which ultimately had to be rejected. It was named a Compound Back-Lit Parabolic Concentrator, CBPC, and was proposed as a possible solution to the SPC deficiency.

The concept employs two parabolic trough reflectors. The reflector on the right is a segment of a parabola whose focal point lies above and to the left of the left hand edge of the back facing array. The left hand reflector is a segment of a similar parabola whose focal point lies above and to the right of the right hand edge of the solar array. The design accommodates 5° sun misalignment by configuring the reflectors to be oversized. When the sun is on axis, the width of the reflected light at the array exceeds the width of the array by an amount such that when the sun is off axis and the light is defocused and aberrated, the array remains illuminated. However, the shaded area under the array proved to be the weakness of this concept. With a sun axis shift, the shaded area also shifts and the reflective behavior of the two mirror segments becomes unequal. One of the mirrors only illuminates a portion of the array while

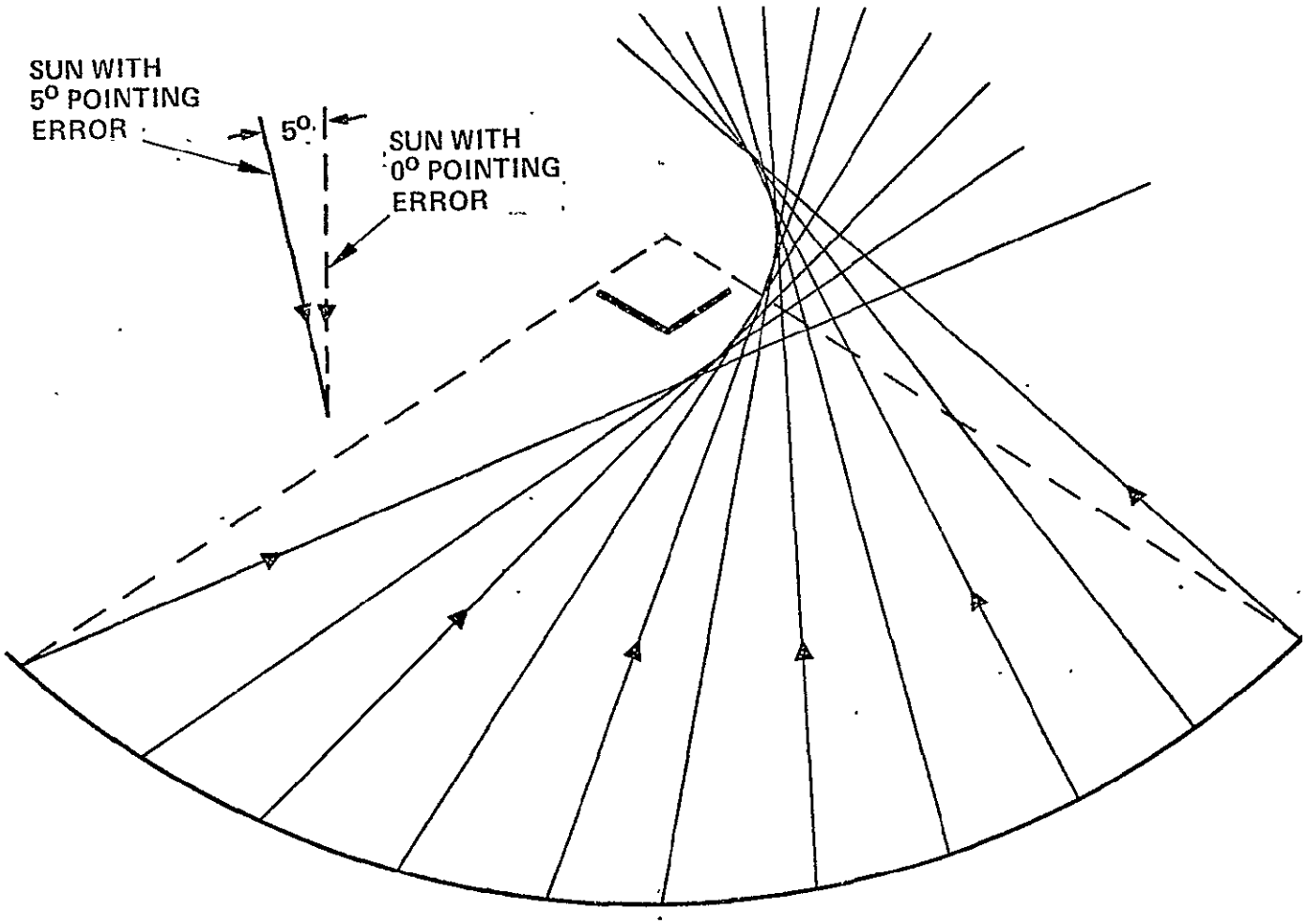

FIGURE 2.2-3. WHY SPC CANNOT MEET 15% NONUNIFORM ILLUMINATION LIMIT

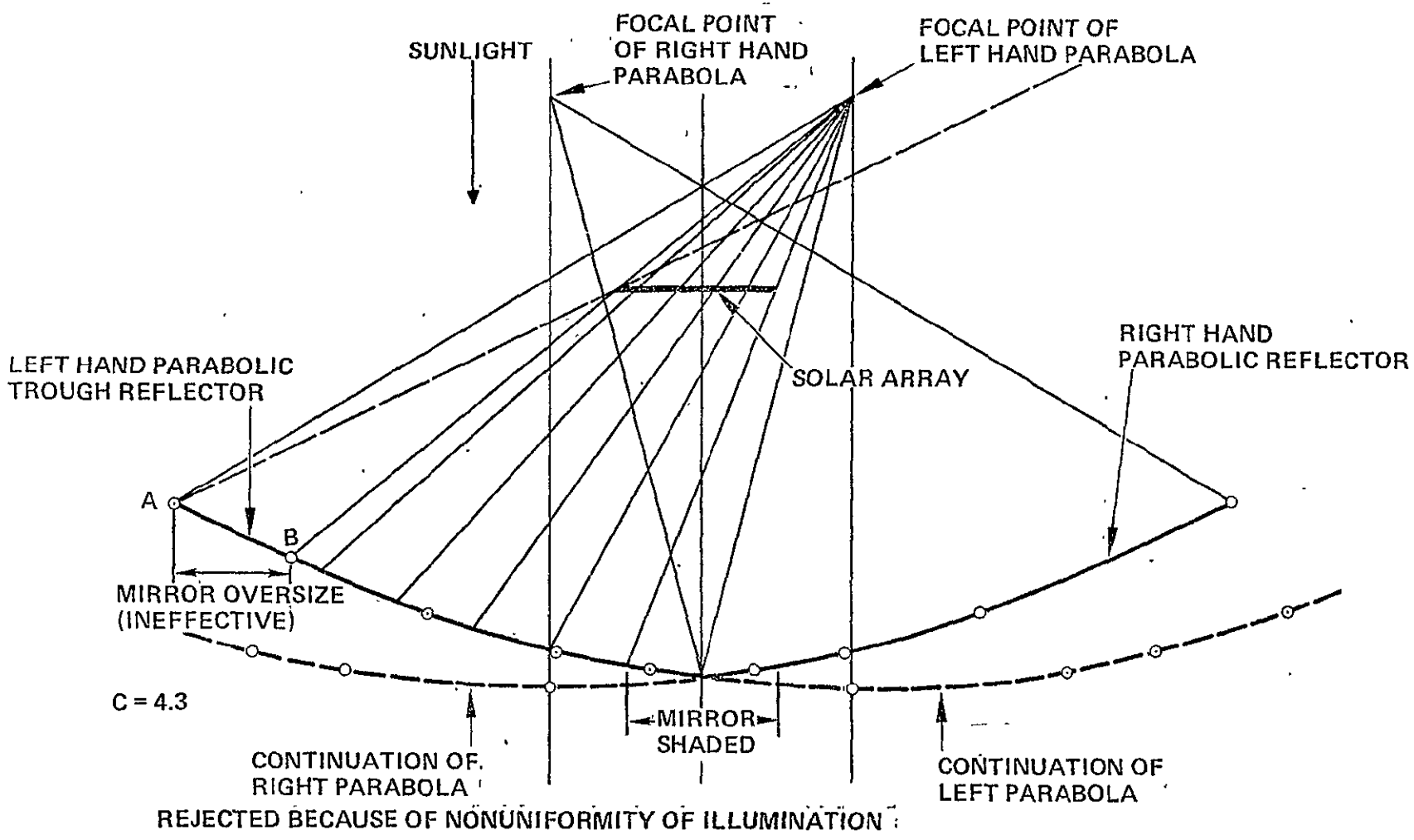

FIGURE 2.2-4. COMPOUND BACK-LIT PARABOLIC CONCENTRATOR, CBPC

the other illuminates it entirely. The resulting nonuniformity of the illumination was found to be unacceptable and the concept was eliminated from further consideration.

2.3 Description of Concepts Accepted for Evaluation

An initial screening of all known candidate concepts identified six concepts which satisfied the technical requirements listed in Section 1.0. Each of these will now be considered in detail.

2.3.1 The two dimensional flat plate trough (2D-FPT) shown in Figure 2.3-1 is a front-lit design which has been studied in some detail for space applications (References 2 and 3). Large values can be achieved by using extremely large mirrors and employing multiple reflections before light is received on the panel. However, the mass of the structure necessary to maintain these large mirrors limits the specific power of the array to an unacceptably low value. When limited to single reflection, smaller mirrors results for $C_g < 2$, however, as C_g approaches 3, the mirror size becomes infinite. A practical limit of approximately 2 has been established as the optimum (Reference 2). Variation in the concentration ratio below the maximum is accomplished by simply changing the mirror tilt angle. With a flat mirror, a shift in the sun's vector produces a corresponding shift in the reflected beam. To assure complete and thus uniform illumination of the array with a $\pm 5^{\circ}$ sun axis shift, the mirror is designed to be oversized such that the array is still totally illuminated by the shifted beam. In this manner, the concept meets all of the technical requirements.

2.3.2 The two dimensional compound parabolic concentrator illustrated in Figure 2.3-2 is a front-lit design which has been extensively studied (References 1 and 4). Each mirror is a segment of a parabola. When properly configured, it inherently accommodates the $\pm 5^{\circ}$ sun shift. Within

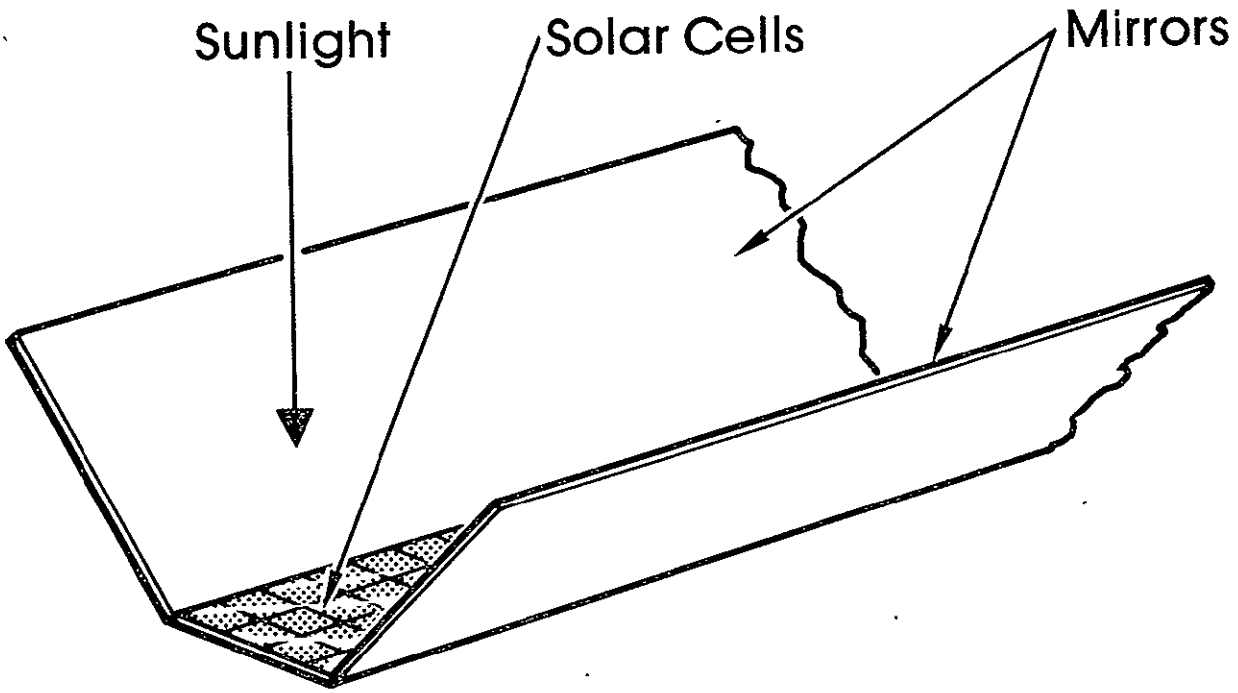

Fig. 2.3-1 - Two dimensional front-lit flat plate trough concentrator (2D-FPT)

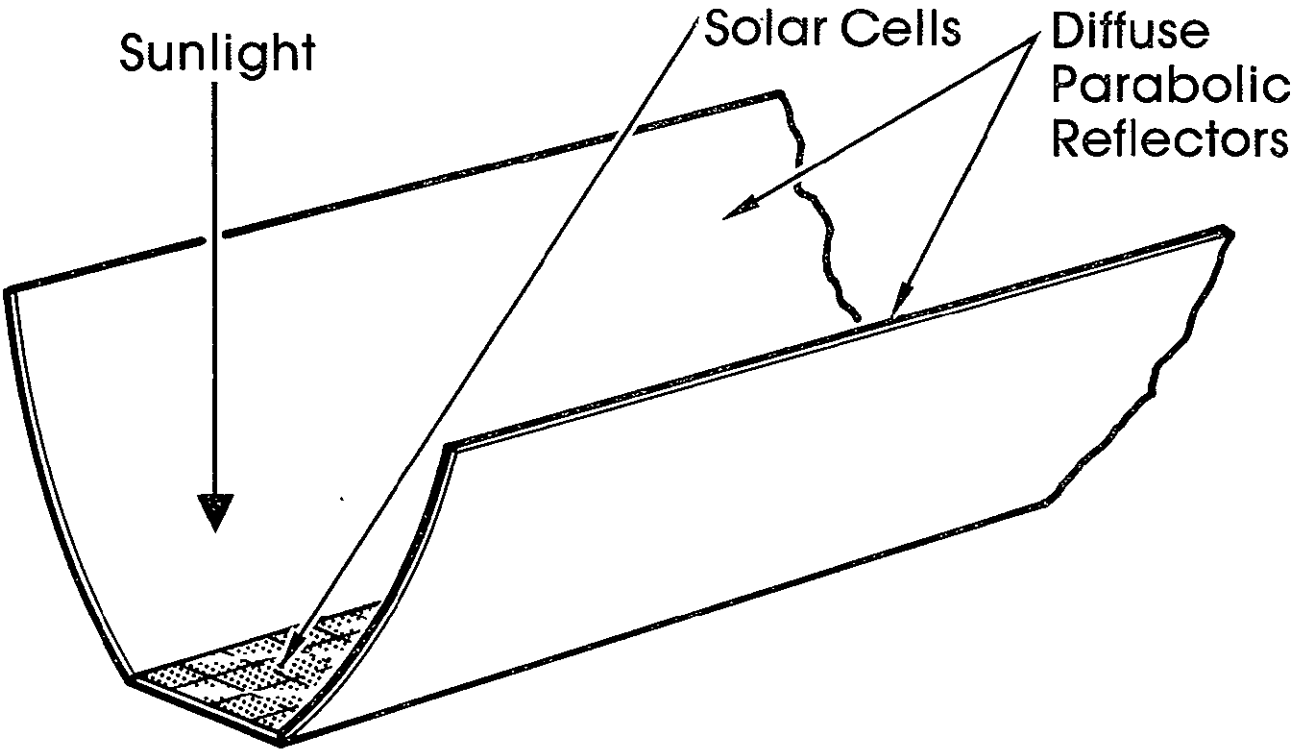

Fig. 2.3-2 - Front lit compound parabolic concentrator (CPC)

this sun angle, the maximum C_g achievable is 11.3, but the area ratio R becomes unacceptably high above a C_g of about 5. With specular mirrors, this concept produces extremely non-uniform illumination and is unacceptable. However, by introducing a sufficiently diffuse mirror surface, the illumination non-uniformity meets the 15% requirement, but at the penalty of a high reflection loss. Variation in C_g is accomplished by mirror tilting.

2.3.3 The three dimensional, back-lit, multiple flat plate concentrator (3D-MFPC) shown in Figure 2.3-3 produces uniform illumination and accommodates sun axis shift by mirror oversizing. Mirrors are provided in orthogonal sets of 4. With no sun misalignment and, hence, no mirror oversizing, any value of C_g is theoretically attainable. However, a theoretical upper limit of $C_g = 131$ results when the mirrors are oversized for a 5^o sun misalignment. When actual deployment and support structure are taken into account, mass considerations create a practical upper limit of C_g on the order of only 6 or 7. Variability in C_g below the maximum is accomplished by rolling up selected mirrors or by changing mirror tilt angles.

2.3.4 The reflexicon shown in Figure 2.3-4 is a back-lit design. Here, the mirrors and array are truncated cones. By varying cone angles and array to mirror distance, configurations with maximum C_g's of any magnitude are achievable if mirrors are not oversized for sun misalignment. The illumination is somewhat non-uniform but meets the 15% criteria. With oversizing, upper limits to C_g exist, however, mass considerations limit C_g to 11 or 12. C_g variability is accomplished by moving entire conical mirror assemblies vertically (along the axis of symmetry) until they no longer illuminate the array.

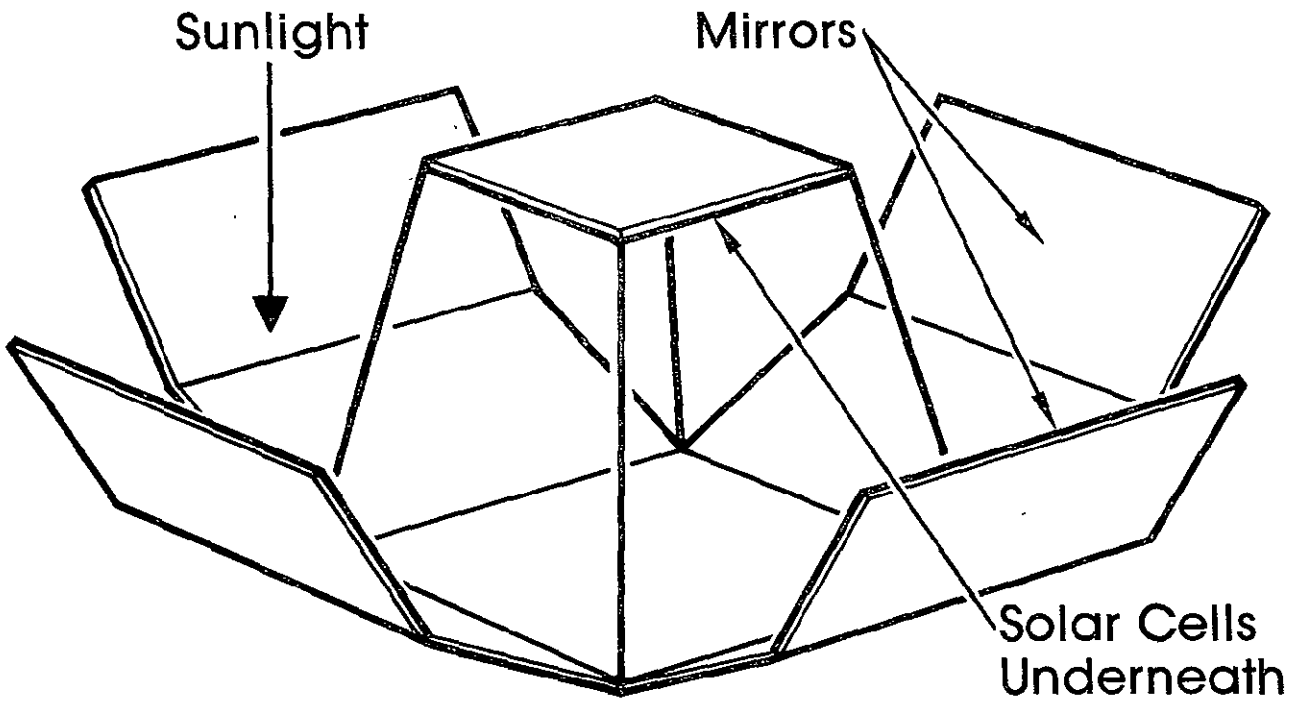

Fig.2.3-3 - Back-lit three-dimensional multiple flat plate concentrator (3D-MFPC)

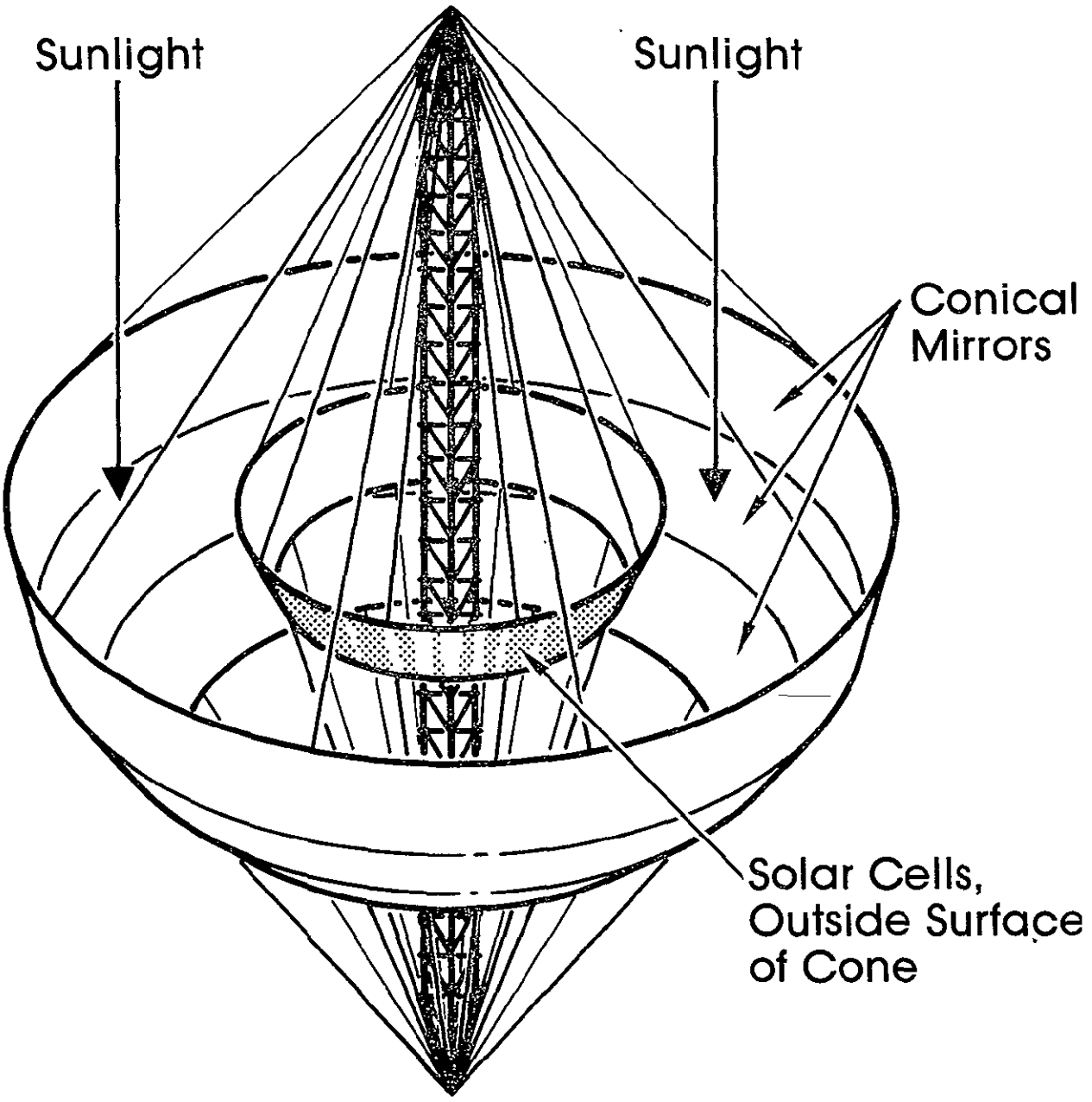

Fig. 2.3-4 - Back-lit reflexicon concentrator

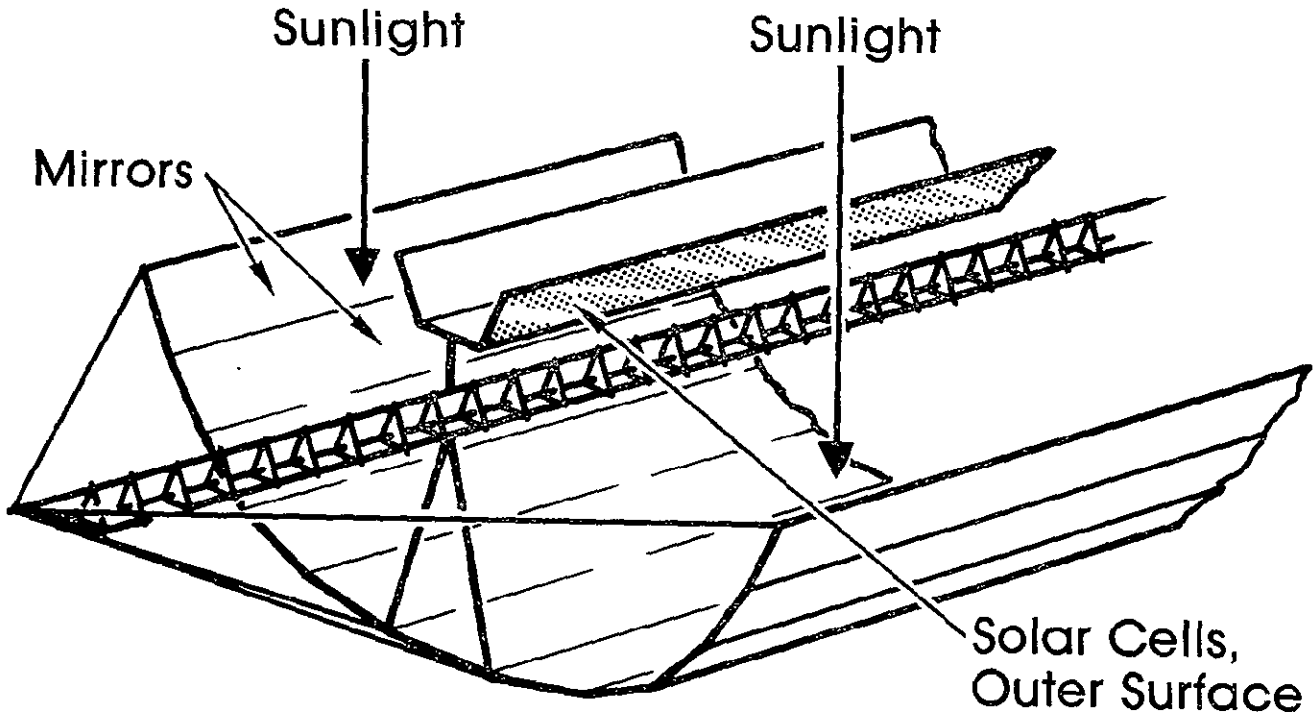

Fig. 2.3-5 - Two-dimensional back-lit multiple flat plate concentrator (MFPC)

2.3.5 Passive and semi-active multiple flat plate concentrators (MFPC) are actually two variations of a single two dimensional, back-lit design (Figure 2.3-5). They differ from the 3D-MFPC only in that they are configured in two dimensions. In the passive version each flat plate mirror is oversized to accommodate sun axis shift. Mass considerations limit C_g to about 7 in this version although slightly higher values are theoretically possible. Variability in C_g below the maximum is accomplished by rolling up select Kapton mirrors. The semi-active version has each mirror end independently and automatically aligned with the solar axis within 1^o by a simple bimetallic device which senses misalignment and corrects as required after the entire assembly has been aligned by the spacecraft control system. Since the mirrors are now oversized for only 1^o sun misalignment, higher values of C_g are theoretically achievable, however the practical mass-limited C_g appears to be about 18. In this version, C_g variability is accomplished by individual mirror tilting.

2.4 Concept Evaluation Procedure

This section summarizes the procedure that was followed to comparatively evaluate the candidate concepts described in Section 2.3.

Two basic evaluations were performed. The first was an evaluation of the predicted performance of the concepts relative to power output and power to mass ratio (specific power) as a function of solar distance (AU). From the evaluation, comparisons between the concepts were made. The second evaluation was a comparison of the concepts made in terms of a list of cost-related parameters.

To accomplish the predicted performance evaluations of the concepts, a number of assumptions and decisions had to be made and certain fundamental data had to be generated. With regard to the solar array to be enhanced by the concentrators, a baseline solar cell was selected and for this cell a curve of efficiency versus temperature and irradiance level was generated. This work is described in Section 2.4.1.

The 8 micrometer thick Kapton reflectors selected for all concepts were assumed to be coated either with vapor deposited aluminum (VDA) or with a particular "cold mirror" coating developed by the OCLI Co. Based on test data, the VDA reflects 90% of all incident light across the entire light spectrum.

Thus the VDA converts the Kapton into an ordinary or conventional mirror which reflects all incident light. On the other hand, the "cold mirror" coating does not produce an ordinary mirror, but instead is spectrally selective. In principle, a "cold mirror" coating reflects well only across the wavelength band which the solar cell converts to electrical power. It reflects poorly across the remaining light spectrum which is desirable since here the reflected light only increases the cell temperature. An analysis of the

particular OCLI "cold mirror" coating which was selected in conjunction with the selected cells found the total effective reflectance integrated across the usable spectrum to be 64% while the total heat inducing reflectance was 42%. An additional reflection loss of 10% was assumed for all concepts due to mirror shape and surface smoothness deficiencies. Higher losses were used for CPC due to mirror surface texturing and these data were extracted from references 1 and 4.

A thermal analysis of each concentrator concept was then performed from which curves of temperature as a function of C_g, AU, and reflector coating were generated. This effort and the results are summarized in Section 2.4.2. All these analytical data permitted the final power output of the baseline solar array to be calculated for each concept as a function of solar distance, maximum C_g, and type of reflector coating.

Next, considering each concept individually, numerous structural ideas for stowage, deployment, shaping, support and adjustment were proposed and studied. For the idea judged best for that concept, major structural members were sized by stress analysis, ultimately permitting mass estimates to be made as a function of maximum C_g. These data then permitted specific power to be determined for each concentrator concept as a function of C_g for various solar distances and each of two reflector coatings.

The final curves of weight versus maximum C_g are shown in figures 2.4-1, 2.4-2, 2.4-3, and 2.4-4 for the reflexicon, 3D-MFPC, passive MFPC and semi-active MFPC respectively. Weight data on the 2D-FPT was obtained from reference 2 and then modified to make it consistent with the thin solar cell selected for the baseline array as well as with the size of the array. The weight of the CPC solar cell blanket given in reference 6 is based on an

ultra thin silicon cell and cover with essentially the same dimensions as the cell selected for this study. It was, therefore, assumed that the listed weight of the CPC blanket would be essentially the same on a per unit area basis as the weight of the baseline array used in the study. Accordingly, only an adjustment for comparable output size was made on the CPC data. Late in the study, however, it was determined that the construction of the CPC solar cell blanket differed substantially from that used in this study. Most significant of the differences was that while the baseline cell used a 50 micrometer cover glass fastened with 30 micrometers adhesive, the CPC simply used 25 micrometers of adhesive instead of a cover glass. This difference, together with several items accounted for on the baseline, but omitted in the CPC estimate, caused the CPC blanket to weigh approximately ½ of the baseline on a per unit area basis. Therefore, while comparisons between the CPC and the other concepts are valid on a power output basis, a direct comparison of specific mass is not valid.

Final Phase I performance results are discussed in Section 2.4.3 as are the results of the comparisons made relative to other cost related parameters.

FIGURE 2.4-1. WEIGHT ESTIMATE FOR REFLEXICON

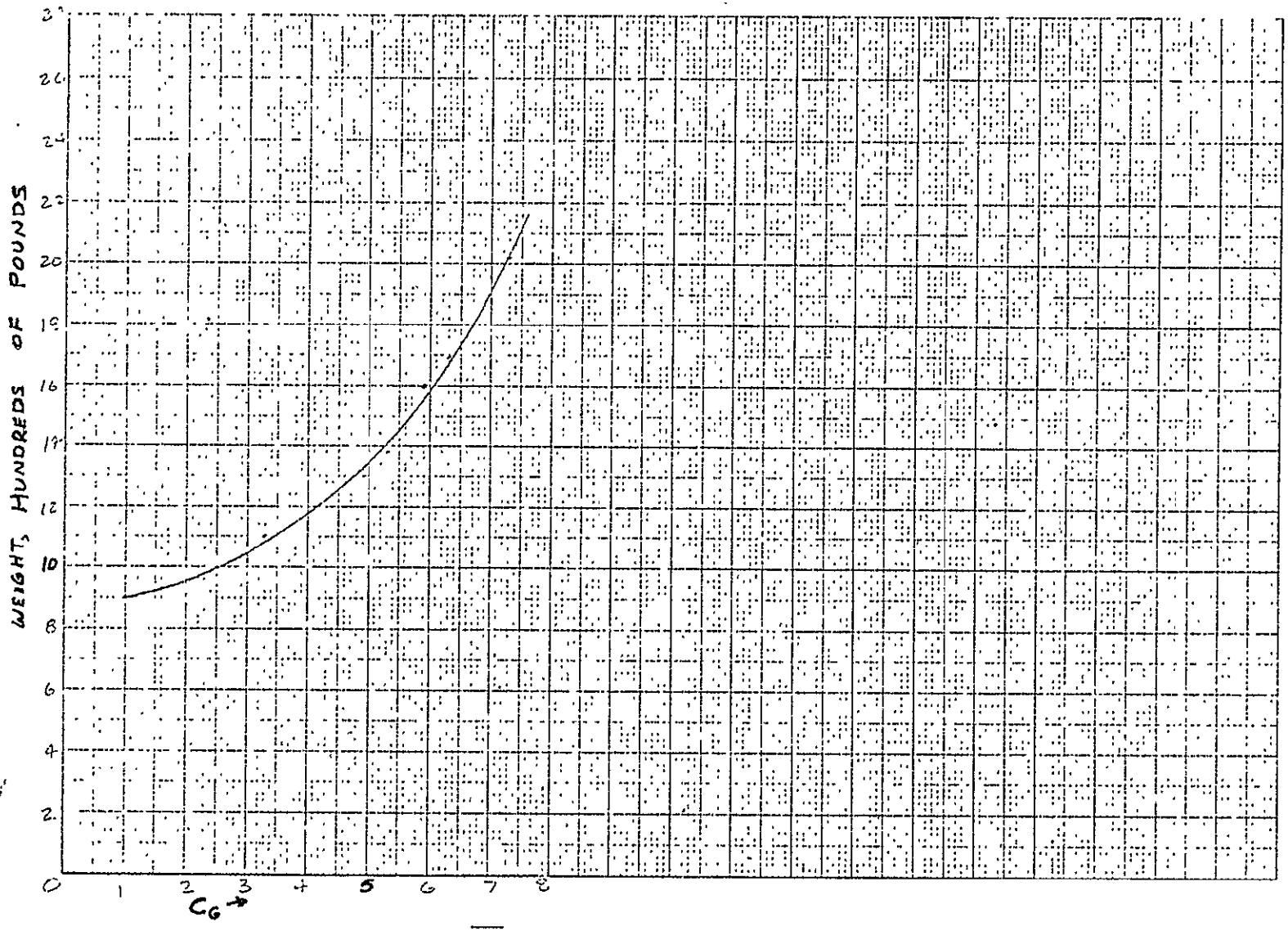

FIGURE 2.4-2. WEIGHT ESTIMATE FOR 3D MFPC

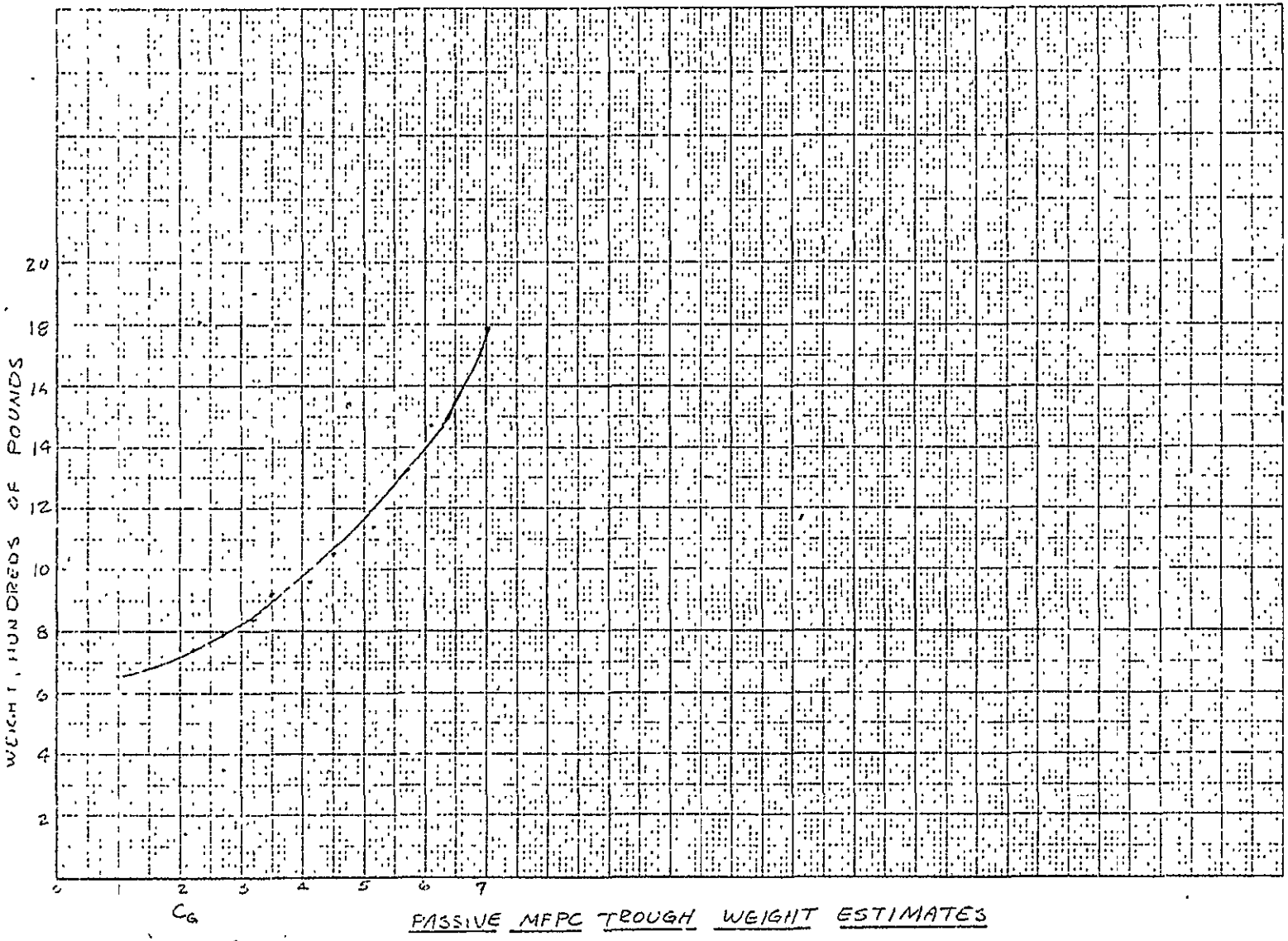

PASSIVE MFPC TROUGH WEIGHT ESTIMATES

FIGURE 2.4-4. WEIGHT ESTIMATE FOR SEMI-ACTIVE MFPC TROUGH

2.4.1 Array Selection and Analysis

For a fair evaluation of the future effectiveness of solar concentrators, the array selected for enhancement should contain the lowest mass cells projected to be available in the same time period. Based on this criterion and projecting forward a few years, the silicon cells selected would be 50 um thick, 13% efficient with 50 um covers. These would be mounted on a flexible substrate of Kapton and glass fabric with a rear thermal control material of second surface aluminized FEP Teflon film. The weight budget for such a solar array is summarized in Table 2.4.1-1. While the achievement of this low weight still requires a scale up to realize production quantities of the thin solar cells and coverglass, no fundamentally new technology is required. The other components of the array are presently available in production quantity.

During launch such a flexible array would be folded or rolled to provide a compact volume. Upon reaching orbit the array would be deployed, then supported in a taut manner by mechanisms attached to the edges of the array. These mechanisms are described elsewhere in this report. The size of such an array has been calculated using the design factors listed in Table 2.4.1-2. To achieve the required 25 kW at 1 AU, 55°C, an array of the proposed construction would need an area of 194 m^2.

The heart of the solar array is the solar cell. Over the past few years, 50 micrometer thick silicon solar cells have been under development for space application. Small quantities of cells have been made with efficiencies near 14% (See Reference 11). The feasibility of producing thin cells in a pilot line production facility has been investigated, demonstrating that production cells with an average efficiency near 12% is possible now (References 12 and 13). With minor improvements, future cells in production quantities are expected to have an average efficiency of 13%.

The characteristics of the solar cell considered baseline for this study are summarized in Table 2.4.1-3. The photovoltaic power capability of the cell is shown in Figure 2.4.1-1. An important property of any solar cell is the inherent sensitivity of its power output with respect to the cell's temperature. This is especially important for the present program because the operating temperature of the cells depends markedly on concentration ratio, AU distance, and concentrator design. An increase in the cell operating temperature, due to enhanced solar irradiance by concentration, causes a slight increase in the cell short-circuit current and a significant decrease in the cell voltage. The

ITEM	MATERIAL	THICKNESS (cm)	% AREA	DENSITY (g/cm^3)	WEIGHT (g/cm^2)
Cover	Ceria Doped Glass	0.005	90	2.6	0.0117
Adhesive	RTV Silicone	0.003	90	1.1	0.0030
Cell	Silicon	0.005	90	2.4	0.0108
Interconnect	Silver and Solder	0.004	10	11.0	0.0044
Adhesive	RTV Silicone & Glass Fabric	0.004	100	1.3	0.0052
Support Sheet	Kapton	0.003	100	1.4	0.0042
Bus	Copper	0.003	40	8.9	0.0106
Adhesive	RTV Silicone & Glass Fabric	0.004	50	1.3	0.0026
Insulator	Kapton	0.003	50	1.4	0.0021
Adhesive	RTV Silicone & Glass Fabric	0.005	100	1.3	0.0065
Thermal Control	Aluminized FEP Teflon	0.005	100	2.2	0.0110
Diodes & Wire		N/A	N/A		0.0010
				TOTAL	0.0731 g/cm^2
					= 0.7 kg/m^2

TABLE 2.4.1-1. UNIT WEIGHT FOR SOLAR PANEL BLANKET

Power requirements	25 kW at 1 AU, 55°C, beginning of life
Cell efficiency	13.0% at 28°C
Design factors	
Assembly loss (fabrication)	3%
Bussing loss	4%
Diode loss	0.5%
Solar constant	135.3 mW/cm^2
Packing factor	90%
Temperature factor (55°C compared to 28°C)	0.88
Initial power (accounts for first 3 losses)	25 kW/0.925 = 27,027 W

Total area (A) is determined by:

Initial power = solar constant x total area x cell efficiency x temperature factor x packing factor

$$27{,}027\ W = 135.3\ \frac{mW}{cm^2} \times A\ cm^2 \times 0.130 \times 0.88 \times 0.90$$

$$A = 194\ m^2$$

TABLE 2.4.1-2. SOLAR ARRAY SIZING ASSUMPTIONS

CELL

2 MIL THICK (2 cm x 2 cm)

N/P 10 OHM-CM SILICON

P/P^+ BACK CONTACT

OPTICAL REFLECTING BACK CONTACT

Ti-Pd-Ag CONTACTS (WITH Al)

DUAL LAYER ANTI-REFLECTIVE FRONT COATING

13% EFFICIENCY AMO AT 27°C

COVER

CERIA DOPED MICROSHEET

2 MIL THICK GLASS

1 MIL THICK SILICONE ADHESIVE

TABLE 2.4.1-3. BASELINE SOLAR CELL FOR CONCENTRATOR ENHANCED SOLAR ARRAYS

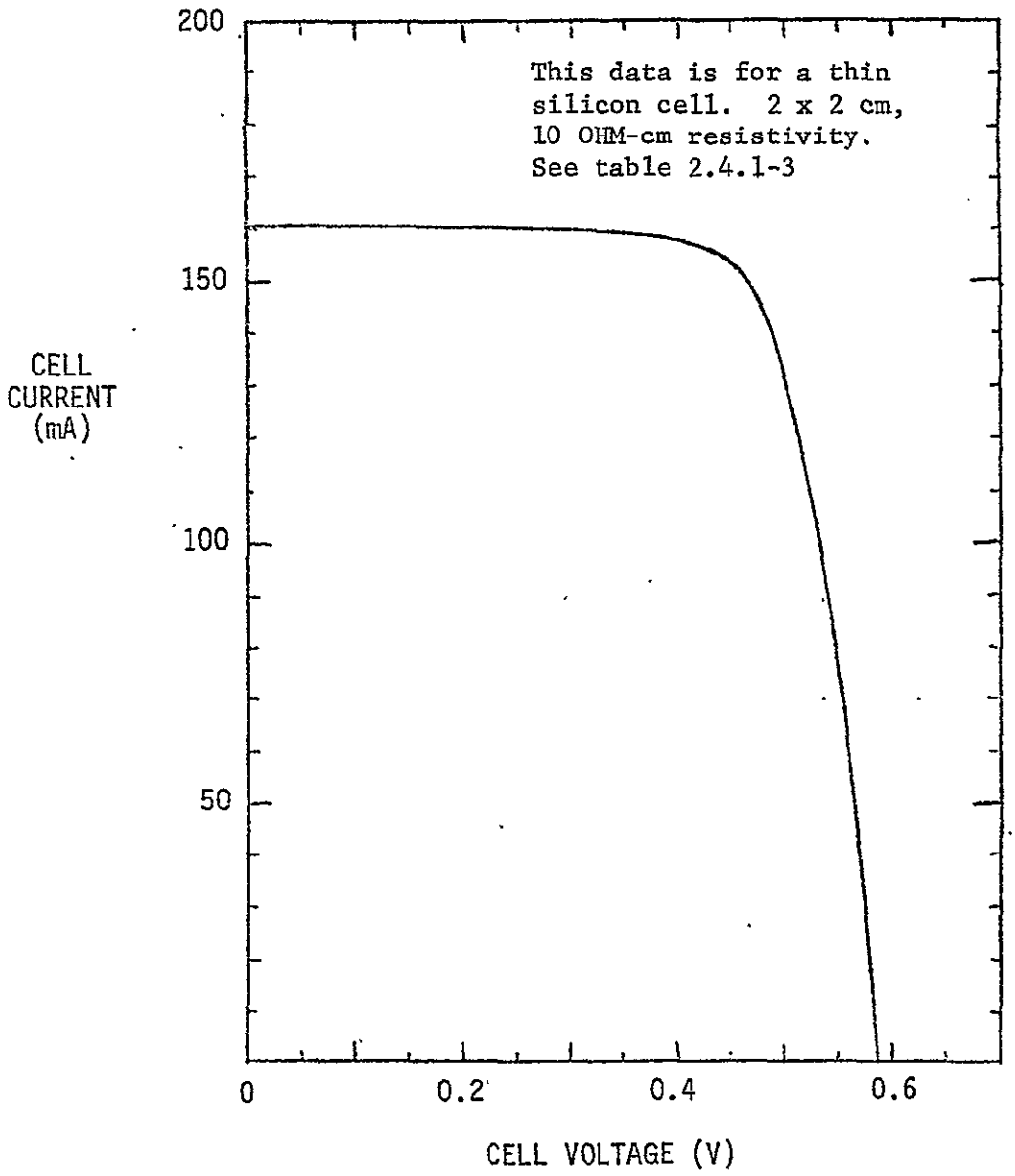

FIGURE 2.4.1-1. PHOTOVOLTAIC RESPONSE FOR BASELINE SOLAR CELL 27°C AT AMO SUN ILLUMINATION

increase in current is typically less than 0.1% per ^{o}C. The decrease of voltage with temperature is typically near 2.2 mV per ^{o}C. Both of these dependencies, and therefore the temperature dependence of cell power, depends slightly on cell design features. The expected temperature dependency for the baseline 50 micrometer cell of this study is shown in Figure 2.4.1-2. This dependency was established by compiling measured data on various, existing types of silicon cells and projecting to the baseline cell (References, 13, 14 and 15).

The operating temperature of cells depends upon the amount of sunlight actually absorbed by the cells. Figure 2.4.1-3 shows the useful current response of the cell as a function of the wavelength of incident light. A key feature to this is the lack of response at wavelengths much longer than 1.1 micrometers. These longer wavelengths contribute only to heating the cell, not to useful electrical energy. The heating of the cell actually reduces the cell output as indicated in Figure 2.4.1-2. Since about one-fourth of sunlight energy is at these longer wavelengths, anything done to the cell to enhance reflectance of this long wavelength light contributes to increased efficiency of the cell. Of course, as much absorbtion as possible is desired at shorter wavelength where direct photovoltaic conversion occurs. Using the specified (Table 2.4.1-1) dual anti-reflective layer for low reflection of short wavelengths and the reflective back contact to reflect part of the long wavelengths, the predicted reflectance of the baseline cell is presented in Figure 2.4.1-3. Both Figures 2.4.1-3 and 2.4.1-4 were used elsewhere in this report to establish trade-offs in optimizing power by considering the effect of using "cold" mirrors (visible reflecting, IR transmitting) for the concentrator surfaces.

The final factor that needs to be considered for solar cells is the effect of non-normal sunlight illumination. In general, concentrator systems will cause the light to impinge on the array at a wide range of incident angles. The effect of angle of incidence on cell power is summarized in Figure 2.4.1-5. As long as the incident angle is within 60^{o} of normal, the power drop off with angle can be approximated by the cosine of the angle.

While the solar cell is the most important part of any array, thereby receiving the most attention in this report, the other array components also are needed to make a practical array. The choice of a 50 micrometer thick cover was based on the thinnest glass that can be cast in production quantity. While not presently available is such quantity, it could be produced if a market were developed. The other array components, listed in Table 2.4.1-1, are conventional, available materials.

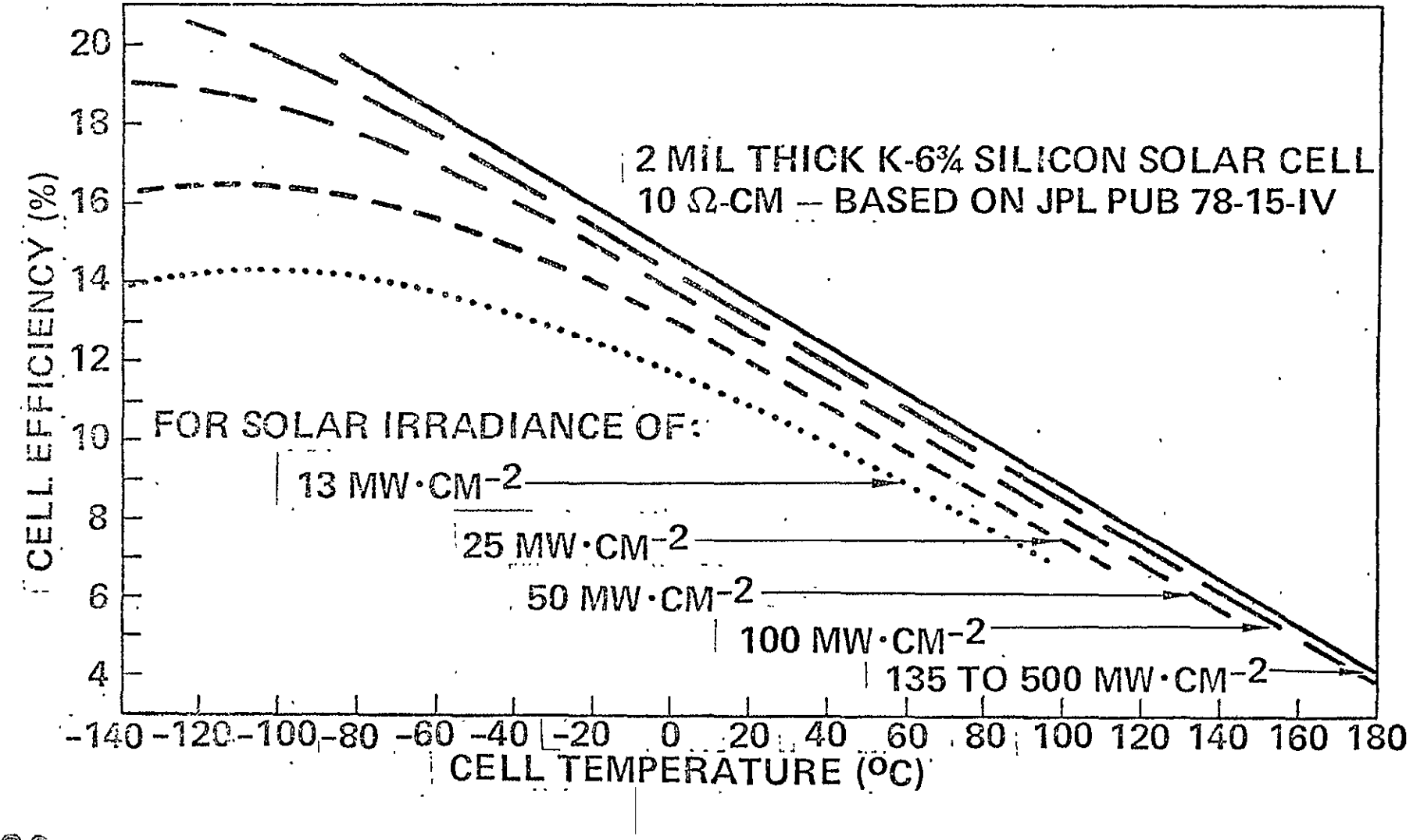

FIGURE 2.4.1-2. SOLAR CELL EFFICIENCY FOR BASELINE SOLAR CELL

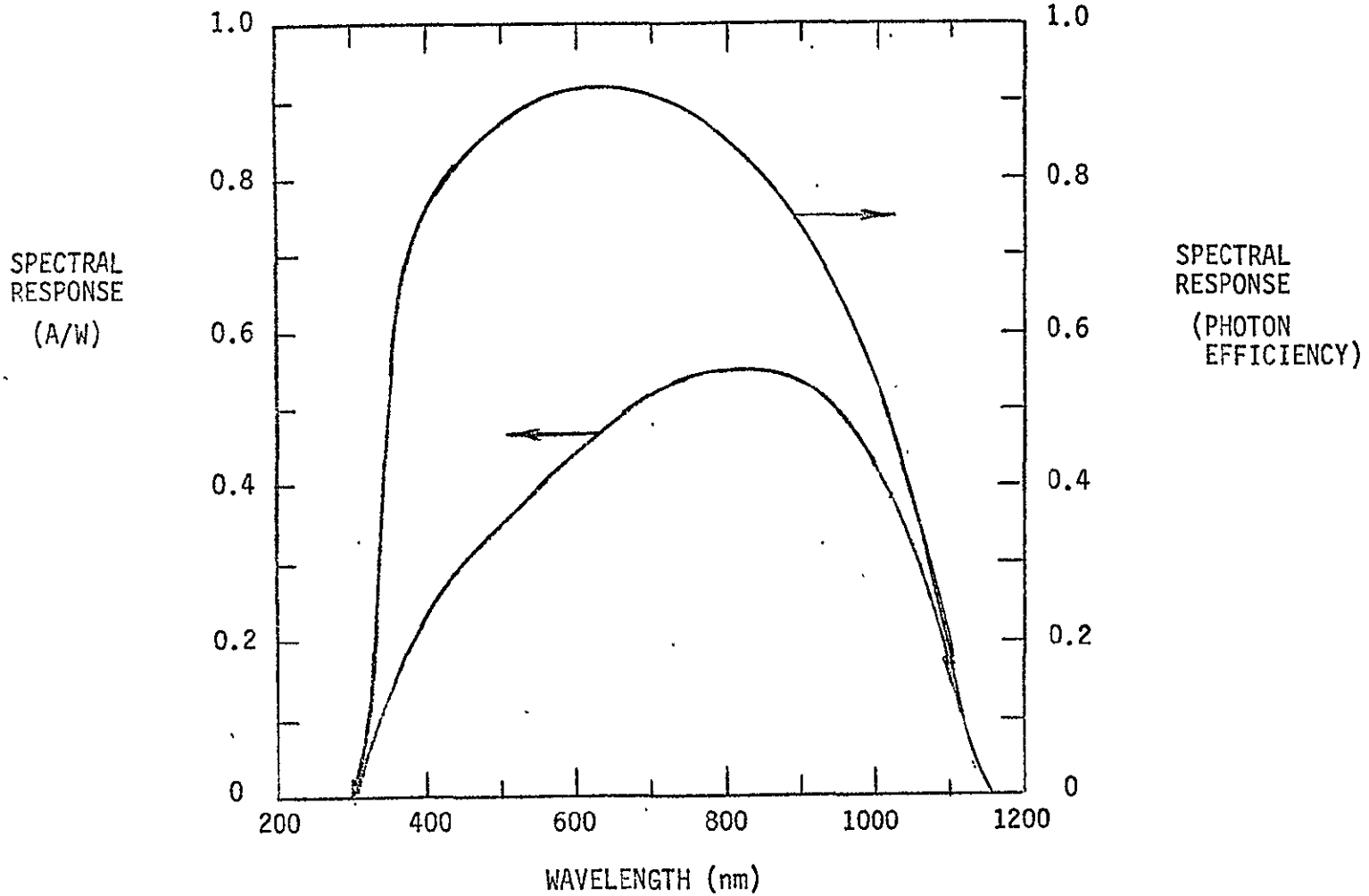

FIGURE 2.4.1-3. SPECTRAL RESPONSE FOR BASELINE SOLAR CELL

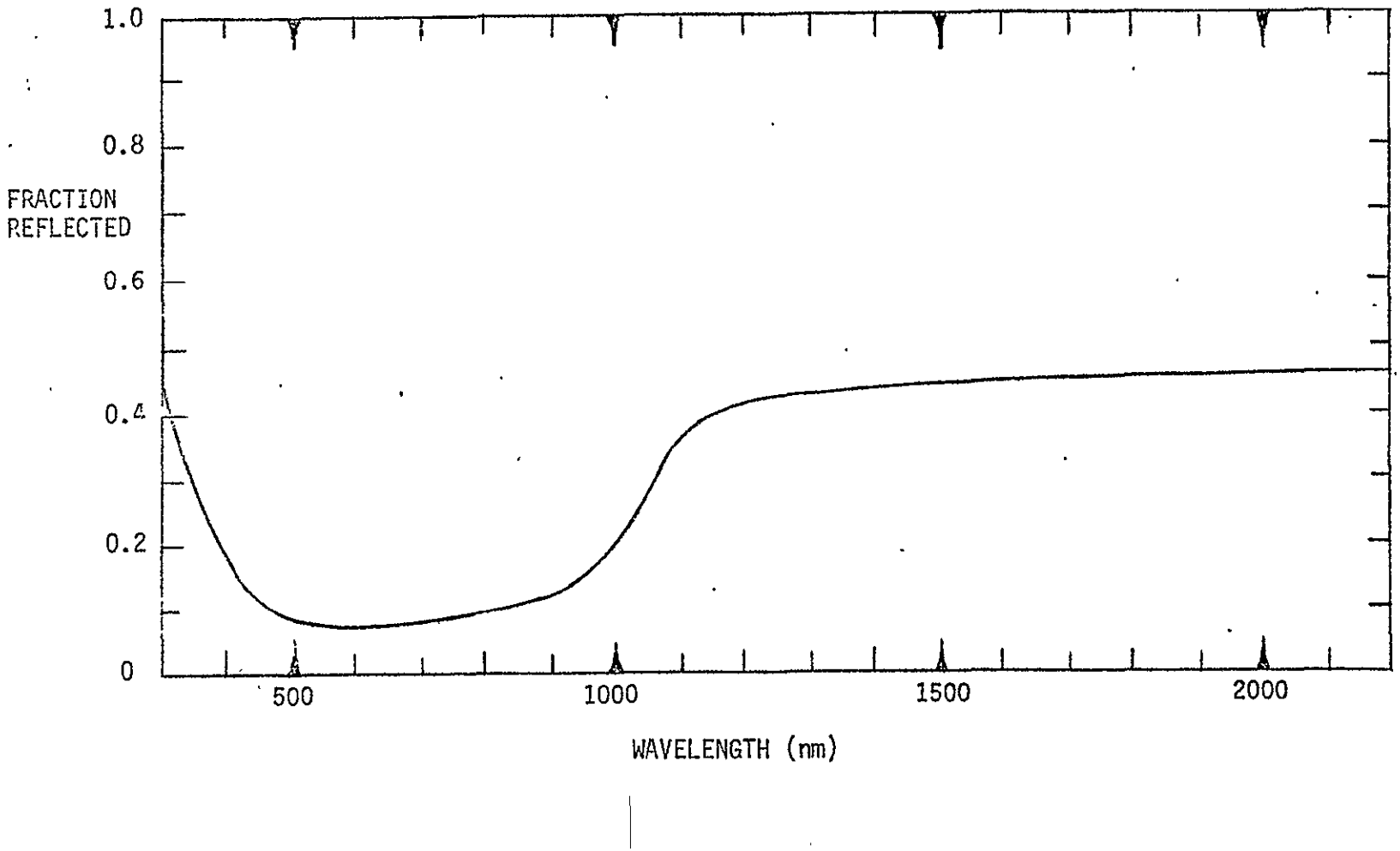

FIGURE 2.4.1-4. SPECTRAL REFLECTANCE FOR BASELINE SOLAR CELL

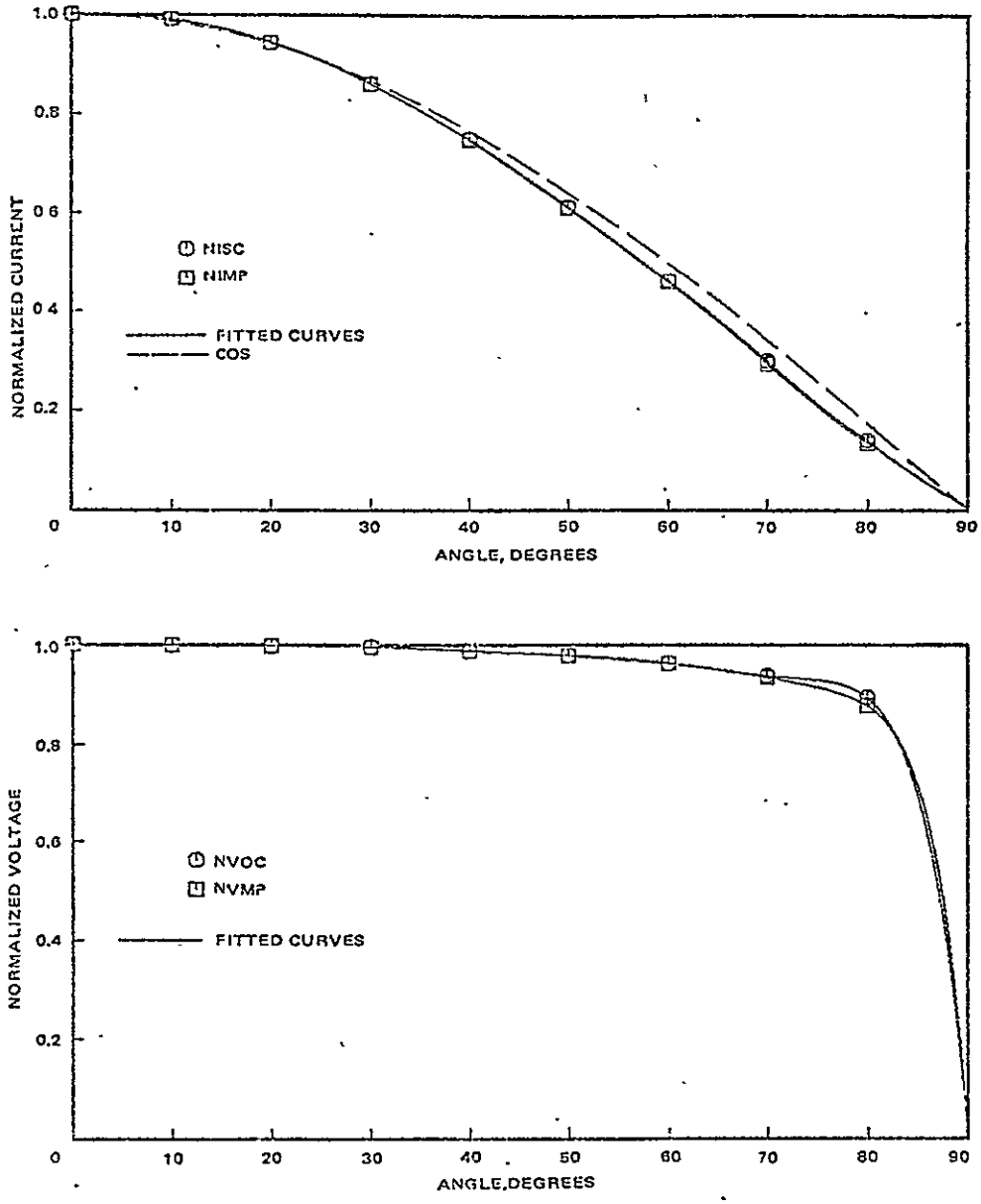

NOTE: In both curves above, circles and squares proved to be essentially coincident within the precision of the measurements.

FIGURE 2.4.1-5. ANGULAR RESPONSE FOR BASELINE SOLAR CELL AMO ILLUMINATION

2.4.2 Phase I - Thermal Analysis

Solar Array and Reflector Coating Thermal Characteristics

Solar Array temperatures for the several candidate concentrator design concepts considered in Phase I were calculated parametrically as functions of solar distance, geometric concentration ratio, and concentrator surface finish. In all cases the array was assumed to utilize 2 mil silicon solar cells possessing projected thermal/optical radiation properties and electrical efficiencies comparable to the K6 3/4 type cell. In addition, all designs analyzed utilize backlit arrays and, therefore, were assumed to be covered with 2 mil silvered Teflon on the back side to minimize absorbed solar heat loads (solar absorptance, α = .1, total hemispherical emittance ϵ =.66). Temperature data on the front lit designs were obtained from reference 2 for the 2D-FPT, and reference 6 for the CPC.

The projected spectral reflectance for the assumed solar cell is shown in Figure 2.4.2-1. The resulting open circuit solar absorptance is 0.79. Total hemispherical emittance was taken as 0.80. Cell electrical efficiency was considered in the calculation of array front (cell) side solar loads, i.e., the effective cell absorptance was taken as the difference between the open circuit absorptance and the efficiency. Assembled efficiency data as functions of temperature and solar irradiance are shown in Figure 2.4.1-2 (Section 2.4.1). Array temperatures were calculated iteratively using these temperature dependent data.

Three reflector coatings were assumed in the initial analysis effort. Vapor deposited aluminum (VDA) was examined because it is the simplest to utilize. However, because the VDA is an ordinary mirror and hence non selective specularly, use results in the highest predicted array temperatures. A

reflectance of 0.9 was assumed, consistent with the Lockheed study (Reference 2). The assumed VDA emittance was 0.04 and absorptance 0.1.

The second finish examined was the OCLI "cold mirror" coating described in the Hughes Aircraft Company's concentrator design study proposal (Reference 5). This coating has the advantage of being "tailored" to reflect primarily in the wavelengths in which the silicon cells are electrically efficient, thus resulting in lower array temperatures. A reflectance of 0.42, an absorptance of 0.26, and an emittance of 0.7 were assumed for this coating. These first two properties are based on the coating spectral reflectance and transmittance data provided by the vendor as presented in Figure 2.4.2-2. Because this coating is very spectrally selective, the effective cell open circuit absorptance for incident illumination reflected from the cold mirror surface is somewhat higher than the value derived for direct solar illumination. This is a result of the coating being highly transparent to solar energy in the longer wavelengths (where the solar cells have a moderately high reflectance) and highly reflective in the 0.5 to 0.9 wavelength region where the cells have high absorptance. The cell open circuit absorptance for solar energy received from the cold mirror reflector was calculated to be 0.87. This effect is somewhat offset by the fact that the effective cell efficiency (again, based on incident energy reflected from the cold mirror) is somewhat higher for the same reasons. Spectral analysis of cell electrical response has shown that a cell receiving unconcentrated solar energy reflected from the cold mirror will produce only 64 percent of the power produced by a cell receiving direct solar irradiation, assuming a fixed cell temperature. However, because only 42 percent of the total direct energy is reflected onto the first cell, its effective efficiency is $\frac{.64}{.42}$ or 1.52 times the efficiency derived for direct illumination.

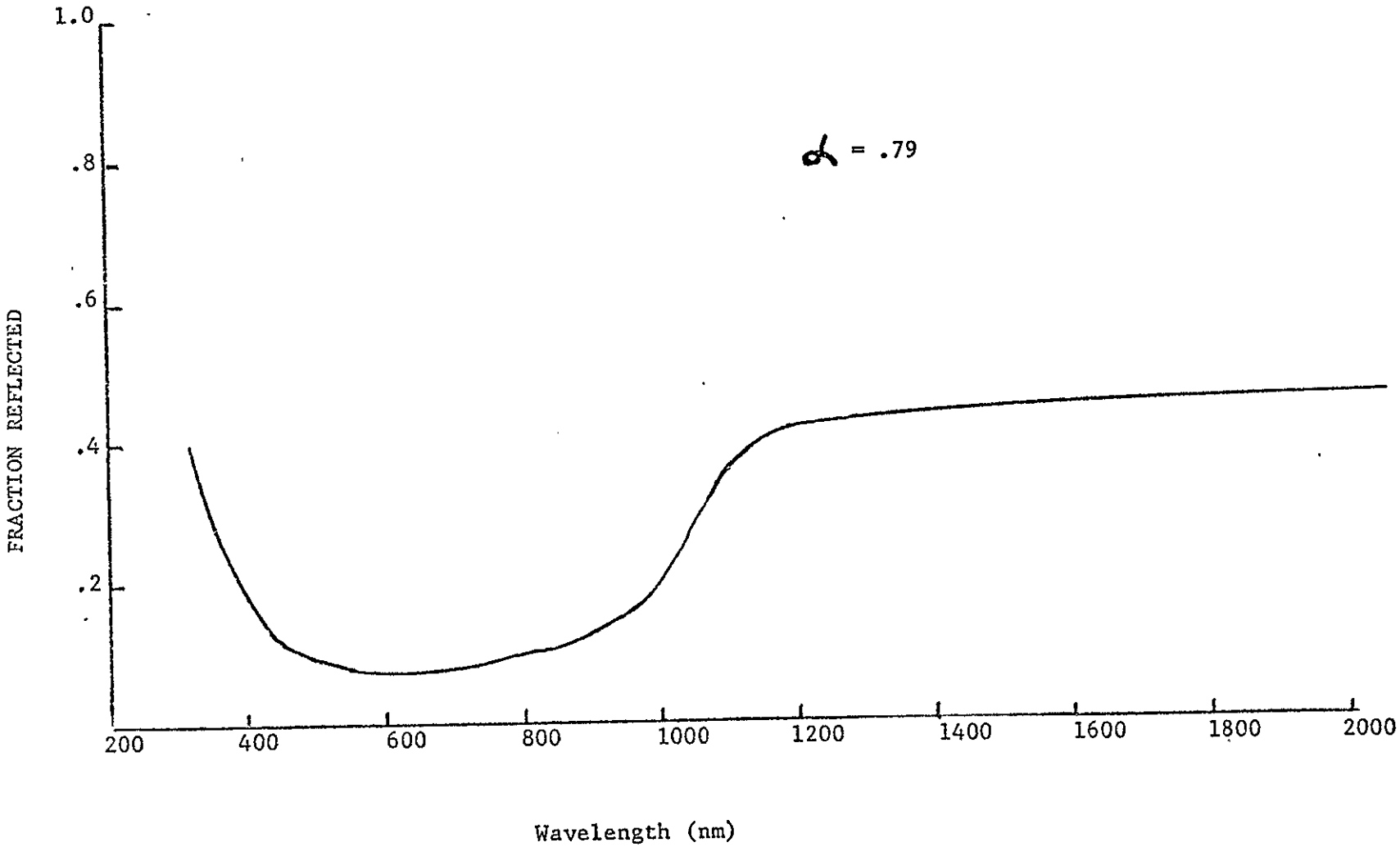

FIGURE 2.4.2-1. PREDICTED SOLAR CELL SPECTRAL REFLECTANCE

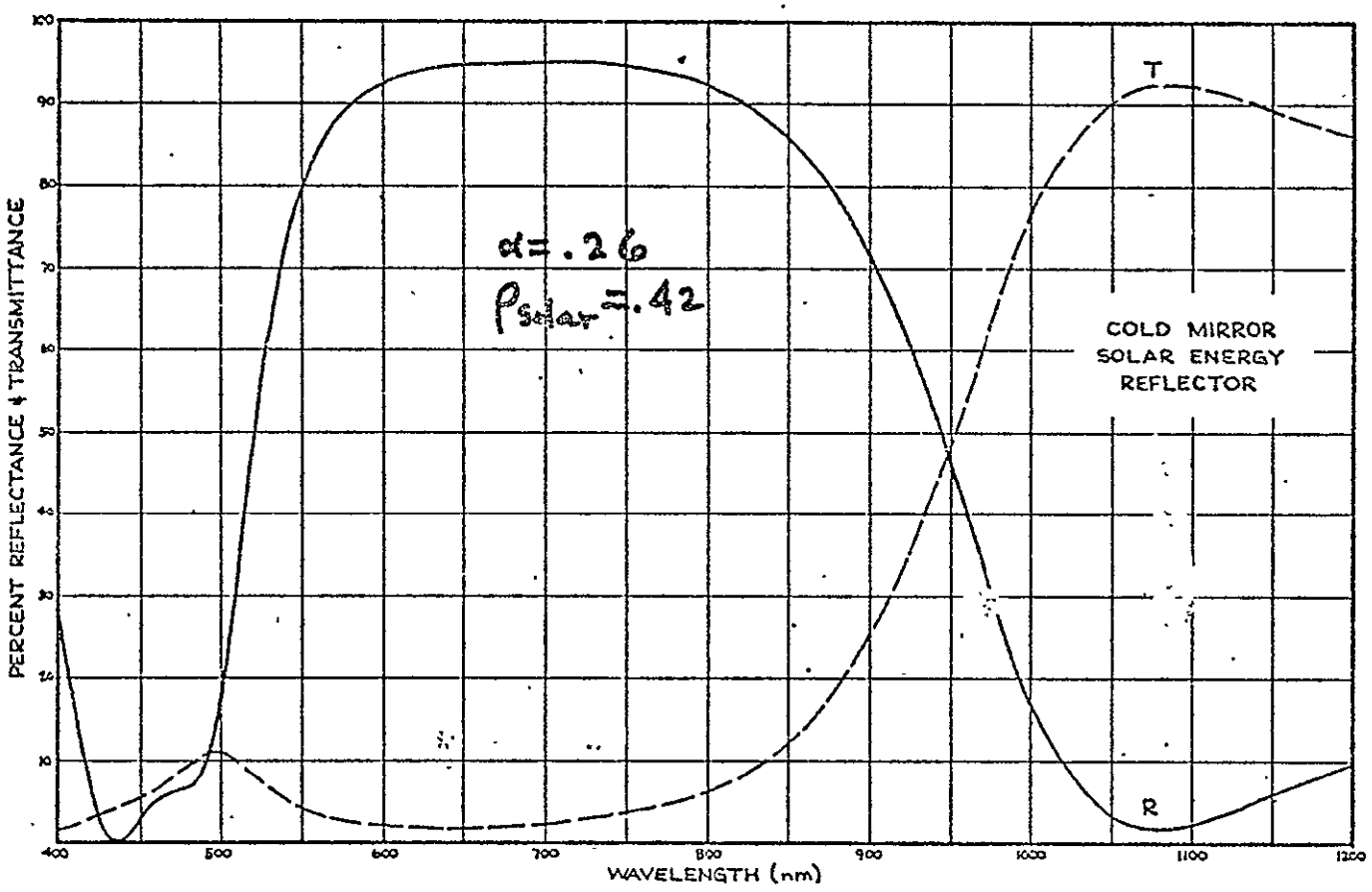

FIGURE 2.4.2-2. OCLI "COLD MIRROR" SPECTRAL REFLECTANCE AND TRANSMITTANCE

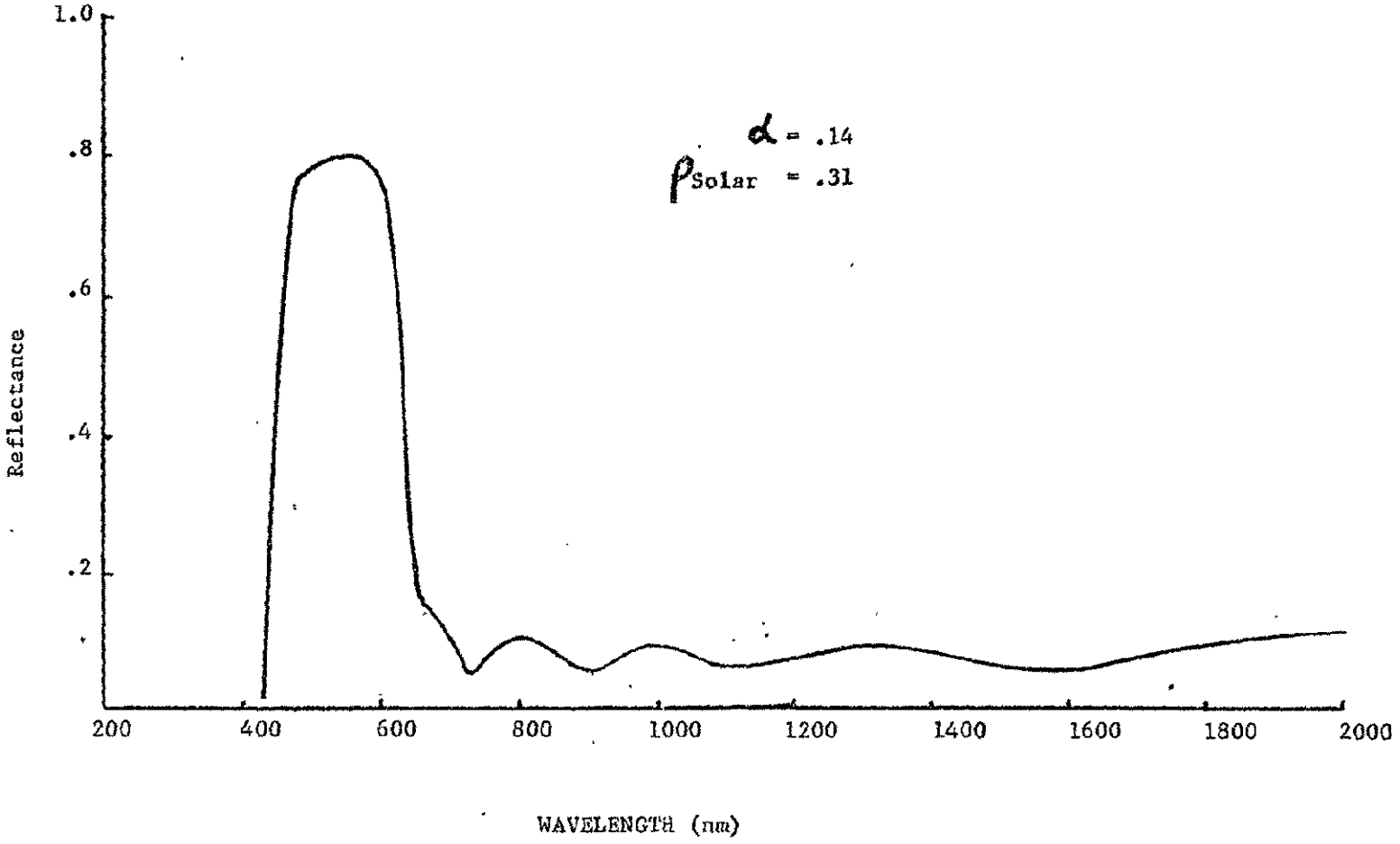

FIGURE 2.4.2-3. VALTEK COATING SPECTRAL REFLECTANCE

Similar adjustments were not required for the VDA reflector finish because its reflectance is relatively flat across the solar wavelengths.

The third finish considered was a germanium coating supplied by Valtek. This coating has a high reflectance in the wavelengths from about 0.4 to 0.65 microns, meaning that a large fraction of the solar energy above 0.65 to which the cells are responsive is lost. Because the total reflectance is only 0.31, use of this coating results in lower array temperatures. However, because this advantage does not compensate for the reduced energy available to the cells, this coating was not retained as a candidate reflector finish. Valtek coating spectral reflectance data are shown in Figure 2.4.2-3.

All calculations, regardless of assumed reflector front side finish, were based on a reflector backside emittance of 0.5, which is consistent with a 1/2 mil thick Kapton reflector substrate. It was also assumed that imperfections in the reflector surface will cause only 90 percent of the reflected solar load to be directed into the array.

Array Temperature Predictions

Because of the numerous candidate concentrator design concepts and the many possible configurations of a given concept, a comprehensive thermal analysis of all designs and configurations of interest was considered beyond the scope of this limited study. Instead, two of the thermally more straightforward concepts were analyzed in detail for a given configuration which, in each case, preliminary optimization studies indicated gave near maximum specific power, neglecting temperature effects. The two designs analyzed were the passive multiple flat plate concentrator (MFPC) and the 3-D MFPC.

Figure 2.4.2-4 schematically depicts the elements of the thermal models developed for these two designs. As shown, the solar array was

treated as a single node as were each of the symmetric pairs of reflector panels. Solar heat loads, both direct and reflected, were considered for each of these nodes. Infrared radiation interchange between the various reflector nodes and between these dones and the array was included.

Predicted array temperatures as a function of solar distance and geometric concentration ratio are shown in Figure 2.4.2-5 and 2.4.2-6 for the passive MFPC and the 3-D MFPC, respectively, assuming the cold mirror reflector coating. The geometric configuration of either design was set by the selection of the H/L ratio, where

H = distance from array to inboard edge of first reflector plate, measured parallel to reflector axis of symmetry

L = array width.

The overall length of one wing of the passive MFPC was taken as 1.5 times the overall width, which it is believed will result in a favorable (minimum weight) structural design arrangement. This is explained in Section 3.1.7.

The concentration ratios shown in the figures represent those resulting from deleting appropriate pairs of reflector plates. This is representative of the reflector plate furling or rolling-up technique selected as the means for varying concentration ratio of this design.

The dashed portions of the temperature curves indicate those regions of solar intensity and/or concentration ratio where the irradiance on the array fell outside the ranges shown on the cell efficiency curves. In the case of irradiances above 500 mw/cm^2 the efficiency data for 500 mw/cm^2 were used. Justification for this decision is contained in Figure 2.4.1-2. For values below 25 mw/cm^2, linear extrapolation was assumed. These regions do not encompass conditions of primary concern, either because array temperatures

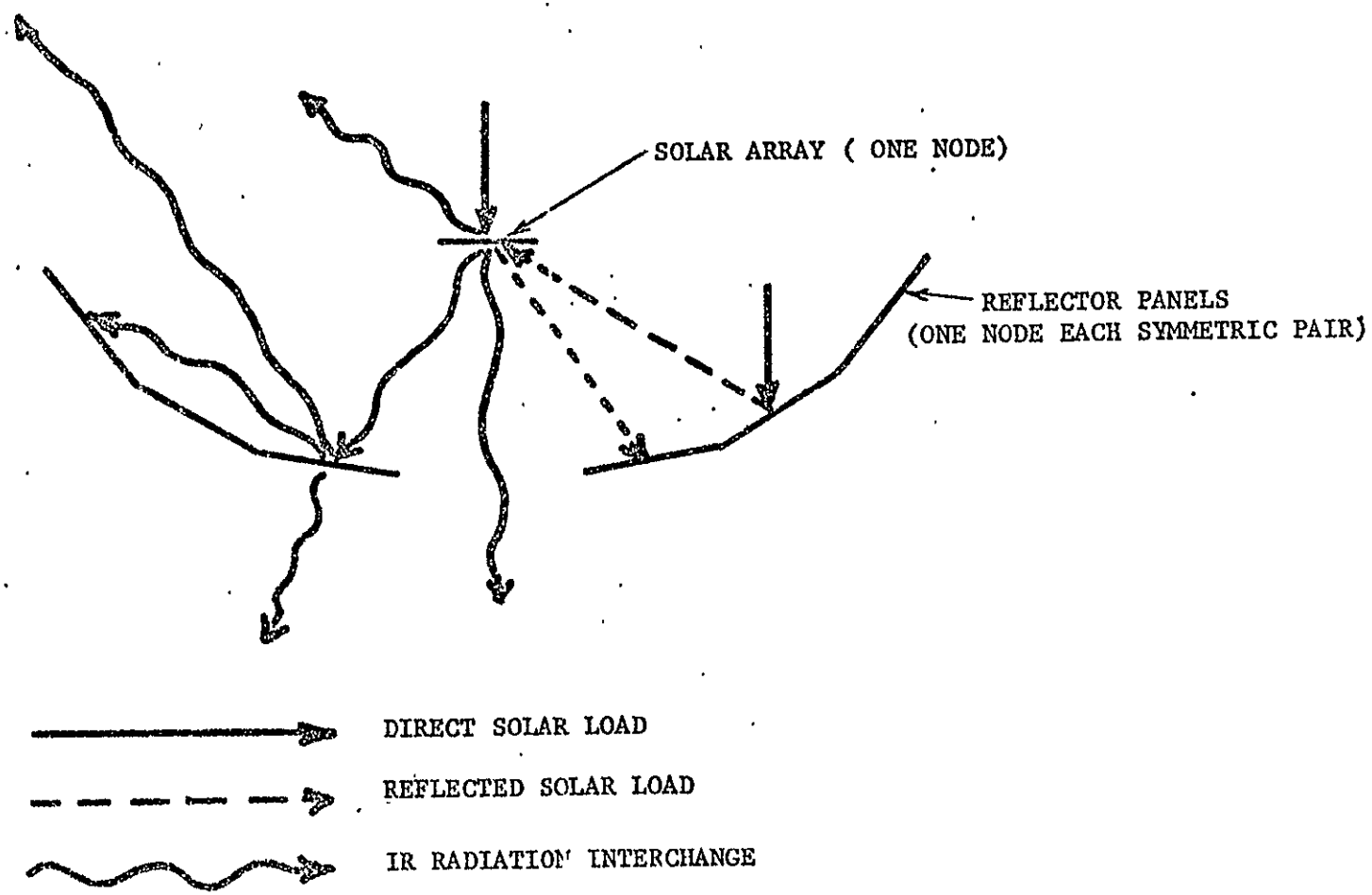

FIGURE 2.4.2-4. CONCENTRATOR THERMAL MODEL

exceed the allowable 150°C upper limit, or are so low that they have little effect on array output.

A comparison of the resulting temperatures for these two design concepts show little or no difference at a given concentration ratio and solar distance. This suggests that the differences in these designs, largely, the view from the arrays to the reflector plates, have small influence on the array temperatures. Intuitively, the infrared loads on the array from the reflector should be small at the high concentration ratios because array temperatures are substantially higher than those of the reflector. At lower concentrations, the array view factors to the reflector are small because of fewer plates being deployed. To quantify this supposition, array temperatures were recalculated over the same ranges of concentration ratios and solar distances, neglecting radiation interchange with the reflector. These results are presented in Figure 2.4.2-7 as the difference between the predicted temperatures including interchange and those neglecting interchange plotted against array temperature neglecting interchange. As indicated, this difference in temperatures is relatively small and appears to correlate with array temperature level.

These results led to the conclusion that the data shown in Figures 2.4.2-5 and 2.4.2-6 could be used for a broad range of MFPC configurations (i.e., other H/L values) with sufficient accuracy for the purposes of this comparative study.

Furthermore, the results shown in Figure 2.4.2-7 were utilized to easily calculate array temperatures for much higher concentration ratios characteristic of the active MFPC design. The resulting temperatures for this extrapolation are shown in Figure 2.4.2-8, again only for the cold mirror reflector coating.

The reflexicon concentrator design could have been treated in the same manner except for one important difference. The conically shaped array (approximated by trapezoids) has a small but significant view of itself (backside surface) which restricts rejection of the front side solar load to space. A simplified analytical model, comparable to the no radiation exchange model described above, was developed to which the array self blocking was added. The temperatures derived from this model were compared with those neglecting the blocking. The resulting temperature differences are shown in Figure 2.4.2-9 as a function of solar distance and concentration ratio. By combining these data with the reflector interchange effects of Figure 2.4.2-7, estimates of reflexicon array temperatures were developed as shown in Figure 2.4.2-10.

As indicated, all of the foregoing temperature predictions were based on the cold mirror reflector coating. Similar passive MFPC and 3-D MFPC array temperatures were developed, as indicated in Figures 2.4.2-11 and 2.4.2-12, based on a VDA reflector coating. As can be seen, these temperatures are significantly higher than those shown for the cold mirror reflector. A similar analysis of reflector radiation interchange effects indicated that the reflector infrared loads to the array could be neglected in the determination of array temperatures. This is consistent with the fact that the low reflector emittance (.04) results in very low radiation coupling terms, while the high reflector backside emittance (.66) results in relatively low reflector temperatures. Based on this finding, the array temperatures at higher concentration ratios (active MFPC) shown in Figure 2.4.2-13 were calculated.

Estimated reflexicon array temperatures for the VDA reflector coating given in Figure 2.4.2-14, were developed using data similar to that shown in Figure 2.4.2-9.

Finally, the effects of finish degradation (i.e., increase in solar absorptance) of the silvered Teflon covering the backside of solar array (common to all backlit designs) were examined for the passive MFPC operating at 1 AU. The Teflon absorptance was assumed to increase from 0.1 to 0.2, which is typical of 7 to 10 years exposure in a geosynchronous orbit and significantly more severe than degradation expected in interplanetary missions. The predicted array temperature increases are shown in Figure 2.4.2-15 as a function of concentration ratio for both candidate reflector coatings. As indicated, these effects are relatively small at higher concentration ratios, increasing to almost $20^{o}C$ at a concentration ratio of 1.0 with a cold mirror reflector.

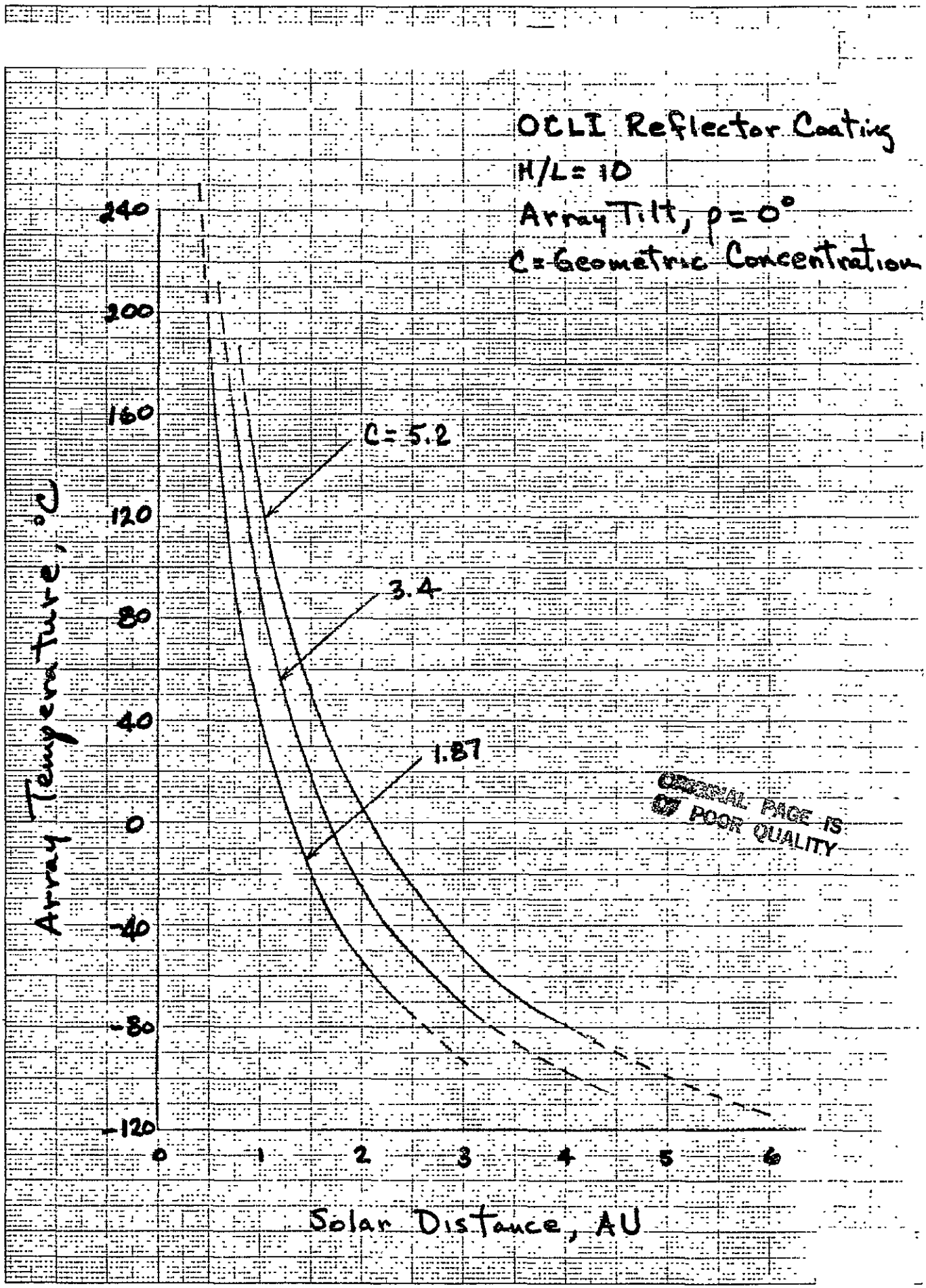

FIGURE 2.4.2-5. MFPC SOLAR ARRAY TEMPERATURES

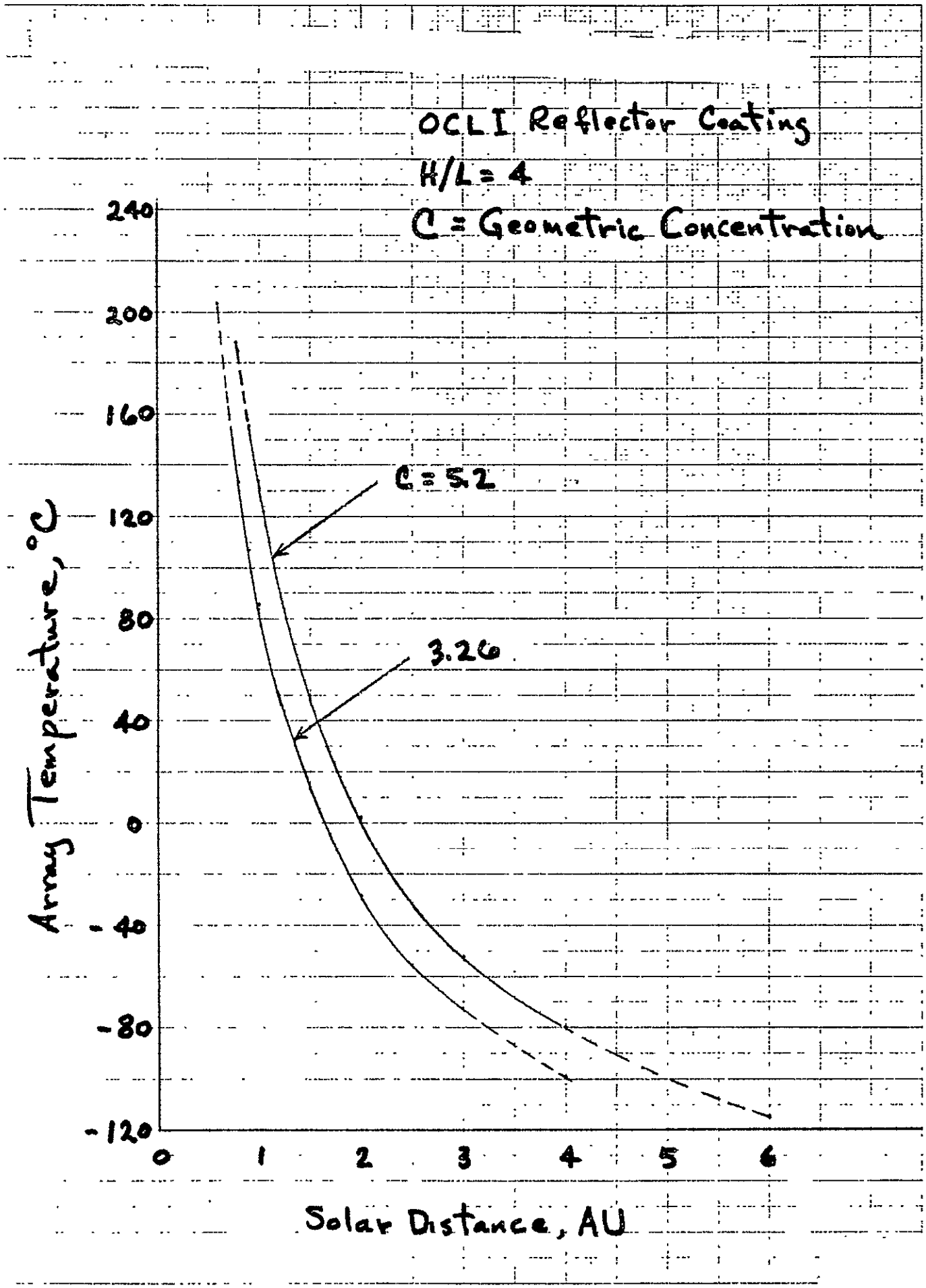

FIGURE 2.4.2-6. 3D MFPC SOLAR ARRAY TEMPERATURES

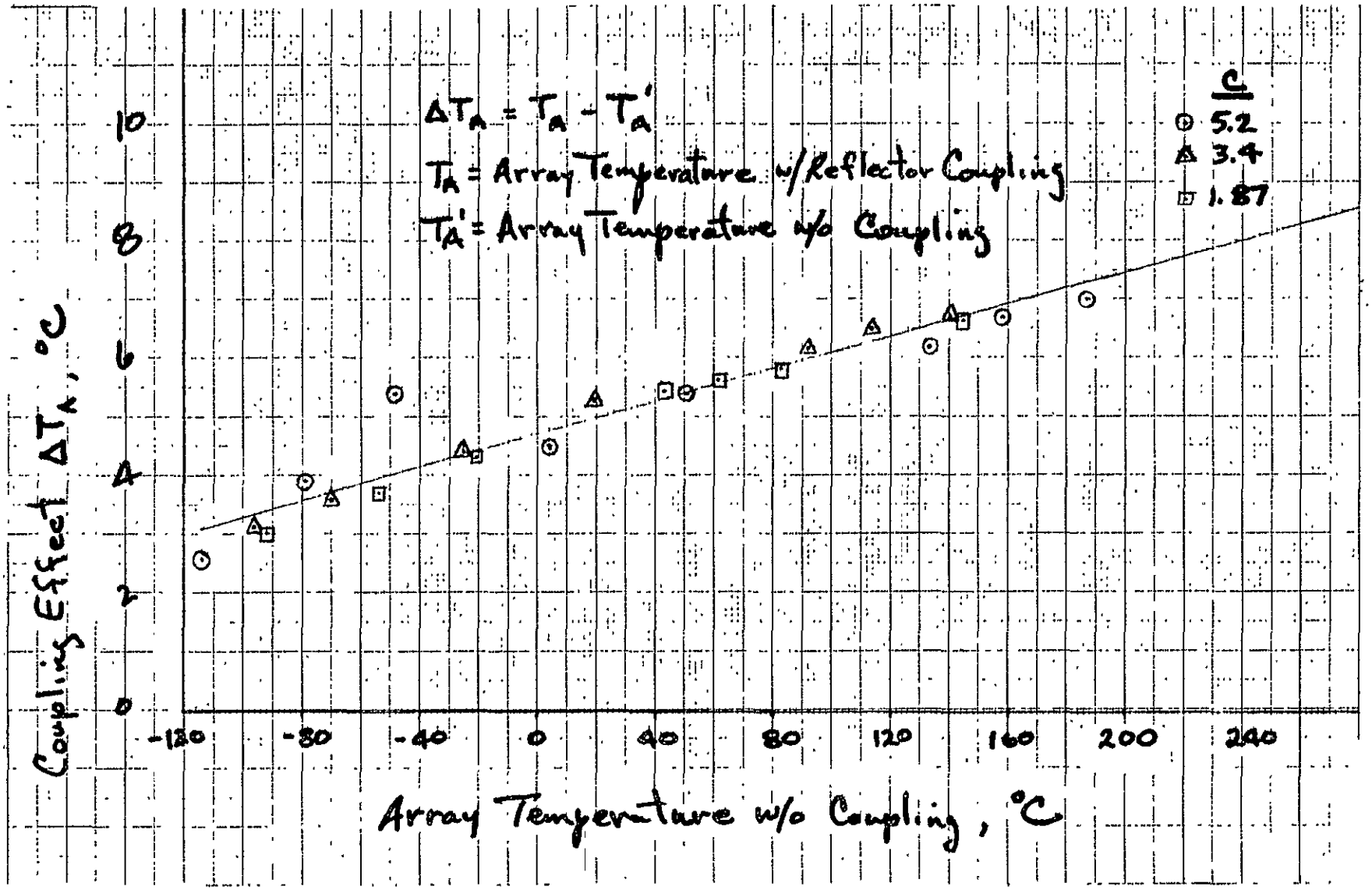

FIGURE 2.4.2-7. ARRAY/REFLECTOR RADIATION INTERCHANGE EFFECTS

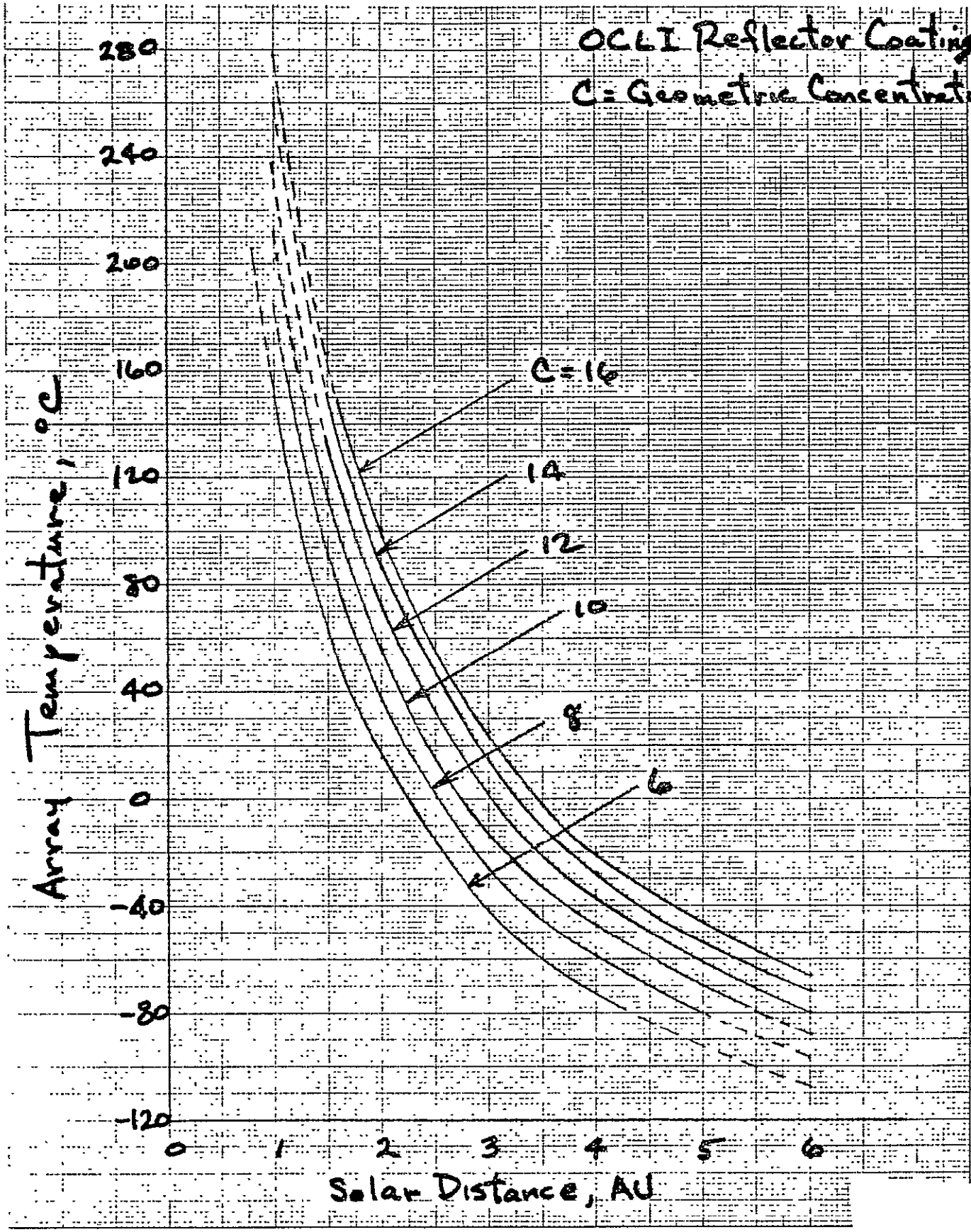

FIGURE 2.4.2-8. EXTRAPOLATED CONCENTRATED ARRAY TEMPERATURES AT HIGH CONCENTRATION RATIOS - MFPC

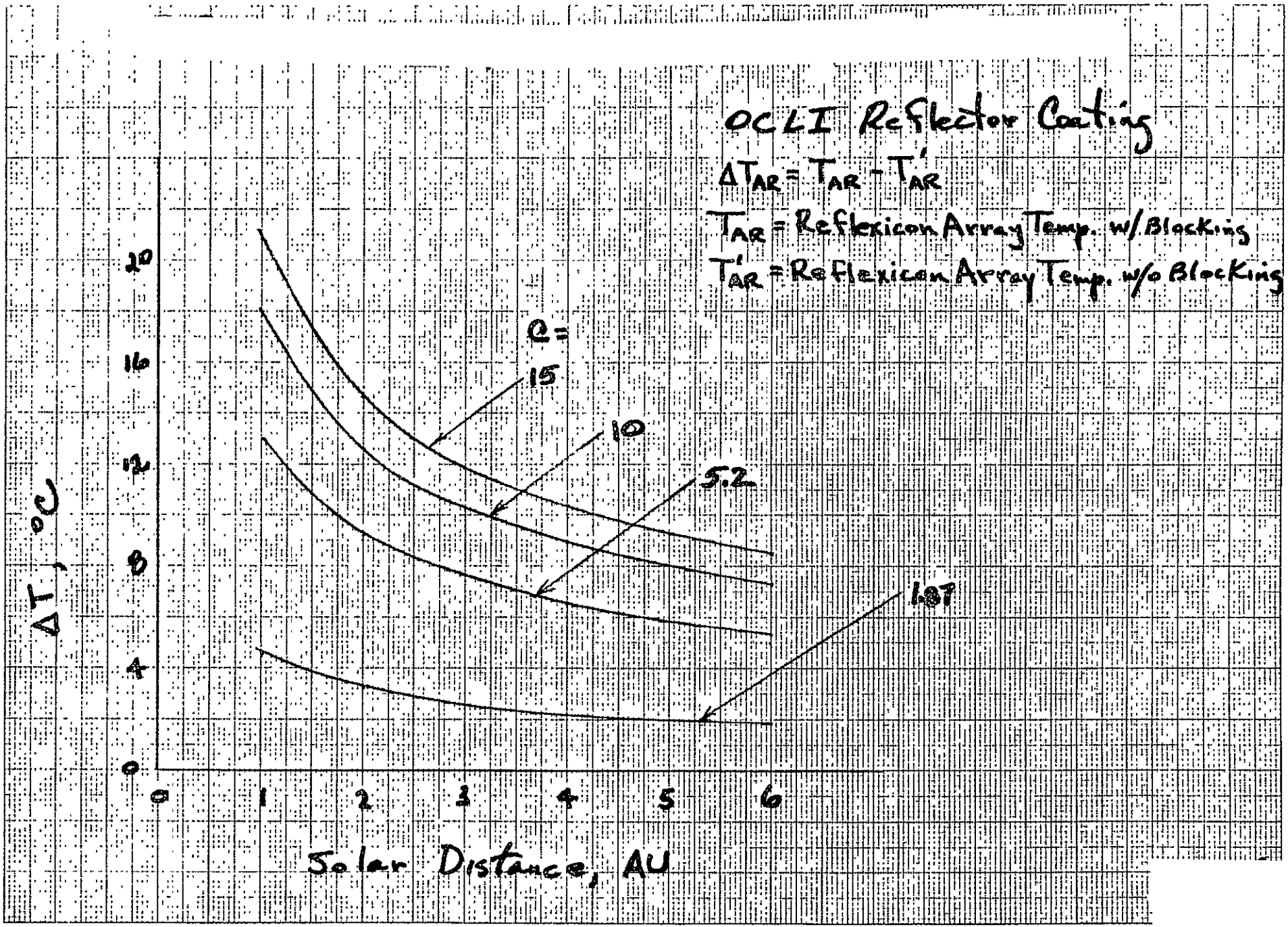

FIGURE 2.4.2-9. REFLEXICON ARRAY SELF BLOCKING EFFECTS

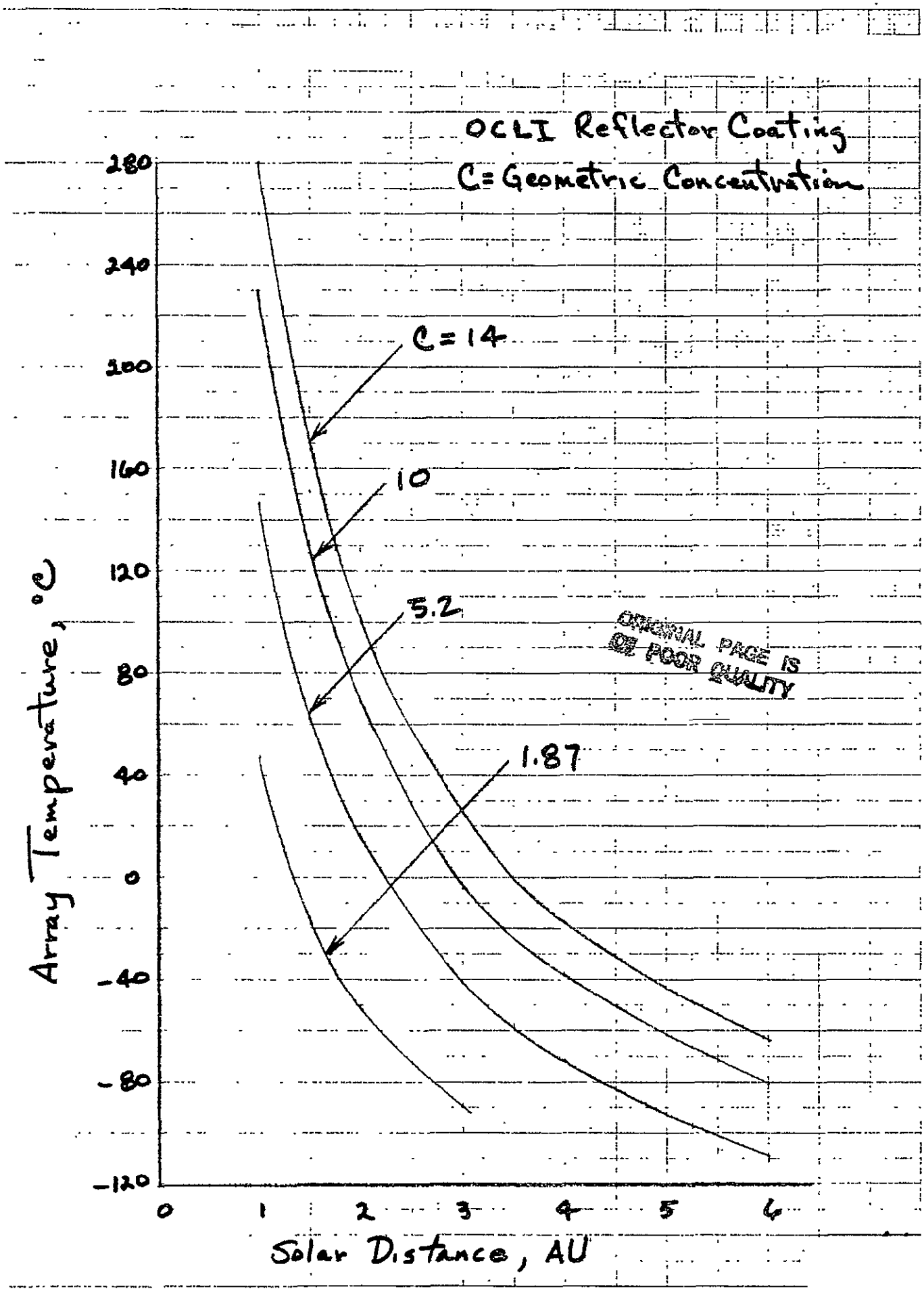

FIGURE 2.4.2-10. ESTIMATED REFLEXICON ARRAY TEMPERATURES

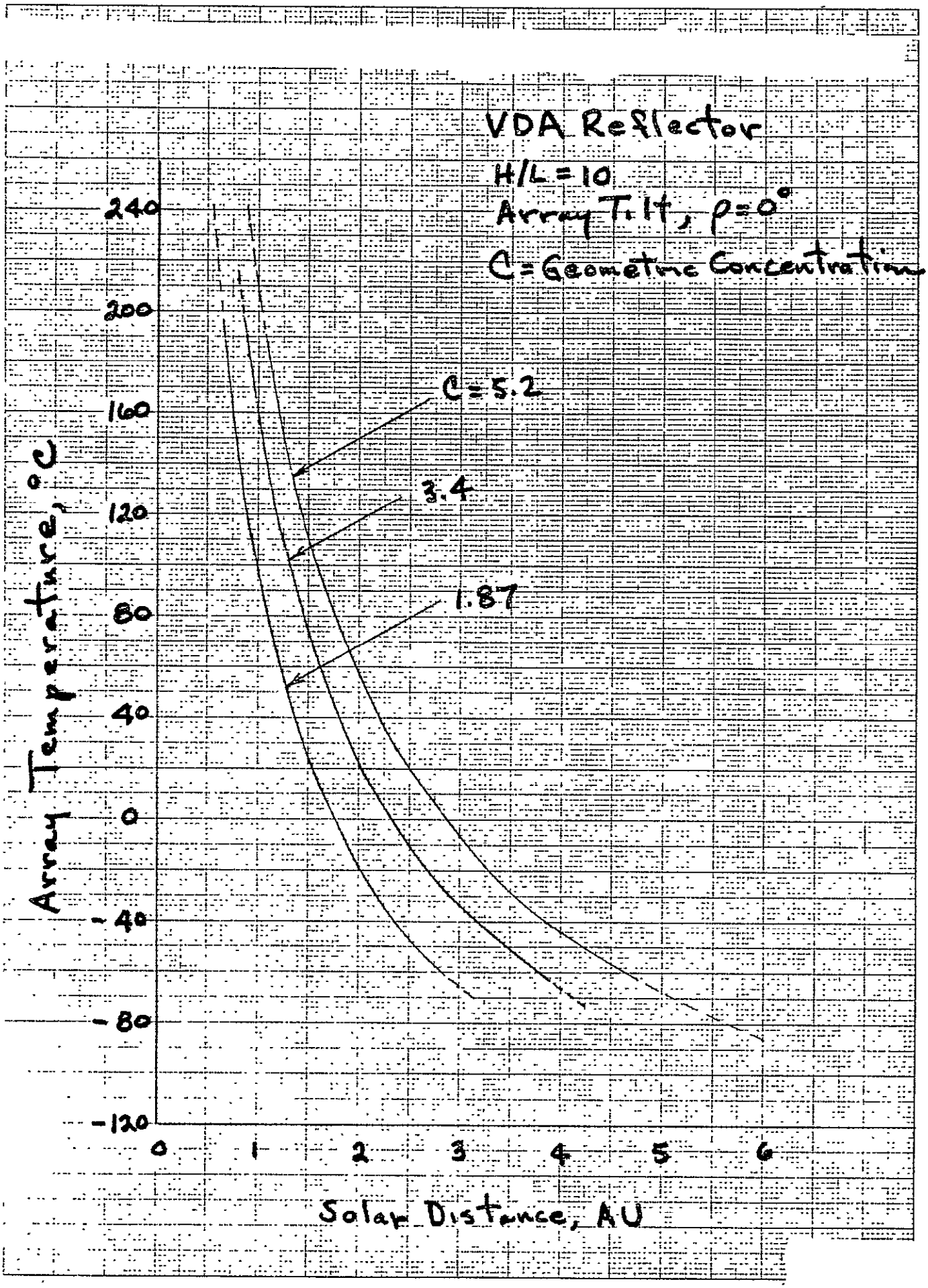

FIGURE 2.4.2-11. MFPC SOLAR ARRAY TEMPERATURES

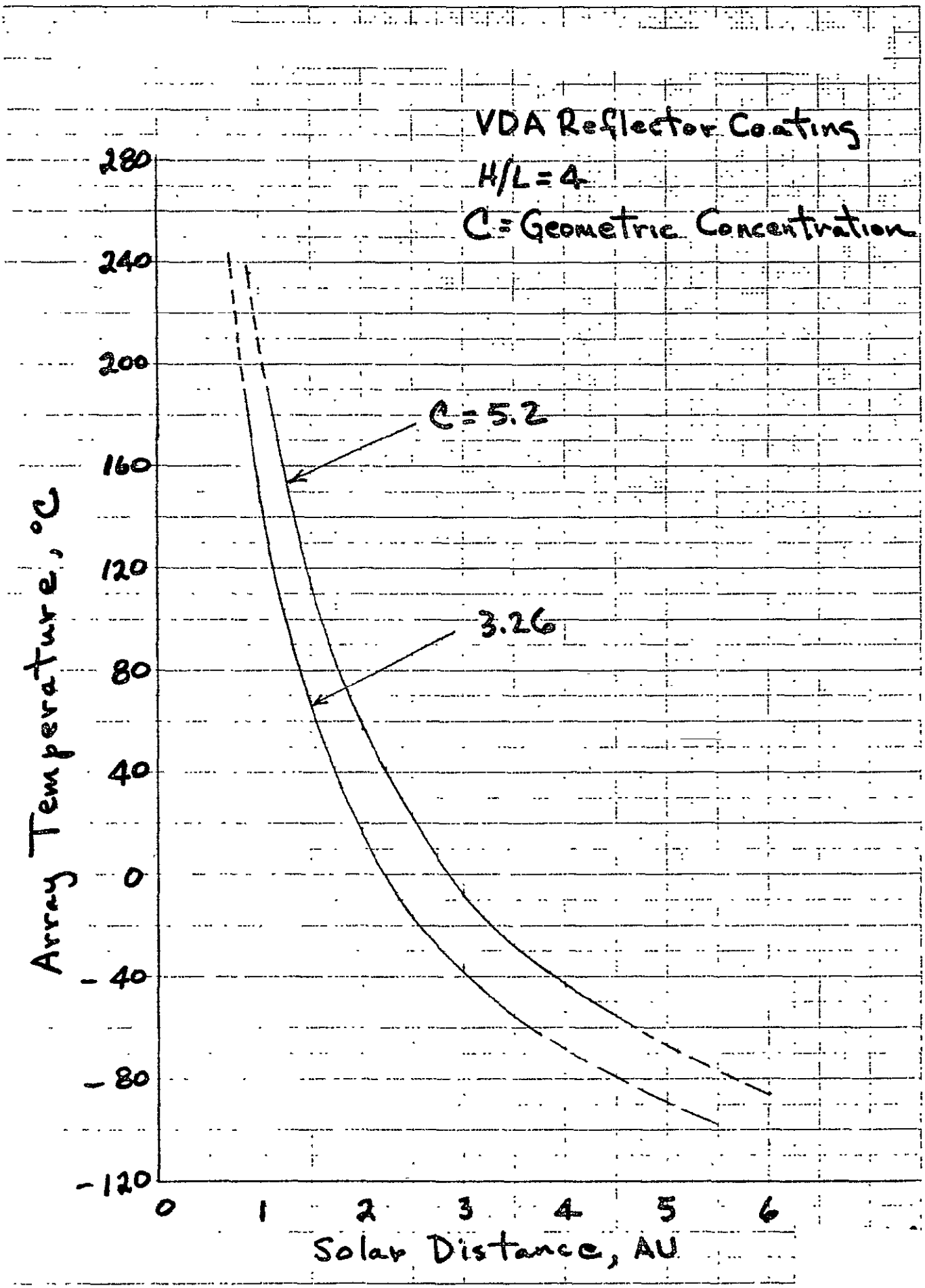

FIGURE 2.4.2-12. 3D MFPC SOLAR ARRAY TEMPERATURES

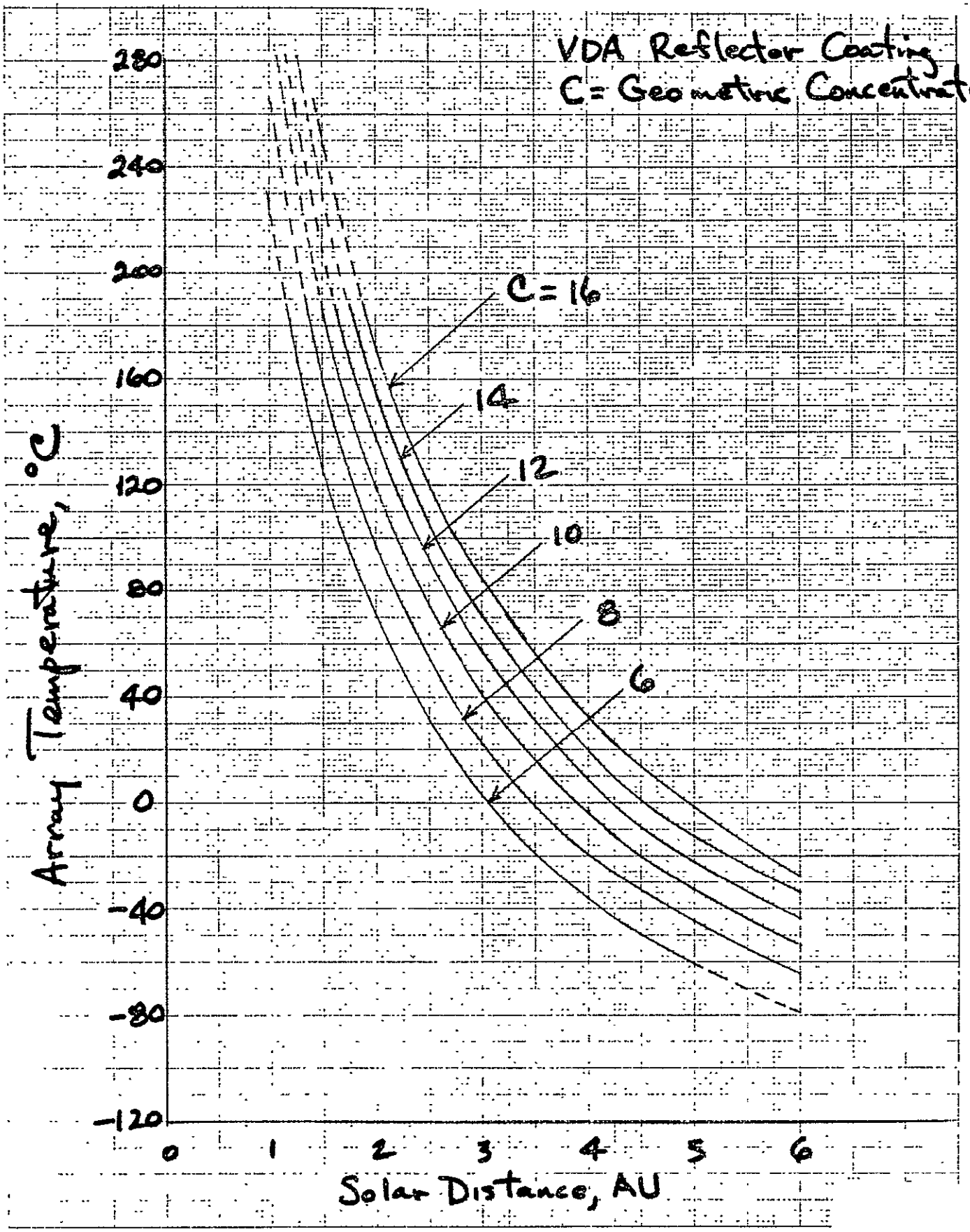

FIGURE 2.4.2-13. EXTRAPOLATED CONCENTRATED ARRAY TEMPERATURES AT HIGH CONCENTRATION RATIOS - MFPC

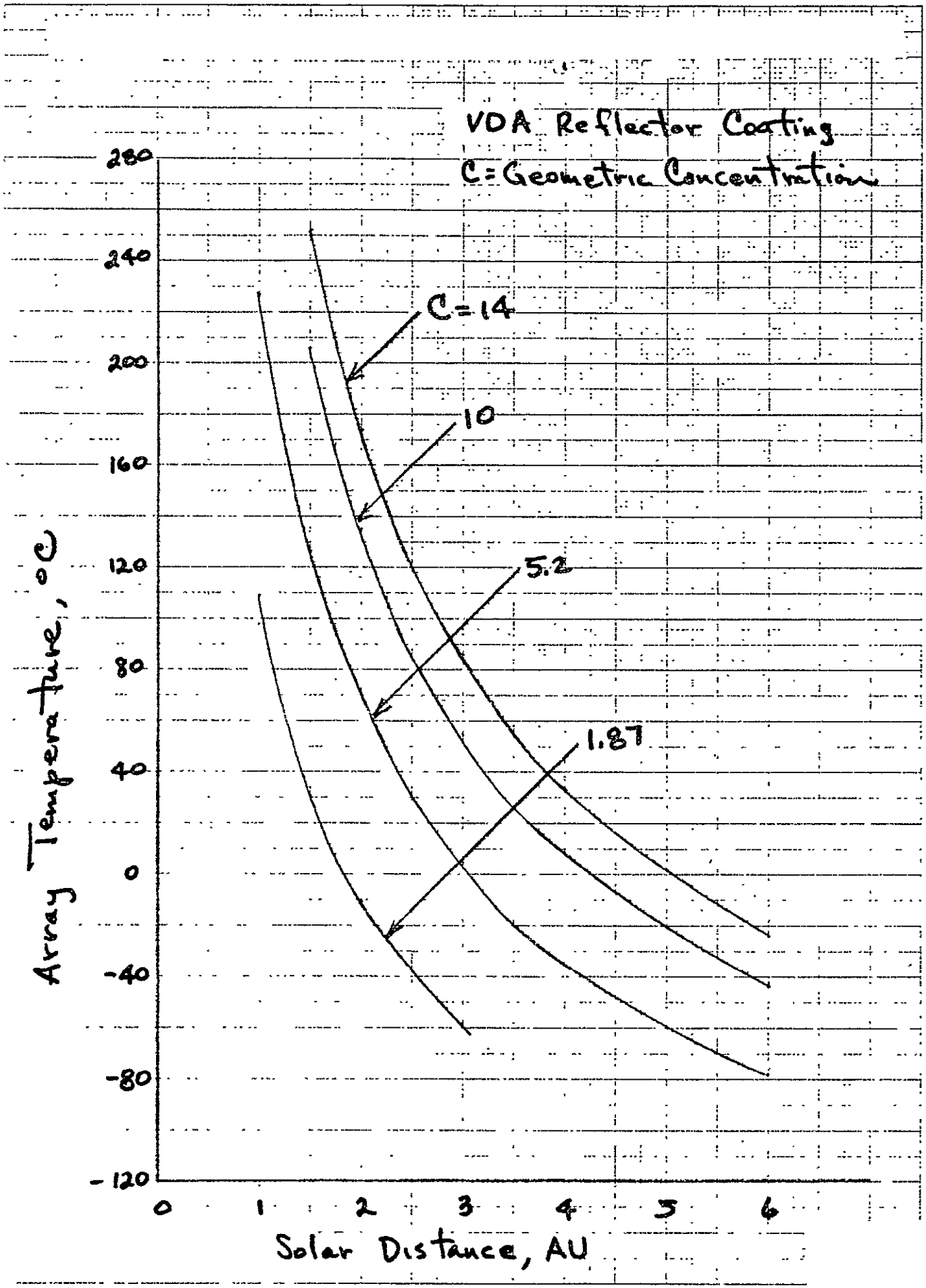

FIGURE 2.4.2-14. ESTIMATED REFLEXICON ARRAY TEMPERATURES

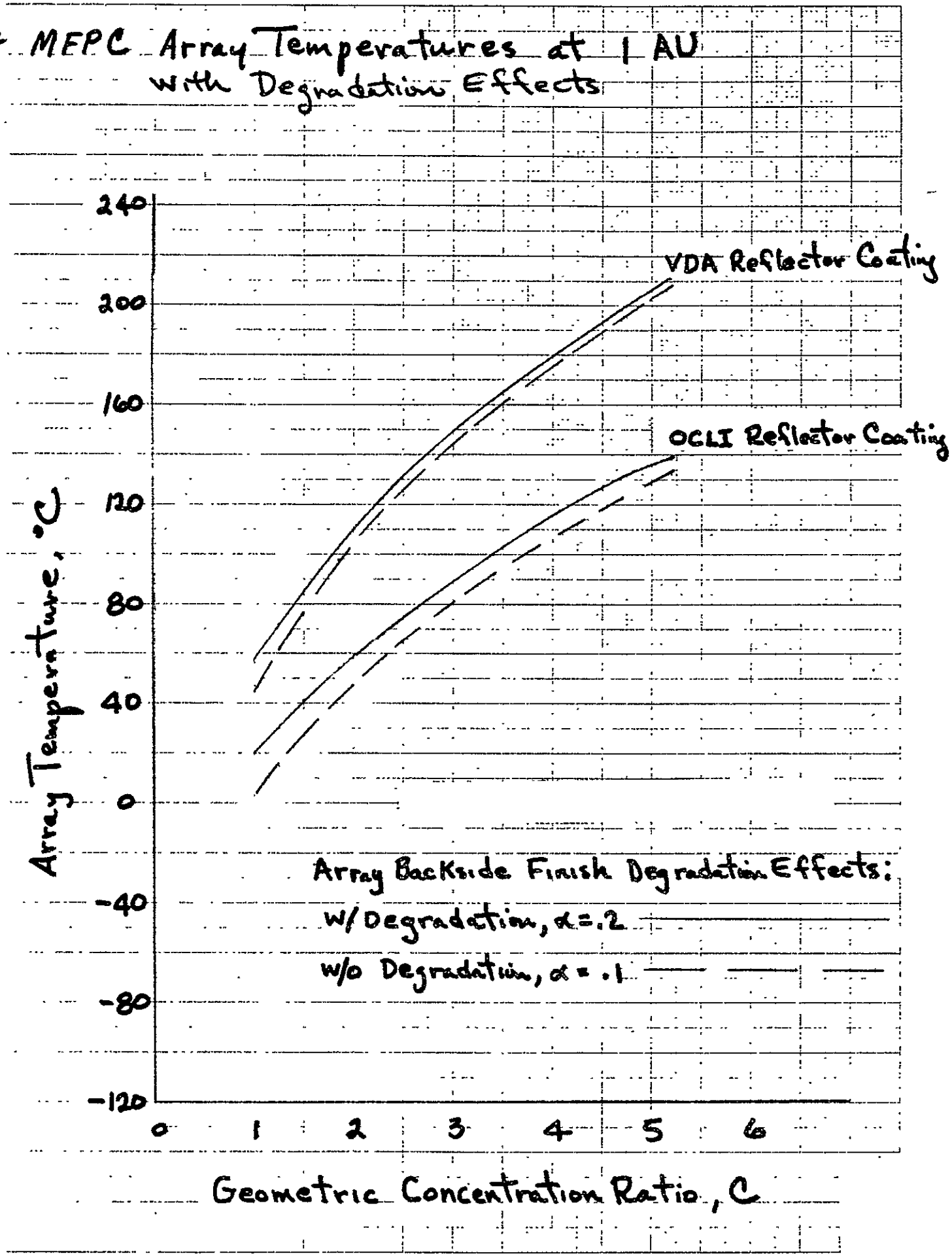

FIGURE 2.4.2-15. MFPC ARRAY TEMPERATURES AT 1 AU WITH DEGRADATION EFFECTS

2.4.3 Phase I - Concept Optimization and Evaluations Results

The basic calculation procedure followed in predicting the performance of each concept is described by Figures 2.4.3-1 and 2.4.3-1 (continued). These figures illustrate the step by step procedure by a specific example calculation. The procedure was merely repeated, parametrically varying AU and C_g for each concept and for each of the two reflector coatings considered. This procedure was not applied to the 2 front-lit configurations inasmuch as performance data on these designs was obtainable from References 2 and 6. The data obtained from these references was of course adjusted to eliminate differences in starting array size, solar cell and cover dimensions and solar cell efficiencies.

For purposes of comparison, the performance of an unconcentrated planar SEP array was also calculated. For calculating specific power, the weight of the SEP array was obtained from Reference 2 and adjusted to eliminate differences with the baseline array relative to cell type, array size, and efficiency.

Configuration Optimization

Performance results are presented in Figure 2.4.3-3 for one particular concept, the semi-active MFPC. Here, specific power is plotted versus the maximum C_g for solar distances of 4 AU and 6 AU, respectively. Every point on either curve represents a different but specific geometric configuration of the same concept; each configuration characterized by the maximum C_g it can deliver and possessing a different number and/or size of mirrors and a different total mass.

Each curve exhibits a maximum which defines the optimum configuration for operating at that solar distance. Since the curves are relatively

GIVEN

- 3D-MFPC CONCEPT CONFIGURED TO PERMIT C_G MAX = 5.2
- OCLI COATING
- BASELINE SOLAR ARRAY (25 KW AT 1 AU AND 55°C), CELL EFFICIENCY AT 55°C = 11.5%

FIND

SPECIFIC POWER AT 6 AU AND C_G = 5.2

$$\text{POWER OUTPUT} = \frac{25 \times C_e}{(AU)^2} \times \frac{\text{(CELL EFFICIENCY AT TEMP FOR 6 AU)}}{\text{(CELL EFFICIENCY AT 55°C)}} \text{ KW}$$

- FOR OCLI COATING $C_e = C_G \times 0.90 \times 0.64 = 0.576 \times C_G = 0.576 \times 5.2 = 2.99$
- FROM TEMP CURVE FOR THIS CONCEPT, WHEN C_G = 5.2 AND AU = 6, T = -115°C

FIGURE 2.4.3-1. EXAMPLE TO ILLUSTRATE PROCEDURE USED TO CALCULATE SPECIFIC POWER

- AT 1 AU WITH NO REFLECTOR, SOLAR IRRADIANCE = 135 $\frac{\text{MILLIWATTS}}{\text{CM}^2}$. AT 6 AU AND WITH AN EFFECTIVE CONCENTRATIO RATIO OF 2.99, IRRADIANCE BECOMES = 135 X 2.99 ÷ AU^2 = 11.2 $\frac{\text{MILLIWATTS}}{\text{CM}^2}$

- FROM CELL EFFICIENCY CURVE, WHEN T = -115°C, AND IRRADIANCE = 11.2, EFFICIENCY = 13.8%

THEREFORE, POWER OUTPUT = $\frac{25 \text{ X } 2.99}{36} \text{ X } \frac{13.8}{11.5}$ = 2.5 KW

- FROM WEIGHT VERSUS C_G CONFIGURATION CURVE, 3D-MFPC SYSTEM WEIGHT = 544 KG

SPECIFIC POWER AT 6 AU = $\frac{2.5 \text{ KW}}{544 \text{ KG}}$ = 0.0046 KW/KG

FIGURE 2.4.3-1. EXAMPLE TO ILLUSTRATE PROCEDURE USED TO CALCULATE SPECIFIC POWER (CONTINUED)

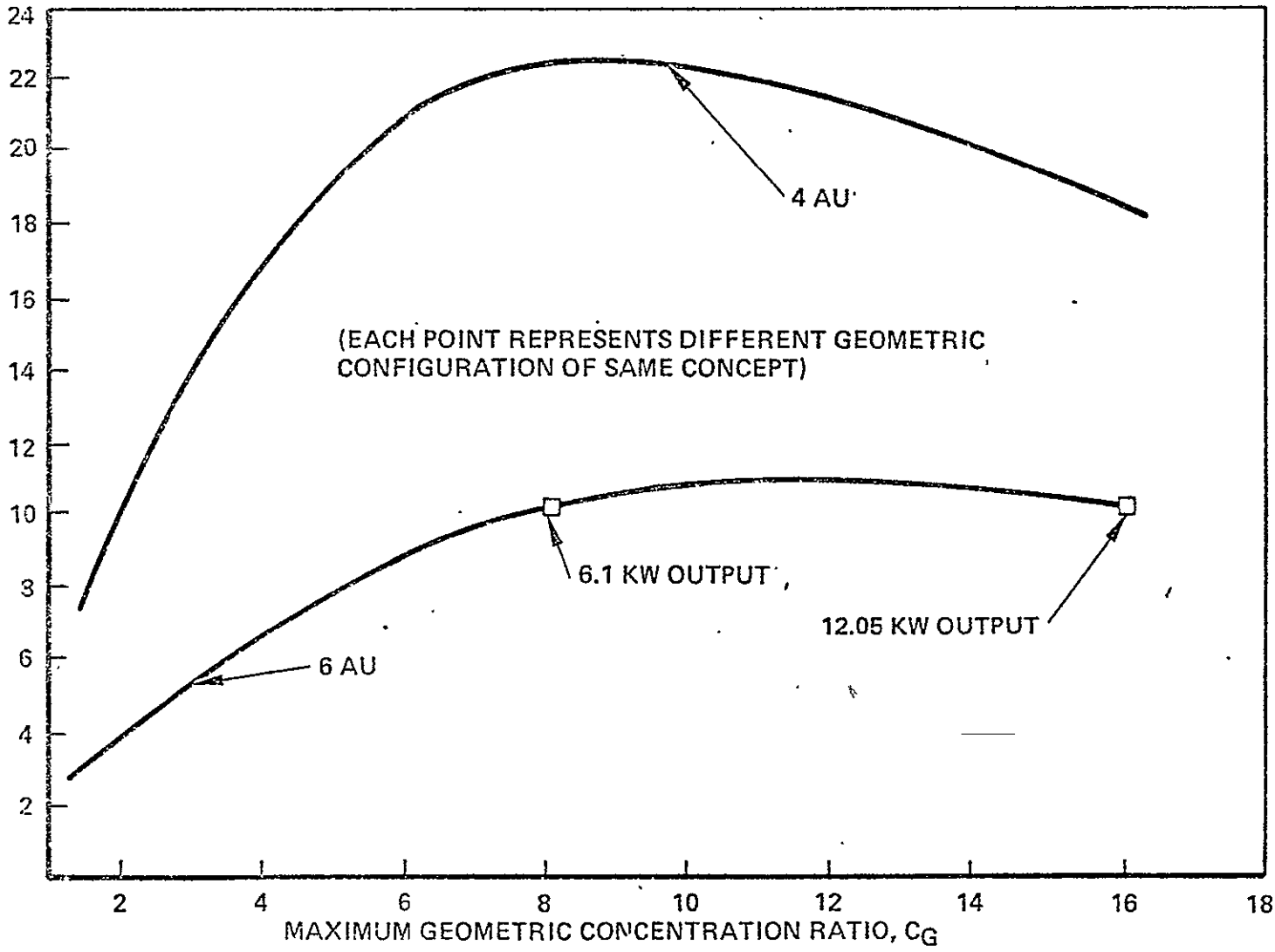

FIGURE 2.4.3-3. TYPICAL SPECIFIC POWER VS. C_G CURVES FOR ACTIVE MFPC CONCEPTUAL DESIGN

flat at the maximum, a range of choices are available, all of which maximize specific power. Within this range of choices, the most cost effective choice is clearly the configuration with the highest C_g since this one will use the fewest solar cells for any required power output. For example, in Figure 2.4.3-3 at 6 AU, the maximum occurs between C_g = 8 and 16. Therefore, for primary operation at 6 AU, the C_g = 16 configuration appears best, yet both deliver about 10 watts per Kg which is approximately the maximum value possible. On the other hand, C_g = 16 would be a very poor choice if operation were intended primarily at 4 AU. At this distance, the figure shows that the C_g = 10 configuration would deliver 25% more watts per Kg than would the C_g = 16. The shape of the curves in the figure are typical of all the concentrator concepts studied.

Concentrator Concept Evaluation Results

Relative to specific power and power output performance, concentrator concept ranking varied with solar distance. When optimized for primary operation at 1 AU, the 2D-Front lit flat plate trough (2D-FPT) with VDA coated mirrors proved best with a 25% improvement in specific power over an unconcentrated silicon cell array (114 versus 91 w/kg). The other concepts showed little improvement in specific power over an unconcentrated array with either mirror coating studied for silicon solar cells. The 2D-FPT was also the best performer in power output at 1 AU, generating 35.8 kw. These 1 AU results are shown in Figure 2.4.3-4.

Table 2.4.3-1 summarizes the results of the various concepts when optimized for operation at 6 AU but examined between 1 AU and 6 AU. At 6 AU, the reflexicon is the best candidate if specific power is the sole criterion for judgment. The semi-active MFPC, with nearly the same specific power,

appears more attractive than the reflexicon because of its reduced structural complexity and higher concentration ratio which reduces the number of cells needed.

Independent of power performance, each concept was additionally evaluated in terms of cost related parameters such as deployment simplicity, freedom from stability and control problems, intrinsic reliability, simplicity of concentration ratio variability, compatibility with existing solar array designs, earth testability, restrictions on attached spacecraft, etc. This was accomplished by polling a selected group of spacecraft designers and assigning a numerical rating to their admittedly subjective opinions.

The consensus was that the 2D-FPT concept could be implemented at the lowest cost and with the fewest technical difficulties. the CPC concept was ranked very close to the leader, and then the three MFPC concepts formed a group with admittedly greater complexity, but still well within the limits of existing technology. The reflexicon was judged to be the most expensive and complex if the six design concepts.

Conclusions for Phase I

Based on a combined evaluation of specific power and subjective design criteria, the 2D-FPC appears to be the best concentrator design for arrays using silicon solar cells at 1 AU. At distances greater than 1.5 AU, some version of the two dimensional MFPC appears best for enhancing the performance of silicon solar cell arrays. At 6 AU the semi-active MFPC used in conjunction with ultra-thin silicon cells shows dramatic improvements over planar arrays.

Table 2.4.3-1 CONCENTRATED ARRAY PERFORMANCE COMPARISONS

THIN CELL SILICON ARRAY 6 AU OPTIMIZED CONFIGURATIONS

13% CELL AMO 27°C

		Unconcentrated Sep Array with Thin cells	2D-FPT	CPC	3D-MFPC	Reflexicon	Passive MF-PC (20 mirrors)	Semi-Active MFPC-(44 mirrors
POWER OUTPUT	1AU	25KW	35.2KW	29.2KW	28.9KW	28.9KW	28.9KW	28.9KW
	1.5AU	14.2KW	21.3KW	29.2KW	34.3KW	34.3 KW	34.3KW	34.3KW
	2AU	7.9KW	13.9KW	21.7KW	27.6KW	33.4KW	29.6KW	34.9KW
	4AU	1.8KW	3.2KW	7.1KW	10.2KW	15.6KW	11.7KW	22.0KW
	6AU	0.7KW	1.3KW	2.7KW	4.34KW	7.6KW	5.2KW	12.1KW
Optimum Conc. Ratio at 6AU, C_g		--	1.81	4.66	6	10	7	16
Total Conc. Array Mass		273kg	307kg	329kg	717kg	664kg	816kg	1175kg
Power to Mass at 6AU		2.6 w/kg	4.1 w/kg	8.2 w/kg	6.0 w/kg	11.4 w/kg	6.3 w/kg	10.8 w/kg

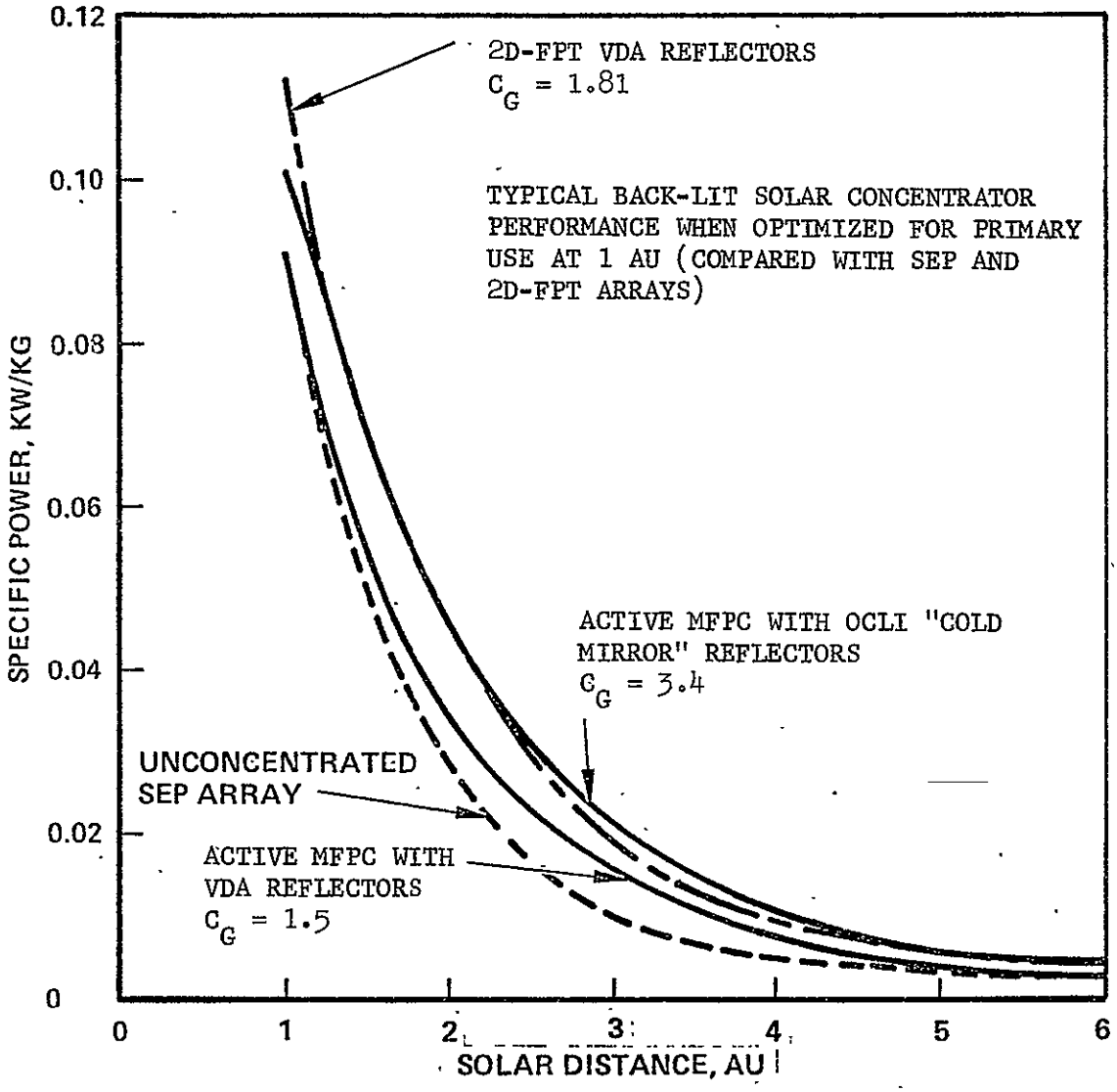

FIGURE 2.4.3-4. CONCENTRATOR PERFORMANCE AT 1 AU

At large solar distances, the Vapor Deposited Aluminum reflector coating (VDA) produced a much better power output performance from every concept than did the particular cold mirror coating that was also considered. This was found to be the case in spite of the fact that VDA, with its nonselective high solar reflectance, results in the highest predicted array temperatures. At large solar distances where irradiance levels and temperatures are low, cell efficiency tends to be less sensitive to temperature change. Thus, the reduction in temperature produced by substituting the cold mirror coating for the VDA yields only small benefit. However, since the cold mirror only reflects 64% of the solar spectrum that is useable by the cells (as opposed to 90% for the VDA) the power output is reduced significantly. The detrimental effect outweighs, by far, the beneficial effect producing a net loss.

At 1 AU, however, the situation is somewhat different. With VDA coated reflectors, the temperatures are so high that the maximum allowable concentration ratio (C_g) is limited to approximately 3 if the 150°C array temperature limit is not to be exceeded. However, with cold mirror coated reflectors, the reduction in temperature is so significant that concentration ratios up to $C_g = 6$ are achievable before the 150°C temp limit is exceeded. This factor of 2 increase in concentration (from $C_g = 3$ to $C_g = 6$) more than compensates for the lower total reflectance of the cold mirror as opposed to the VDA (.64 versus .90). Thus, a net improvement in power output can be realized from a cold mirror coating at 1 AU with any concept that can generate high concentration ratios; i.e., $C_g >> 3$. Specific power, on the other hand, may or may not be improved by the cold mirror at 1 AU. This depends on the rate with which the mass of the concept increases with increasing C_g. Of the concepts evaluated, the front-lit 2D-FPT performed the same with VDA as it did with the cold-mirror, because concentration ratios greater than $C_g = 2$ are not achievable without unreasonable mirror size. With the diffuse mirror CPC, the cold-mirror reduces the overall reflection efficiency to unacceptable levels. The remaining back-lit designs all show only minor improvement in specific power such that the 2D-FPT with VDA is still superior at 1 AU.

3.0 PHASE II - TECHNICAL SUMMARY

(Semi-active MFPC Design)

3.1 FINAL MFPC CONFIGURATION OPTIMIZATION

3.1.1 Phase II Optimization Objective

The semi-active MFPC configuration selected during Phase I and used as a starting point for Phase II was one that generated a geometric concentration ratio of 16 and that employed a dual V shaped array. The C_G=16 selection was based on Phase I performance studies which found this value to be optimum for maximizing the specific power at 6 AU. The V-shaped array was chosen to reduce angle of incidence effects by causing the reflected light from the mirrors to be received more nearly normal to the array plane. Because of the V-shaped array geometry, each mirror could only illuminate one half of the array, and the mirrors were sized accordingly. A further consideration, which effected the final design in Phase I, was the selection of a $\pm 1^{o}$ tolerance on the accuracy of the individual mirror tracking devices. This dictated the magnitude of the increased width incorporated in the mirror sizing.

One goal of the Phase II study was a re-examination of the semi-active MFPC configuration chosen to achieve the C_G=16 concentration ratio, the objective being to determine if a further reduction in size and/or mass is possible. Specifically, the questions posed were:

a) Is the V-shaped dual array configuration chosen to minimize angle of incidence effects in fact the best choice when traded against other effects it may induce?

b) Has the optimum ratio of array width to mirror distance been determined?

c) Is the tolerance selected on sun tracker accuracy reasonable and achievable?

d) Can a significant refinement of the sizing of the major structural members be achieved within the scope of Phase II?

3.1.2 Optical Design - Equations

The equations for the design of an individual reflector panel are shown in Figures 3.1.2a and 3.1.2b. The method of analysis is to assume an array angle and an array-to-reflector distance. The equations then completely define the reflector geometry, the only variable being the number of panels selected. Using these equations, a computer program was written to design

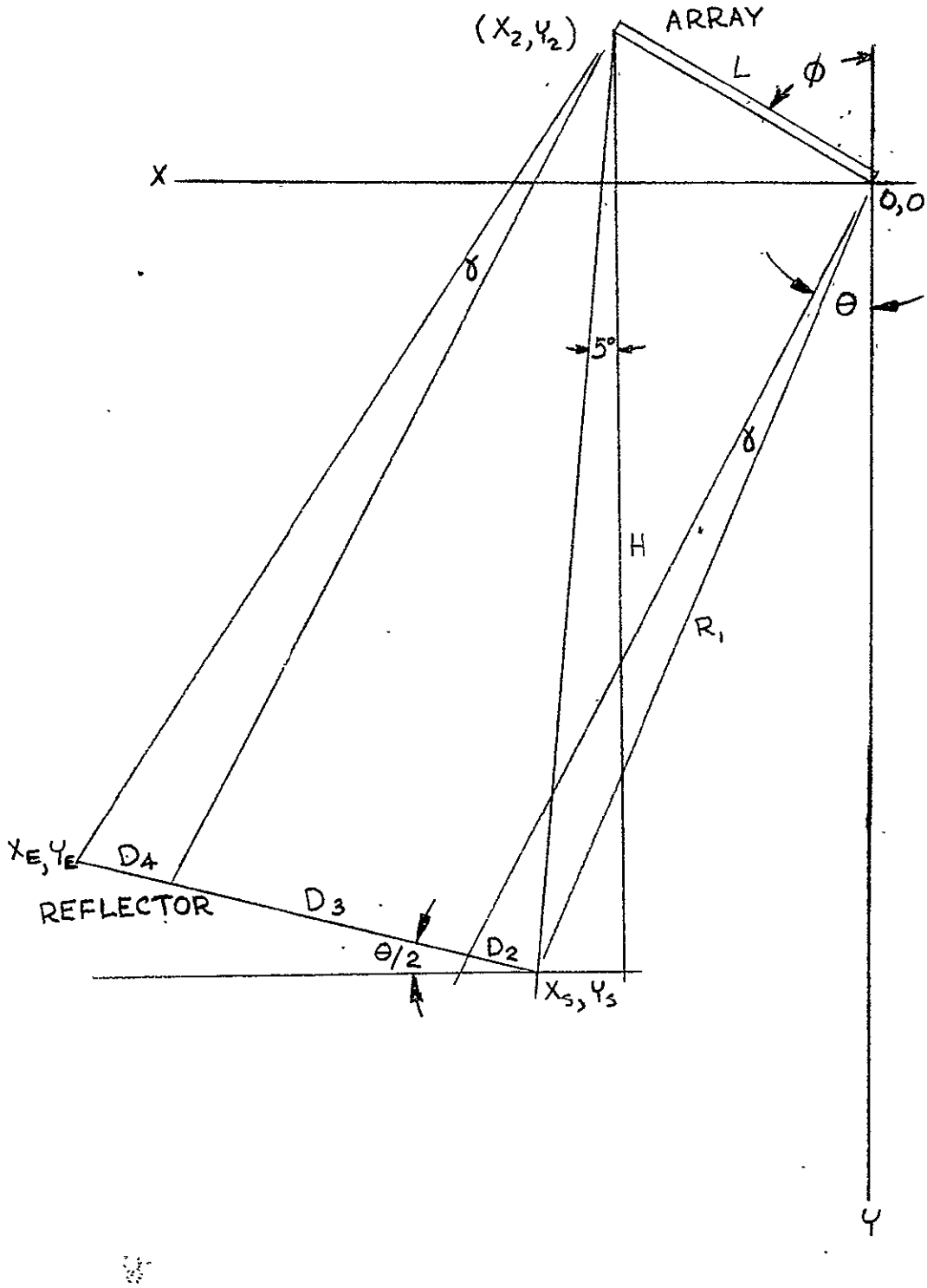

FIGURE 3.1.2a

GEOMETRY FOR OPTICAL DESIGN OF REFLECTOR PANEL

GIVEN: H, ϕ, γ, L (= 1 FOR NORMALIZED PARAMETERS)

① INITIAL VALUES: $X_2 = \sin\phi$, $Y_2 = -\cos\phi$, $X_S = X_2 + H \tan 5°$, $Y_S = H$

② $\theta = 5° + \arctan \frac{X_S}{Y_S}$, $R_1 = \sqrt{X_S^2 + Y_S^2}$

③ $D_2 = \frac{R_1 \sin\gamma}{\cos(\theta/2)}$ $\quad D_3 = \frac{L \sin(180 - \phi - \theta)}{\cos(\theta/2)}$

LIGHT GATHERED = $D_3 \cos(\theta/2)$

④ $X_T = X_S + (D_3 + D_2)\cos(\theta/2)$

$Y_T = Y_S - (D_3 + D_2)\sin(\theta/2)$

⑤ $D_4 = \frac{\sqrt{(X_2 - X_T)^2 + (Y_2 - Y_T)^2}\ \tan\gamma}{\cos(\theta/2)}$

⑥ $D_T = D_2 + D_3 + D_4$ (PANEL WIDTH)

⑦ $X_E = X_S + D_T \cos(\theta/2)$

$Y_E = Y_S - D_T \sin(\theta/2)$

⑧ NEW $X_S = X_E$, $Y_S = Y_E$

⑨ RETURN TO STEP 2

FIGURE 3.1.2b

EQUATIONS FOR OPTICAL DESIGN

reflectors, and using a search method, to select an optimum geometry for a desired concentration ratio.

3.1.3 Mirror Pointing Accuracy

Optical performance of the semi-active MFPC is strongly dependent on the pointing accuracy achieved by the solar tracker. Several mechanisms are discussed in 3.2.2; the common trait is the production of a sunspot, with a feedback system which maintains the spot in a fixed location. One limit on the accuracy achievable is the degree of collimation in the incoming light; at one A U this is $\pm$ 1/2; at 6 A U this limit is $\pm$ 1/12 degree. Another limit is the amount of linear translation produced by an axis shift. A conclusion from the study is that a motion of 1/8 inch should be sufficient to actuate a properly designed feedback mechanism. With a 10 inch separation from the concentrator, this gives an accuracy of $\pm$ .7 degree. Therefore, the selection of an accuracy of $\pm$ 1 degree as the requirement for our solar tracker is confirmed.

3.1.4 Single vs. Dual Arrays

In the Phase I Study, as previously mentioned, configurations in which the array was in two (V-shaped) symmetric sections, at an arbitrary angle to the solar axis were investigated. During Phase II thermal analysis, however, it was determined that a planar array configuration with the array perpendicular to the sun gave equivalent optical performance, with reduced solar cell temperatures. The need to reduce angle of incidence losses with a V-shaped array was therefore re-examined. It was found that these losses are in fact negligible. (See Section 3.1.6) It was, thus, concluded that the superior configuration is the planar array with each mirror illuminating the entire array rather than 1/2 as with the V-shaped array. Obviously, there is some weight savings due to the reduced number of parts; there is also reduced complexity, a cooler array, and a slightly smaller reflector. With a change in array shape, the optimum configuration had to be redetermined using the computerized method of Section 3.1.2.

3.1.5 Specific Geometry Selection

Table 3.1.5(a) shows the dependence of area ratio R on array/reflector spacing H/L, for a required maximum concentration of 16 using a flat array. The optimum R occurs for H/L from 10 to 14. However, to minimize the weight of the end struts, 10 was selected. Note that "R", at 28.7, is about 10% less than the value of 32 developed during Phase I. This alone reduces weight by perhaps

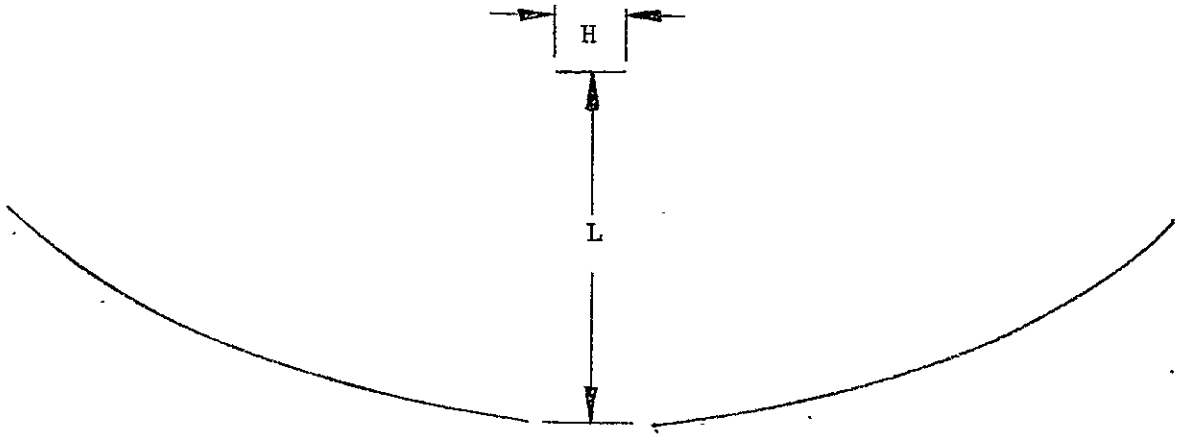

H/L	AREA RATIO	CONCENTRATION
8 or less	---	16 is not achievable
9	31.0	16.37
10	28.7	16.15
12	28.94	16.4
14	28.39	16.05
16	30.14	16.49
18	31.8	16.83

TABLE 3.1.5a

AREAS RATIOS FOR VARIOUS ARRAY/REFLECTOR SPACINGS

5%. Also, the planar array system uses a smaller number of reflector panels, each a larger size; this reduces the number of solar trackers and bearing assemblies required, saving even more weight. The planar array choice will also reduce development cost inasmuch as planar array designs have already been implemented by Hughes as well as by others in the industry.

3.1.6 Angle of Incidence Effects

One problem with the planar array system, especially for smaller values of H/L, is that much of the reflected light impinges on the array at a very shallow angle. This is not desireable, as it causes some of the received light to be reflected from the solar cell. This loss was, therefore, evaluated, using the angle of incidence solar cell data presented in the Phase I report (see Figure 3.1.6(a)). Calculating the light loss for each reflector panel and summing, it was found that the effect was negligible in the light of the benefits to be derived from the planar array. For example, for the concentrator with H/L = 10, the light loss is 2.6%; for H/L = 12, the loss is 1.9%.

3.1.7 Final Size Selection

All calculations and data discussed above has been based on normalized (i.e., dimensionless) parameters. To actually size a concentrator/array system, we must know a) the array area required, and b) the overall aspect ratio desired. The Phase I study used an array area of 1044 square feet for each wing, and generated 12 kW at 6 A U. This reduces to an array area of 86.6 square feet for the 1 kW Phase II study. The aspect ratio can be studied parametrically in the future, but the Phase II scope did not permit such a study and a value had to be selected. The primary structural elements affected by the aspect ratio are the shaping beam, which reduces in weight as the concentrator becomes long and thin, and the central mast, which becomes heavier. As a first estimate of the optimum, we decided to make these masses approximately equal. Based on the phase I study, we felt this would occur at an aspect ratio near 1.5:1. From the weight statement, in 3.4, it can be seen that the shaping beam; at 8.8 pounds, is heavier than the mast and connister, at 7 pounds. From the above reasoning, there may be a slight benefit to be derived from lengthening the concentrator somewhat further. A design which satisfies the above constraints results in L (width of the solar array) equal to 16 inches, a length of 65 feet, and a reflector aperture of 38.8 feet for one wing. These are the final dimensions that were utilized in the weight analysis. The cross-section is shown in Figure 3.1.7a. The array utilized in this system, if unconcentrated and sun facing, would generate 2.08 kw at 1 AU and 0.06 kw at 6 AU. (See figure 3.6.1-1)

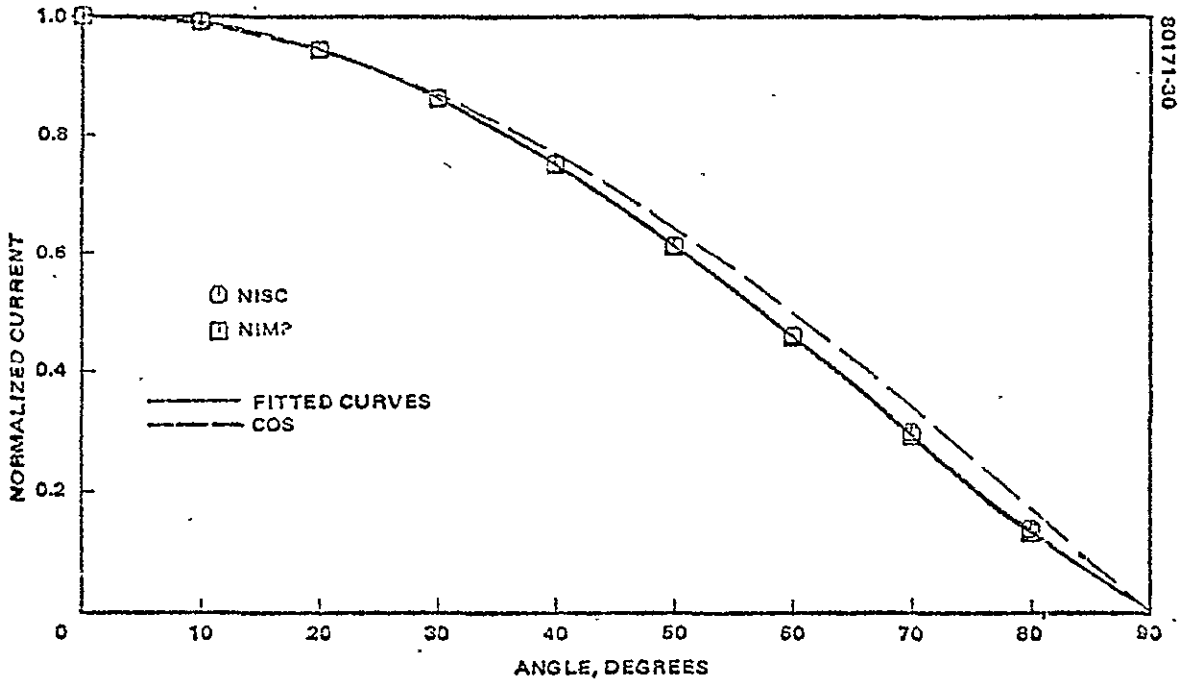

FIGURE 3.1.6a

SOLAR CELL ANGLE-OF-INCIDENCE DATA

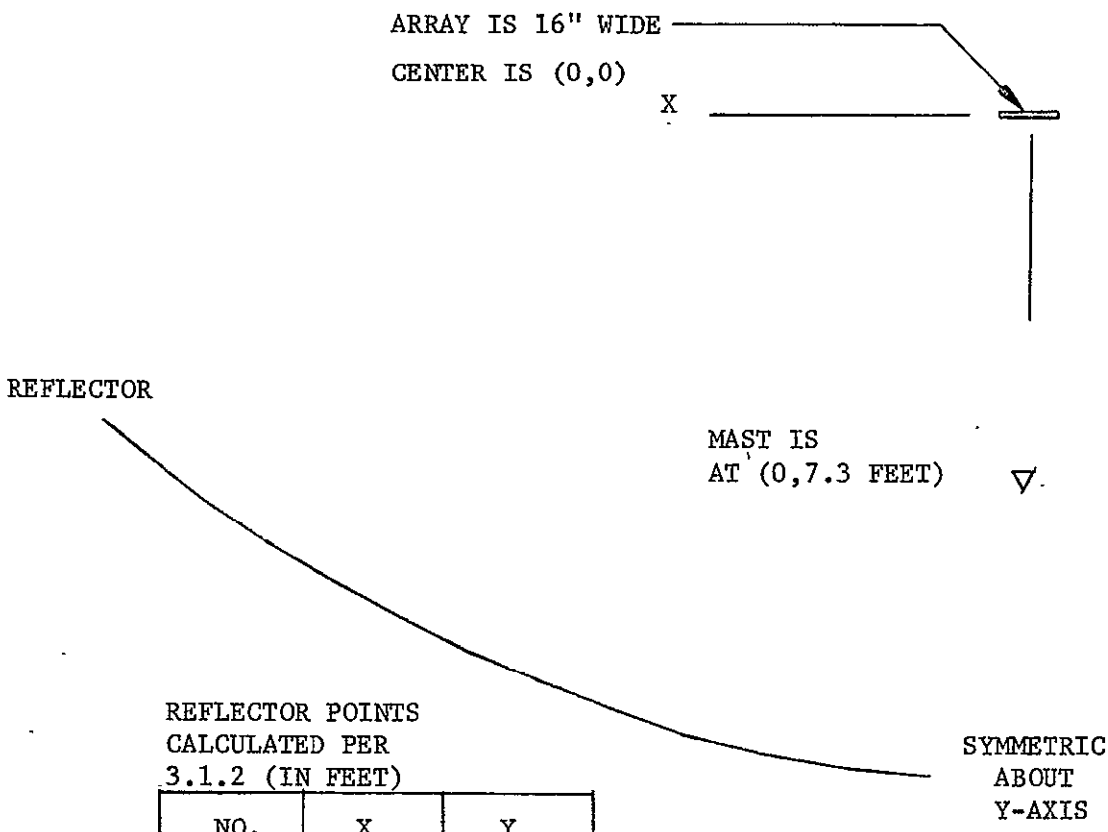

REFLECTOR POINTS
CALCULATED PER
3.1.2 (IN FEET)

NO.	X	Y
1	1.8	13.3
2	3.6	13.2
3	5.4	12.9
4	7.1	12.5
5	8.7	12.0
6	10.3	11.4
7	11.7	10.8
8	13.2	10.2
9	14.6	9.5
10	15.8	8.7
11	17.1	8.0
12	18.2	7.2
13	19.4	6.4

FIGURE 3.1.7a

CROSS SECTION OF CHOSEN REFLECTOR/ARRAY SYSTEM

3.2 Discussion of Drawings

3.2.1 Introduction

Drawings have been prepared to show the system, including the method of attachment to the spacecraft. These drawings which are shown in Appendix B, are intended to show size, configuration, and some proposed details. As will be discussed in the following sections, there are some problems which have not been resolved, and others with several possible solutions. In creating the drawings, mechanisms which Hughes believes to be appropriate at this time were selected; however, the text in many cases discusses possible alternatives. The intent was to show that the problems are solvable, and to permit a reasonable weight estimate to be prepared.

3.2.2 Solar Tracker Mechanisms

The key to the use of the semi-active MFPC is the use of a tracking mechanism which can aim individual mirrors, and which does not require intelligent control from the spacecraft or complex sensing devices. Similar requirements arise in terrestrial applications of solar energy, and several mechanisms have been discussed in the literature. One apparatus uses a reflector which concentrates solar heat onto a bellows filled with fluid. The fluid boils, creating a pressure which is dependent on the temperature, and therefore on the amount of the bellows which is illuminated. Another uses a pair of solar cells, one of which is illuminated when the sun if off-axis clockwise, the other when it is counterclockwise; the output being fed to a D. C. motor. Still another technique focuses light onto a bi-metallic spring (like a home thermostat). The common feature to these approaches is that the effect of an axis shift of the sun relative to the tracker is to cause a motion in some device; i.e., the expansion or contraction of the bellows,

rotation of the motor, or deflection of the bi-metallic spring. This motion is fed into an appropriate linkage which points the system at the new sun position. Note that due to the geometry involved in a system such as the 3-D MFPC, the rotation of the reflector panel must be half that of the sun (or solar tracker) to ensure that the light reflected does not shift.

3.2.3 Selection of the Solar Tracker

The bellows method discussed above is probably not suitable in this application. The large surface area of the bellows makes its temperature strongly dependent on temperatures of surrounding equipment, which will vary widely with solar distance. The solar cell/motor approach is a viable candidate, but at this point, Hughes believes it will require excessive mass. The bi-metallic spring approach is probably the lowest mass, and should be quite responsive. Also, it is very similar in concept to thermal control louver designs, which Hughes and others have flows successfully in mission-critical spacecraft applications. The Hughes mechanism uses a coiled bi-metallic element, with one-half shaded by a mirror. The shade is applied to light received from a parabolic reflector. The parts are aligned such that when the sun is on-axis the shading mirror reflects half the sunlight away, and the Kapton mirror is in the proper position to reflect light on the array. As the sun moves with respect to the concentrator, the bi-metallic spring is either brought into complete light or darkness, causing a temperature change, and generating a restoring torque. One end of the spring is fixed to a shaft, which rides in a bearing on the shaping beam; the other end is fixed to the beam. The concentrator and shading mirrors are also attached to the shaft. Thus the system is always maintained in the proper sun pointing position. A linkage could be used to achieve the 2:1 angle reduction required.

However, Hughes has selected a gear pair, as shown, because less stowage space is required.

3.2.4 Hinges

A large number of self-actuating, self-locking, moment-carrying hinges are required for the system chosen, with our specific configuration using 54. Two basic types are possible candidates. One is a design previously patented by HAC (one of the inventors is a member of this study team) using 2 C-section strips of a spring material, fastened together at the ends to form a slit tube about 2 diameters long. The C-section pieces can be buckled and twisted to collapse the hinge; when released, it straightens and locks. This is an elegant, light-weight mechanism, but suffers from the difficulty of incorporating adjustment of the locked position. Many of the hinges in the MFPC design are required to lock in an off-axis position, and it would be desirable to incorporate an adjustment capability. Therefore, Hughes has selected a traditional-type hinge for this study with 2 tubular elements, a pivot pin, and a positive latch bar. The locked position can be varied by moving the pivot mounting of the latch.

3.2.5 Constant-Tension Device

As the concentrator moves away from the sun, the Kapton temperature will vary substantially, causing a change in length. A means of compensating for this motion, which will be on the order of 3-4 inches, while still maintaining uniform tension, is required. Such a capability was incorporated into the chosen reflector end-bearing device. This bearing allows both axial and rotational motion of the Kapton at the attach end fitting of the shaft. A constant-tension spring attached to the outboard end of the shaft provides the necessary force. Note that this equipment is required on one

end of the mirror only.

3.2.6 End Truss Network

A network of struts and cables is required at each end of the reflector system. The 2 shaping beams are made of graphite-epoxy, in multiple segments, connected with the self-actuating hinges discussed above. Two transverse compression struts, each in two pieces with a hinge, and 10 in-plane cables as shown in the drawing, form a partial "bicycle wheel" system to transfer torsional loads into the central column. An axial compression strut serves as the attach point for the Kapton tension cables; one goes to each reflector pivot mechanism. This minimizes the bending load imposed on the shaping beam. Note that the inboard axial compression strut carries the torque from the central column mast to the spacecraft attach point.

3.2.7 Central Mast

The central mast is a standard coilable lattice column which deploys from a compact cannister. Such masts have been used in space and are extremely light weight efficient structures. The primary load that must be carried by this mast is axial compression which is defined by the tension in the Kapton mirrors and solar array. The tension load is calculated to total 14 pounds.

The basic equations for sizing the central mast were taken from "Parametric Data for Coilable Lattice Booms for Deploying and Supporting Solar Cell Arrays from Spacecraft," prepared for VPL by AEC - Able Engineering Co., Inc. Purchase Order No. JS-685133. The equations use constants based on fiberglass-epoxy properties. To reduce weight, the equations were modified to reflect high strength graphite-epoxy properties instead and to allow buckling of the individual rod elements simultaneous with overall column buckling.

Using a 2x safety factor, the required mast is only 4 inches in diameter. This is considerably smaller than would be required for a fiberglass-epoxy mast, thus a substantial weight savings is realized. Note that the mast on the drawing is not shown to scale, but is shown larger for clarity.

3.2.8 Stowage

As shown in the deployment sketch, the concentrator/solar array assembly is stowed as basically a rectangular box, with 6 struts projecting from each end. The "box" is about 48 inches wide by 24 inches high by 30 inches long, and the struts project a maximum of 48 inches on each side. A support pallet would be required; this has not been studied. The design of the spacecraft-side interface, and the relative positions of the two power modules with relation to the spacecraft when stowed in the shuttle bay, have also not been investigated.

3.2.9 Deployment

The overall sequencing of the deployment has been determined, but much work needs to be completed on the specific details, especially the proper stowage of the cables to ensure freedom from tangling.

The first step is to release the three struts on each end, and the shaping beams. These deploy and lock in place automatically when released. It may be necessary to provide specific sequencing of this actuation. The central column then deploys, pulling out the solar array and the Kapton reflector elements. Since the constant-tension mechanism is collapsed, the tension forces are very small at this time. As the mast reaches the full length, the reflector panels are completely extended, and the constant-tension spring is pulled out, applying the required loads to ensure reflector panel flatness.

3.3 STRUCTURAL CONSIDERATIONS

The primary structure in the semi-active MFPC aside from the deployable central mast is the shaping beam at each end of the Kapton reflector strips. The shaping beam controls the positions of the ends of the Kapton strips.

A structural analysis was performed to determine the shaping beam cross section. This enabled a determination of the structural weight contained in the beam and a design concept to be initiated for the shaping beam latch mechanism. The analysis used the following assumptions:

1) The beam will be a circular cross section tube
2) The material will be graphite epoxy with an elastic modulus of twenty million psi along the axis of the tube
3) The only loads that the tube must react are the components of the Kapton tension that act in the plane of the curved shaping beam due to the angles of the cable network at each end of the array
4) The criteria for the tube size is that the deflection of the end of the tube not exceed two feet and that the strength be adequate.

A finite element model of half of the shaping beam was created using the SPAR program. A computer plot of this model is included in Appendix A. A plot showing the undeformed and deformed shape is also included. A preliminary calculation of the beam stress and deformation as a uniformly loaded cantilever beam gave a preliminary cross section of 1.5 inches O.D. with a .028 inch wall thickness. The results of the analysis using this cross section are shown in Appendix A. The maximum deflection of the shaping beam was 13.1 inches, well within the desired two feet. The maximum moment was 473 in-lb which produced a stress level of just over 10,000 psi. This stress level is low compared to the allowable stress of approximately 60,000 psi for a 6Y70-E42 graphite epoxy composite. Therefore the analysis substantiated the design choice of a graphite epoxy tube 1.5 in. O.D. with .028 in. wall for the shaping beam.

The remaining structural effort was concentrated on an overview of the structural design to assess the feasibility. The design has a wire braced strut that ties the shaping beam and the solar cell array to the central mast. This strut constrains the torsional movement of the shaping beam system so that the torsional stiffness of the central mast now determines the torsional frequency of the system. This is an attempt to produce as high a torsional frequency as possible.

3.4 WEIGHT SUMMARY

The weights shown below are for one wing, generating 1/2 kilowatt at 6 A.U.

REFLECTOR	WEIGHT, LBS.
Kapton	5.5
Graphite/Epoxy End Beams	8.8
Shaping Beam Locking Hinges - .08 lb x 48 required	3.8
Central Mast	3.0
Cannister	4.0
Axial End Struts	
Inboard	1.5
Outboard	1.3
Transverse Compression Struts	
Mast - Array .90 lb. x 2 required	1.8
Mast - Reflector .75 lb. x 2 required	1.5
Solar Tracker Mechanism	
.5 lb. x 48 required	24.0
Reflector Pivots	
Outboard Side - .22 x 24 required	5.3
Inboard Side - .12 x 24 required	2.9
Kapton Support Rod and Attach Rod	4.0
Cables	3.0
Total Reflector and Structure Weight	70.4
SOLAR ARRAY	
Blanket & Cushion	11.4
Shaft & Bearings	1.8
Slip Ring Assembly	2.9
Drum	2.9
Tension Spring & Brake	1.4
Total Array	20.4
Total Weight	90.8 lb
+ 8% Deployment & Pallet	7.2
	98.0
2 Wings Required - Total	196.0 lb. (89.0 kg)

3.5 Modularity

There are two possible ways to add concentrated solar power assemblies. One method is to simply add additional modules axially; this has the minimum effect on the spacecraft, but requires stronger, stiffer central mast and end struts, for a weight penalty, and makes deployment somewhat more complex. Also, there will be some power loss and increased weight due to the longer power cables required. Only even numbers of power assemblies can be used, due to the requirement to maintain the center of gravity at the spacecraft; for example, if 2.4 kW is required, this can be achieved with 5 modules, but a sixth (or ballast weights) must be carried for balance. The alternative is to add assemblies as spokes from the spacecraft; this is lighter weight, and has no penalties from the power module viewpoint, but it complicates the spacecraft side interface. If many modules are used, the spacecraft field of view is blocked in some directions (this could be a serious problem for some scientific missions) and a large radius is required from the spacecraft center to the mounting interface (see 3.5a).

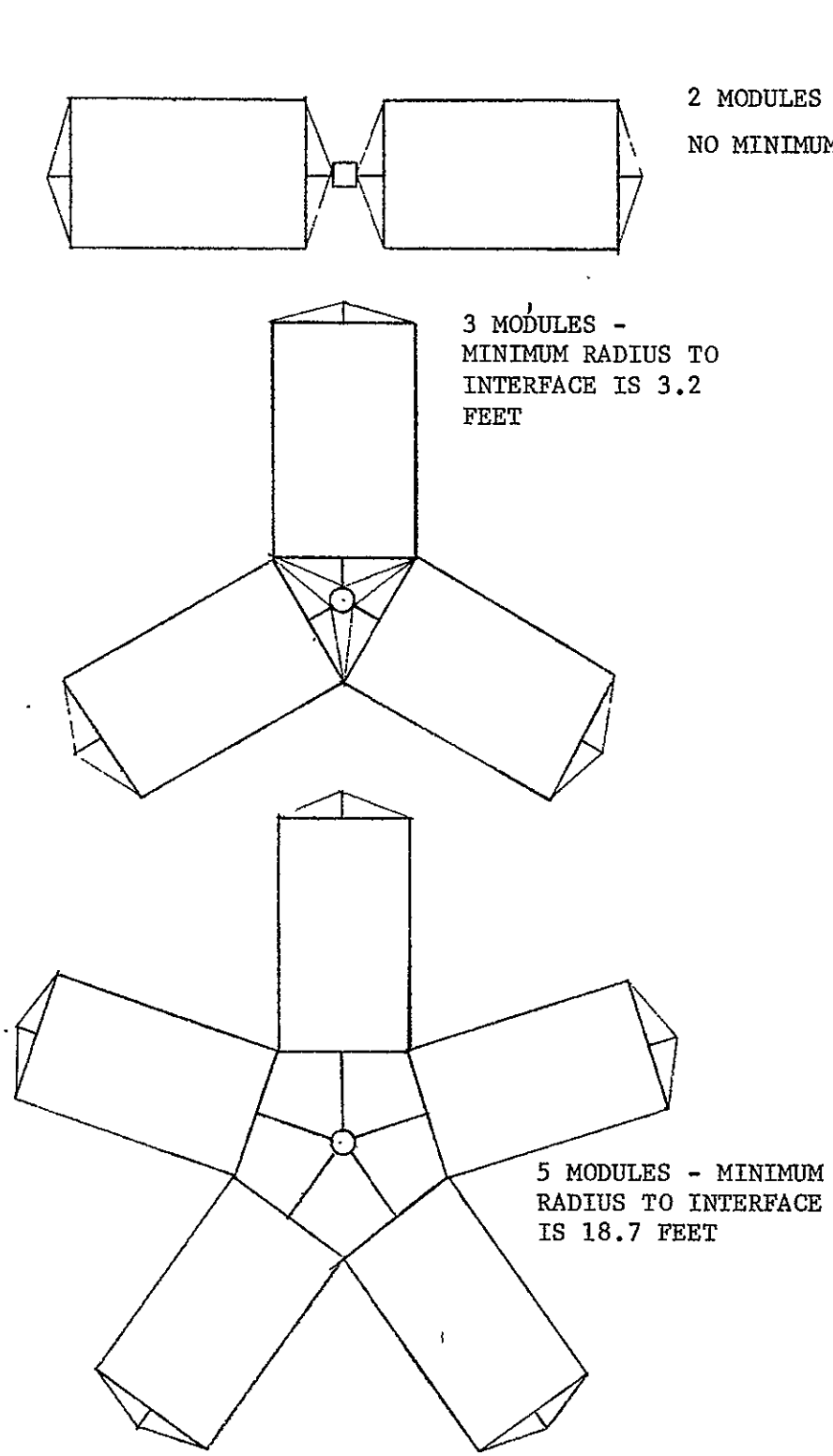

FIGURE 3.5a

MOUNTING OF MULTIPLE MODULES CIRCUMFERENTIALLY

3.6 PERFORMANCE SUMMERY

The following is a summary of the performance characteristics of the Phase II semi-active MFPC power module as described in the drawings of Appendix B and discussed in Section 3.2.

3.6.1 Output Performance

General Description: A back-lit, trough type, semi-active Multiple Flat Plate Concentrator system divided into two equal wings.

Solar Array Description: Each wing contains a flexible rolled-up solar cell blanket which deploys as a planar array.

Array area = 86.7 sq. ft. per wing (16 inches X 65 Ft)

Cells: 50 micrometers thick with a 50 micrometers glass cover, 13% efficient.

Starting Power: Unconcentrated array, if sun facing, can deliver 1 kw per wing at 1 AU, AMO, BOL, and 55°C. *

Concentrator: Back lit configuration (Array backside faces the sun)

Area Ratio: 28.7

Mirrors: 24 per wing provide uniform illumination (12 each side)

Length per mirror = 67 ft.

Width per mirror = variable,

(19 inch average)

17.3 minimum

21.6 maximum

Material: 8 micrometers thick Kapton, first surface VDA coated.

Geometric Concentration Ratio, C_G: stepwise variable from 16.15 maximum to 0.75 minimum in approximately 0.1 increments

Reflection Losses: VDA reflectivity loss 10%

Geometric Distortion loss 10%

Angle of incidence loss 2.6%

* See table 3.6.1-1

Reflection Efficiency: 78.9%

Effective Concentration Ratio: 12.7 Maximum

System Weight: 44.5 kg per wing, 89 kg total

Output: See table 3.6.-1 and Figure 3.6.1-1

Table 3.6.1-1

Array Performance - Total for Both Wings

AU	Concentrated Array Power Output (KW)	Specific Power (Watts/KG)	C_g Employed	Array Temp. ^oC	Array Power If Unconcentrated
1	2.62	29.3	3	145°	2.08
1.5	2.72	30.7	6	126°	1.14
2	2.83	31.7	12	137°	0.65
4	1.79	20.0	16.1	32°	0.15
6	.98	11.0		-28°	0.06

3.6.2 Dynamic Performance of Phase II Concentrator Design

A lumped mass analysis of torsional frequency, assuming loads are rigidly tied to the central mast by the end trusses, gives a natural frequency of .012 Hz. Calculations are shown in Appendix C. This is only slightly less than the .015 Hz quoted by GE (reference 6) but considerable lower than the 0.4 Hz stated by Lockheed (reference2) as an objective. However, both the above numbers were caluulated for a bending mode; neither referenced study analyzed for torsional frequency, which HAC believes is really the lowest frequency mode in long open trough structures of this type.

FIGURE 3.6.1-1 POWER OUTPUT OF SEMI-ACTIVE MFPC VS AU

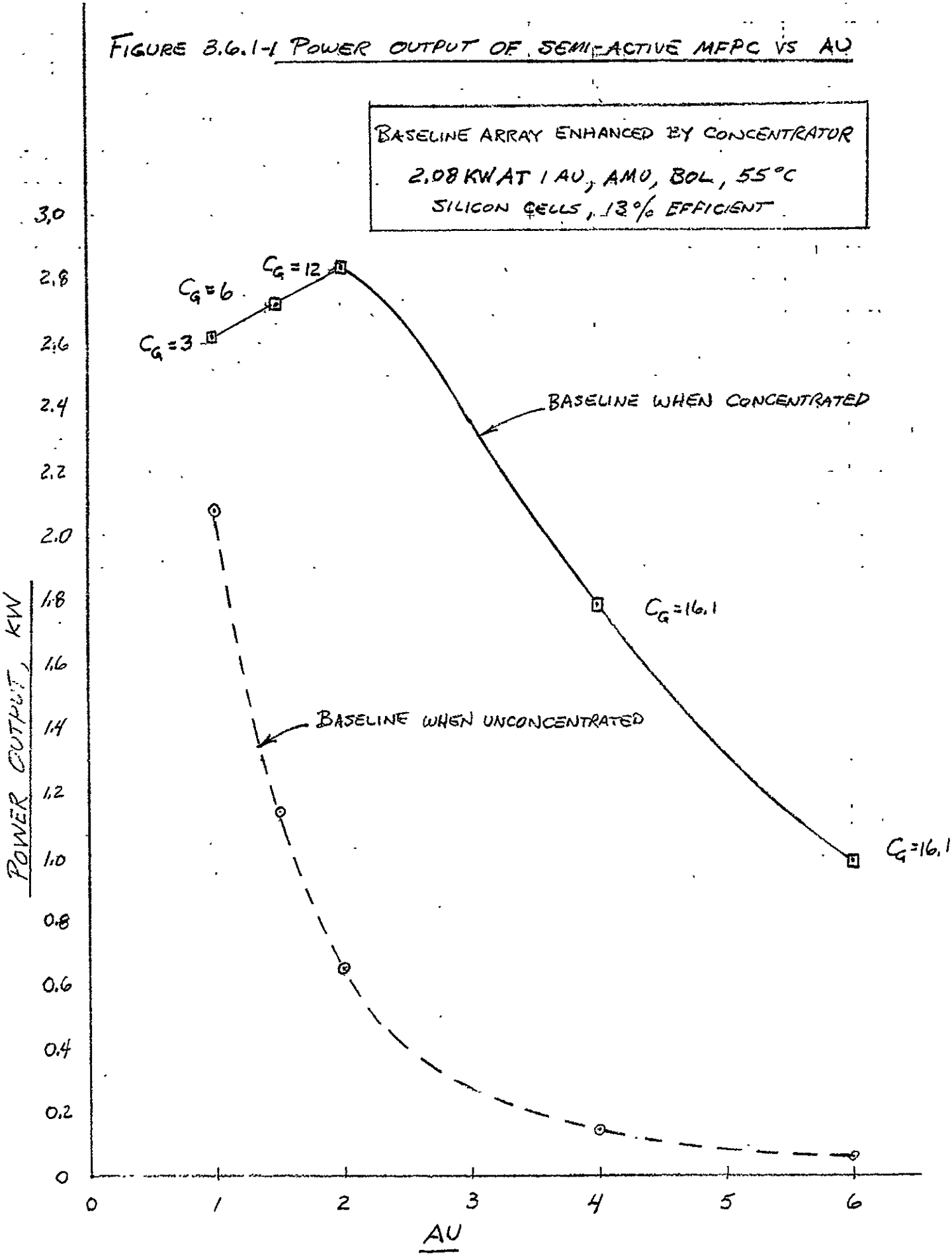

3.6.3 Thermal Performance - Phase II Design

The thermal analysis performed in Phase I (described in Section 2.4.2) was directly applicable to the further development of the active and passive MFPC concentrator designs undertaken in Phase II, this being largely a refinement of the structural design and a scaling down of the configuration for a 1 KW unconcentrated array.

Typical reflector temperatures, shown in Figure 3.6.3-1, were provided as support to an investigation of possible material degradation in the anticipated concentrator mission environments. These temperatures are representative of near maximum levels, i.e., those reflector "plates" most nearly normal to the sunline. The small view to the solar array and, in the case of a VDA reflector finish, the low front side emittance make reflector temperatures relatively insensitive to the design configuration.

To aid in the comparison of concentrator performance characteristics, unconcentrated array temperatures were calculated, utilizing the 2 mil K6 3/4 cell properties and efficiencies derived for the Phase I analysis. These temperatures were determined by the same technique of iterating array temperature and efficiency and are presented in Figure 3.6.3-2 as function of solar distance.

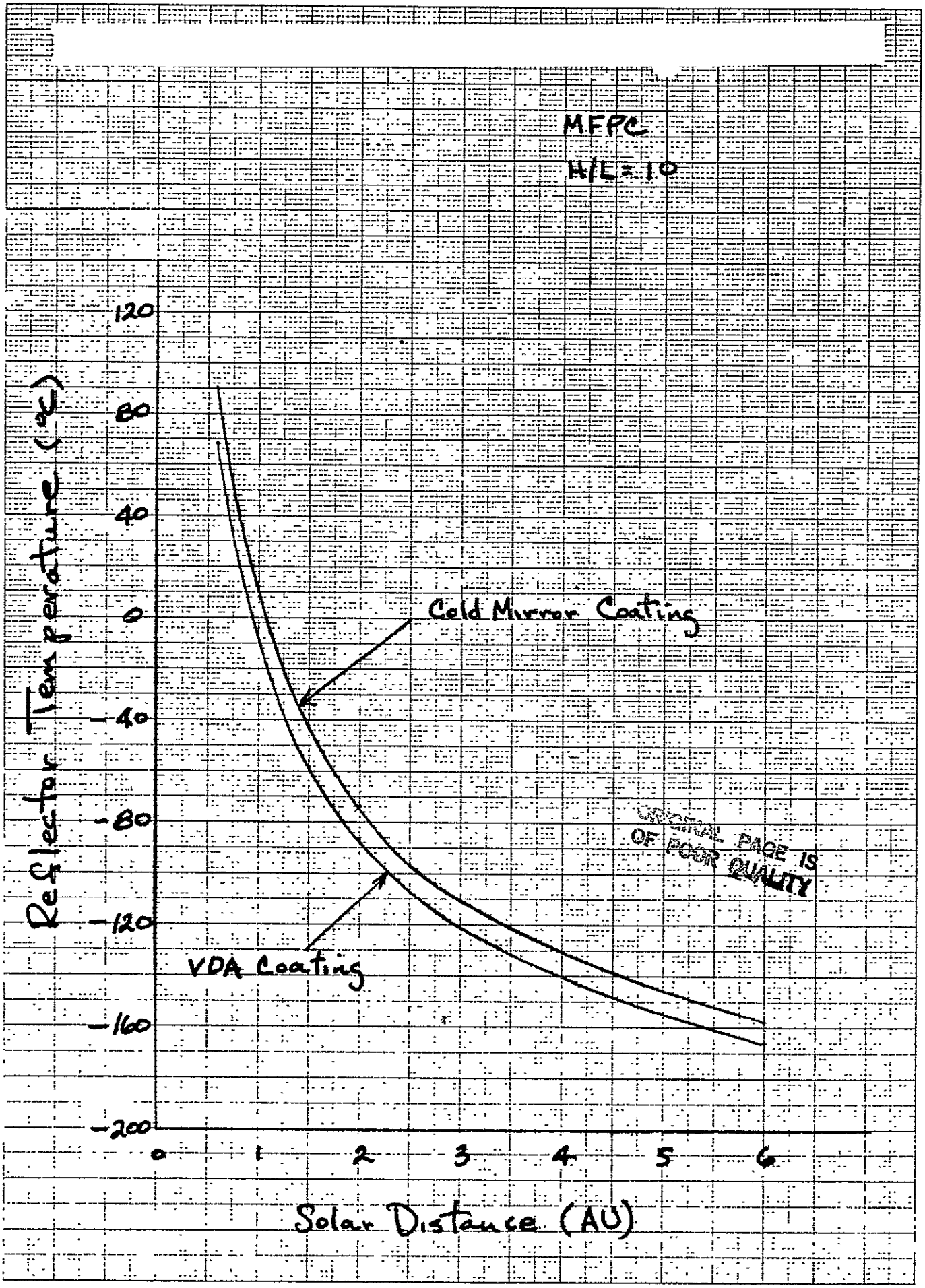

FIGURE 3.6.3-1. TYPICAL CONCENTRATOR REFLECTOR TEMPERATURES

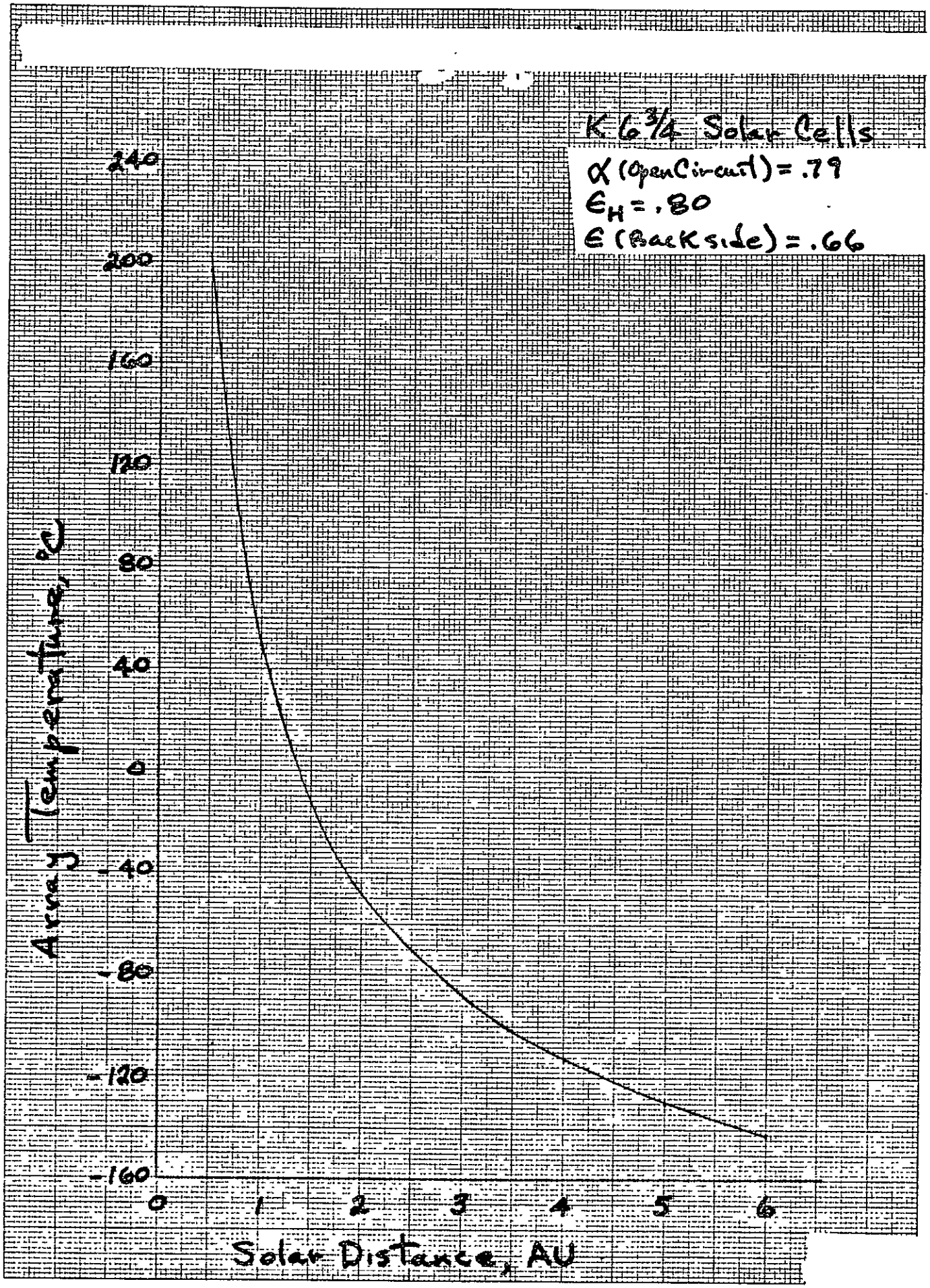

FIGURE 3.6.3-2. UNCONCENTRATED ARRAY TEMPERATURES-NORMAL TO SUNLINE

3.6.4 Anticipated Performance of Mirrors in Space Environment

The reflectors on the multiple flat plate concentrator design proposed by HAC would be made using first surface mirrors of 8 micrometers Kapton (Polyimide) film coated on one side with vacuum deposited aluminum. The coating will be at least 1000 A^{o} thick, to result in an initial reflectivity of 90-92%.

The use of the thin, VDA coated Kapton in space, for long periods of time, raises the question of possible degradation, either of the aluminum coating or the Kapton substrate. This degradation could result from several sources; e.g., temperature build-up from IR radiation from the sun, cross-link induced Kapton embrittlement due to UV and particulate radiation, aluminum coating loss as a result of Kapton embrittlement, and possible micrometeoroid erosion of the VDA. Another possible source of damage, which can be avoided by proper design, is impact damage from Mercury ions from an ion engine in missions which utilize such an engine. These deteriorating influences are discussed below.

Using the known $\frac{\alpha}{\epsilon}$ ratio for the VDA coated Kapton film, it has been calculated that the equilibrium temperature of the film, with the aluminum surface facing the sun, will range from $-10^{o}C$ at 1 AU to as low as $-167^{o}C$ at 6 AU. (See Section 3.6.3). The fact that the film will, at all times, be at a low temperature should inhibit degradation due to UV absorption, which in the case of Kapton, is mostly molecular chain cross-linking.

While in most cases the above statement is true, if any UV is absorbed by the Kapton, the possibility exists that at temperatures substantially below the Kapton glass transition point (where molecular activity is lessened) another effect might come into play. In this case the lower temperatures might enhance embrittlement by increasing the half life of the free radicals

generated by the UV radiation. The longer half lives could then result in increased recombinations with the net result of a higher degree of cross-linking per unit of radiation. Of course, if the VDA coating is impervious to UV radiation, this effect cannot occur. (The backside of the Kapton should never face the sun). The entire hypothesis, including the extent to which various thicknessis of VDA screen out the UV radiation, should be investigated by test.

With regard to creep, the ultimate effect of cross-linking is increased strength (and increased brittleness), both of which act to inhibit creep (Ref. 7). Thus, under the 50 psi design tension load creep should be negligible. (A study of Kapton creep on a specacraft, where the temperature was calculated to be $\approx 230^{o}$F and the loading was to be 700 psi, indicated a creep of 1.7% in seven years).Ref. 8. In any case the VDA will protect against UV deterioration. The amount of protection will, of course, be dependent of the amount of VDA employed.

With regard to particulate radiation, the greatest degradation from this source, it is believed could occur in passage through the Van Allen belts. The inner belt, ranging from≈300 to≈1500 miles, will be quickly traversed and should not result in degradation of significance. Passage through the outer belt, at≈10,000 to≈30,000 miles should likewise result in no appreciable degradation due to the short passage time. Particulate impingement damage to either the film or the VDA will be dependent on the time,and flux density. Ref. 9 states, Reflectance degradation in a 2-mil film of Type H Kapton backed by aluminum is strongly dependent upon electron energy. (Ref. 10). The 2-keV electron results are characterized by a peaking of degradation at a wavelength of approximately 0.5 micrometers. The 50-keV electron results and 80 keV electron results show maximum degradation at a wavelength of approximately 0.60 micrometers. For a fluence of 10^{15} electrons/cm^2, 50-keV degradation is some six times the 20-keV degradation, whereas 80-keV degradation is some eight times that at

20-keV." Thus for long term missions the degradation would depend on the deposited dose and dose profile.

Polymer modification or degradation due to outgassing effects will probably be negligible, since the VDA is unaffected by the vacuum, and the Kapton is substantially free of all outgassing components.

Micrometeroid encounters, it is believed can be discounted since, except for shower encounters, a single micrometeoroid would merely affect a very small area, and not cause a rip or large hole. Nevertheless, imbedding thin glass or Kevlar threads in a square weave pattern, e.g. on 2 in. centers would give the construction a rip stop quality, which in terms of tear insurance and added stiffness might be worth the additional weight.

While the possibilities of degrading factors are apparently quite low, assuming the major portion of the mission is further than 1 Au,there are nevertheless, several areas where further research is well justified. One of these research projects should be an investigation of the effects of ionizing radiation on the VDA coating in a vacuum. The second area is a determination of the minimum amount of VDA which will furnish substantial attenuation to the incoming UV and particulate radiation (especially solar protons in 0.5-3KeV energy range).

Another suggested research project is to determine the need to provide tear resistance in the Kapton substrate to contend with: (a) electron doses deposited by electrons with energies $\measuredangle$ 100 KeV (I.E., in traversing the Van Allen belt) followed by (b) micrometeoroid impact.

3.7 ROM COST ESTIMATE SUMMARY

HUGHES
HUGHES AIRCRAFT COMPANY

FOR DESIGN, DEVELOPMENT & MANUFACTURE OF FLIGHT READY CONCENTRATOR SYSTEM. PHASE II DESIGN, (1 KW AT 6 AU)

	COST (MANUF. LEVEL) K$
NON-RECURRING	
DESIGN ENGINEERING	1,135
ANALYSIS & DESIGN SUPPORT (INCLUDES SYSTEMS ENGR. AND MANAGEMENT)	1,485
DEVELOPMENT HARDWARE	
FABRICATION	607
DEVELOPMENT TEST	220
QUAL. TEST HARDWARE FAB.	1,700
QUALIFICATION TEST	440
FLIGHT SYSTEM FABRICATION	3,500
FLIGHT ACCEPTANCE TEST	120
TOTAL	9,207
G&A AND PROFIT	1,840
	11,047

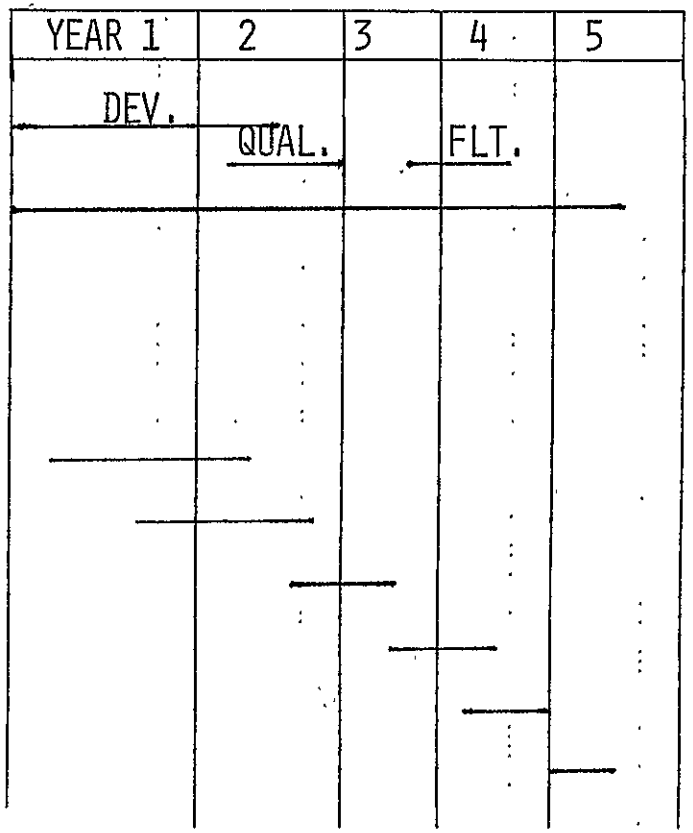

COMPARISON OF ESTIMATED RECURRING COSTS

HUGHES
HUGHES AIRCRAFT COMPANY

- CONCENTRATED ARRAY (1 KW AT 6 AU)
  - 40,000 CELLS AT 15$/CELL — 600 K$
  - REMAINING STRUCTURE (LESS CELLS) — 3.000 K$
  - G&A AND PROFIT — 720 K$

  TOTAL — 4,320 K$

- UNCONCENTRATED ARRAY (1 KW AT 6 AU)
  - REQUIRES 33.3 KW ARRAY AT 1 UA OR 668,000 CELLS AT 15 $/CELL = 10,020 K$
  - ASSUME REMAINING STRUCTURE CAN BE PRODUCED AT HALF THE COST OF A CONCENTRATED SYSTEM

    0.5 X 3,000 = 1,500 K$
  - G&A AND PROFIT = 2,304 K$

  TOTAL — 13,824 K$

<u>CONCLUSION</u>

CONCENTRATED ARRAY AT LEAST 1/3 COST

REFERENCES

1. FINAL REPORT "Winston Solar Concentrators and Evaluation Support", Phase I, Dr. Roland Winston, Univ. of Chicago, JPL contract 954563, September 1977.

2. FINAL REPORT "Concentrator Enhanced Solar Arrays Design Study", Lockheed Missiles and Space Co., Inc. JPL contract 955110, October 1978.

3. FINAL REPORT "Extended Performance SEP Solar Array Study", Lockheed Missiles and Space Co., Inc. NASA contract NAS 8-31352, Marshall Space Flight Center, July 1977.

4. FINAL REPORT "Winston Solar Concentrators and Evaluation Support", Phase II, Dr. Roland Winston, Univ. of Chicago, JPL contract 954563, August 1978.

5. "Proposal for Conceptual Deisgn Study of Concentrator Enhanced Solar Arrays for Space Applications", Hughes Aircraft Company, Reference No. 78(41-10981/E3256-SCG 80211P.

6. "A Flexible-low-mass Concentrator Enhanced Solar Array Design for Future Space Exploration Mission", E. N. Costogue, Paper No. 78-687 presented at AIAA/DGLR -13th International Electric Propulsion Conference, San Diego, Calif./ April 25-27, 1978.

7. Electronic Properties Information Center, Report S-8, Contract AF33(615)2460, Project 7381: Task 738103.

8. TIC #2717.31/118, "Evaluation of Kapton as a Polarizer Top-Material" from R. E. Kelchner to P. W. Bernstein, dated 31 October 1974

9. Giori, G, Yamauchi, T. and Javke, F, "Investigation of Space Radiation Effects in Polymeric Film Forming Materials", NASA CR-132740, dated October 1975.

10. Fogdall, L. B., Connaday, S. S., and Brown, R. R., AIAA 4th Thermophysics Conference, San Francisco, CA, June 1969.

11. John Scott-Monck, "An Overview of Phtovoltaics for Space Application", in Conf. Record of the 13th IEEE Photovoltaic Specialists Conf-1978. pp. 421-428.

12. J. Lindmayer and C. Y. Wrigley, "Ultrathin Silicon Solar Cells", ibid, pp. 450-453.

13. Solarex Corp., "Pilot Line Report, Development of a High Efficiency Thin Silicon Solar Cell", JPL Contract No. 954883, Nov. 1978.

14. R. G. Downing and R. S. Weiss, "Characterization of Solar Cells for Space Application", JPL Publication 78-15, Volumes II (15 Aug. '78), III (1 Sept. '78) and IV (1 Nov. '78).

15. L. J. Goldhammer, "Qualification and Characterization of the K-7 Solar Cell", Hughes Aircraft Co. Report No. SCG 80171R, May 1978.

APPENDIX A

STRESS ANALYSIS COMPUTATIONS

STRESS ANALYSIS

Definition of Terms:

NODE – Point of cable contact with shaping beam.

X, Y, Z – coordinates of node location in referenced X, Y, Z axes

L_x, L_y, L_z – Components of cable lengths from central mast to each node location.

L – cable length

Cable Force – required cable force to produce 0.36 pounds force in Z-direction.

P_x, P_y – components of cable force in the plane of the shaping beam

Beam Element Axes and Force Definition:

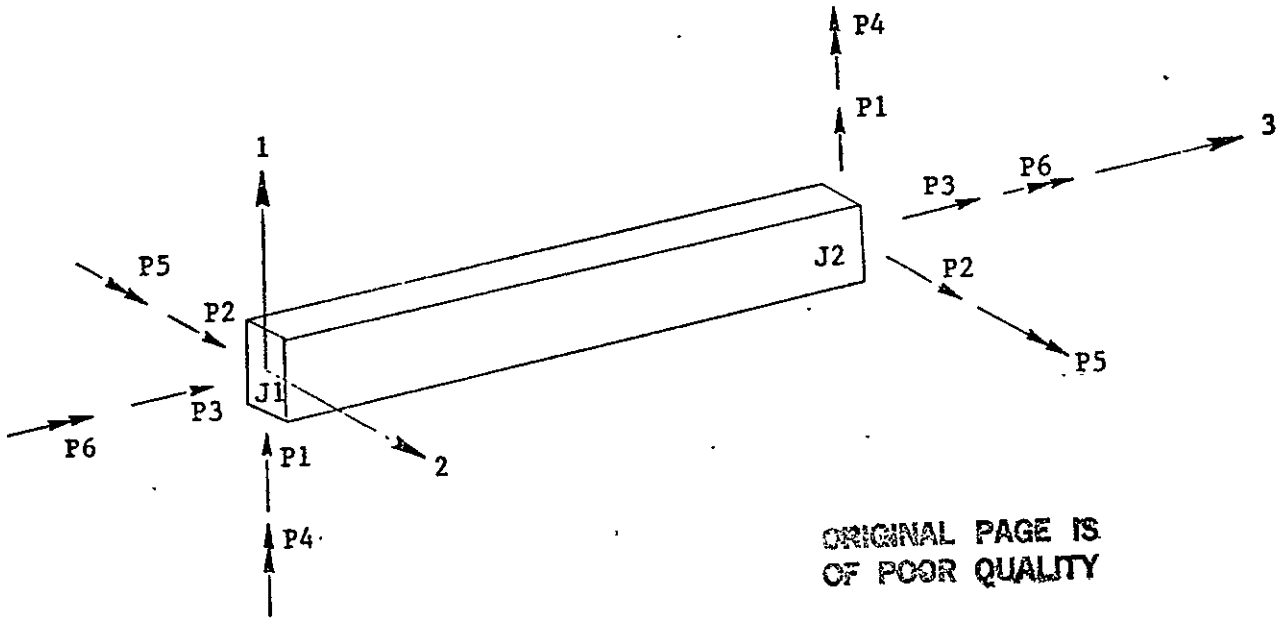

SHAPING BEAM MODEL — GEOMETRY

NODE	X	Y	Z	L_x	L_y	L_z	L
				CABLE LENGTHS			
1	0	159.6	0	0	72.	-96	120.
2	21.6	159.6		21.6	72.		121.9
3	43.2	158.4		43.2	70.8		126.9
4	64.8	154.8		64.8	67.2		133.9
5	85.2	150.		85.2	62.4		142.7
6	104.4	144.		104.4	56.4		152.6
7	123.6	136.8		123.6	49.2		164.1
8	140.4	129.6		140.4	42.		175.2
9	158.4	122.4		158.4	34.8		188.5
10	175.2	114.		175.2	26.4		201.5
11	189.6	104.4		189.6	16.8		213.2
12	205.2	96.		205.2	8.4		226.7
13	218.4	86.4		218.4	-1.2		238.6
14	232.8	76.8	0	232.8	-10.8	-96	252.0

LOADS

NODE	L_x/L	L_y/L	L_z/L	CABLE FORCE	P_x	P_y
1	0	0.60	-0.80	-.45	0	-0.270
2	.1772	.5906	-.7875	-.4571	-.081	-.270
3	.3404	.5579	-.7565	-.4759	-.1620	-.2655
4	.4339	.5019	-.7170	-.5021	-.243	-.252
5	.5971	.4373	-.6721	-.5352	-.3196	-.234
6	.6841	.2616	-.6291	-.5722	-.3914	-.2115
7	.7532	.7998	-.5850	-.6154	-.4635	-.1845
8	.8014	.2397	-.5479	-.6571	-.5266	-.1575
9	.8403	.1846	-.5093	-.7069	-.594	-.1305
10	.8695	.1310	-.4764	-.7557	-.6571	-.0990
11	.8893	.0788	-.4503	-.7995	-.711	-.063
12	.9057	.0371	-.4225	-.8501	-.7695	-.0315
13	.9153	-.0050	-.4023	-.8949	-.8191	.0045
14	.9238	-.0429	-.3810	-.9449	-.8729	.0405

Component in ~~Z~~-direction = 0.36 LB/cable

M. MAGIE 3/28/79

SHAPING BEAM MODEL - GEOMETRY

TUBE SIZE $1\frac{1}{2}$ OD x .028 WALL

GRAPHITE EPOXY $E = 20 \times 10^6$ psi

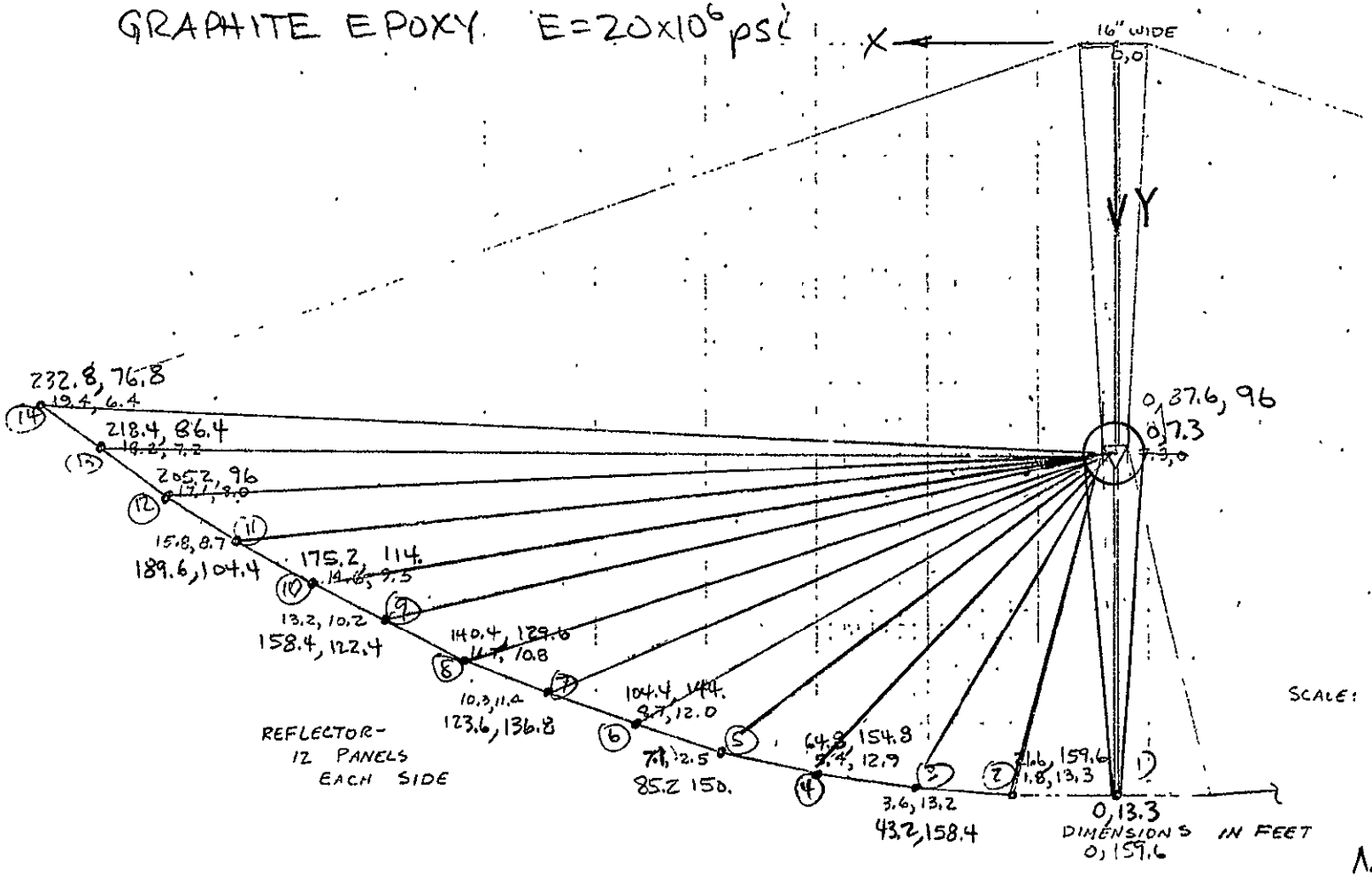

M. MAGIE
3/28/79

CASE 1- 1

*GROUP 1

E21 FORCES, DIVIDED BY 1.0000

INDEX	JOINT	P1	P2	P3	P4	P5	P6
1	1	-1.84	.00	6.59	.00	-473.03	.00
	2	1.84	.00	-6.59	.00	433.30	.00
2	2	-1.93	.00	6.41	.00	-433.30	.00
	3	1.93	.00	-6.41	.00	391.59	.00
3	3	-2.33	.00	6.05	.00	-391.59	.00
	4	2.33	.00	-6.05	.00	340.57	.00
4	4	-2.42	.00	5.70	.00	-340.57	.00
	5	2.42	.00	-5.70	.00	289.81	.00
5	5	-2.51	.00	5.28	.00	-239.81	.00
	6	2.51	.00	-5.28	.00	239.39	.00
6	6	-2.46	.00	4.84	.00	-239.39	.00
	7	2.46	.00	-4.84	.00	188.88	.00
7	7	-2.34	.00	4.37	.00	-188.88	.00
	8	2.34	.00	-4.37	.00	146.20	.00
8	8	-1.89	.00	4.00	.00	-146.19	.00
	9	1.89	.00	-4.00	.00	109.58	.00
9	9	-1.84	.00	3.35	.00	-109.57	.00
	10	1.84	.00	-3.35	.00	75.09	.00
10	10	-1.79	.00	2.62	.00	-75.09	.00
	11	1.79	.00	-2.62	.00	44.03	.00
11	11	-1.15	.00	2.18	.00	-44.03	.00
	12	1.15	.00	-2.18	.00	23.64	.00
12	12	-.97	.00	1.38	.00	-23.63	.00
	13	.97	.00	-1.38	.00	7.82	.00
13	13	-.45	.00	.73	.00	-7.82	.00
	14	.45	.00	-.73	.00	.00	.00

```
EXIT   28.362          0          10
>SPEC 1
 DATA SPACE=     15000


>VIEW 3
>ALL
>EXIT PLTB
```

```
*XQT SSOL
                                SYSV COMPLETED.

EXIT   19.275          3          3
*XQT VPRT
DATA SPACE=     20000


 CASE       F*U                 U*KU                ERR

    1      .2372209+02       .2386415+02      -.5952635-02

EXIT   21.897          9          9
*PRINT STAT REA*DAT*
*PRINT STAT DISP
DATA SPACE=     20000


STATIC DISPLACEMENTS.                                          ID=    1/ 1/  1

JOINT       1             2             6
    1    .000    *    .000    *    .000    *
    2   -.550-04      -.153+00      -.140-01
    3   -.246-01      -.594+00      -.267-01
    4   -.142+00      -.130+01      -.381-01
    5   -.348+00      -.217+01      -.475-01
    6   -.656+00      -.316+01      -.551-01
    7   -.108+01      -.428+01      -.613-01
    8   -.153+01      -.535+01      -.657-01
    9   -.202+01      -.656+01      -.692-01
   10   -.261+01      -.775+01      -.717-01
   11   -.331+01      -.879+01      -.732-01
   12   -.393+01      -.994+01      -.740-01
   13   -.464+01      -.109+02      -.744-01
   14   -.536+01      -.120+02      -.745-01
*PRINT STAT REAC


STATIC REACTIONS,  FORCE ERRORS.                               ID=    1/ 1/  1

JOINT       1             2             6
    1    .659+01*      .134+01*      .473+03*
    2    .264-04       .908-05       .763-04
    3    .990-04       .505-04      -.122-03
    4    .461-03       .278-04       .610-04
    5    .317-03       .823-04       .366-03
    6    .305-02       .104-02       .793-03
    7   -.220-02       .231-02       .000
    8    .226-02      -.375-03      -.262-02
    9    .485-02       .317-02      -.854-03
   10    .117-01      -.207-02      -.671-03
   11    .347-02       .727-02       .427-03
   12   -.491-02       .124-01      -.244-03
   13   -.113-01      -.172-01      -.476-02
   14    .796-02      -.167-01      -.171-02
> XQT GSF

EXIT   23.405          0          7
> XQT PSF
DATA SPACE=     19000

EXIT   26.204          4         14
>PRESET DISPLAY=2
```

ORIGINAL PAGE IS
OF POOR QUALITY

SHAPING BEAM - SPAR MODEL 3/29/79

```
                L, VOL OR      STRUCTURAL     NON-STRUCTURAL
TYPE GROUP      AREA SUM       WEIGHT         WEIGHT
E21    1      .251810+03     .205414+01     .000000



TOTAL                        .205414+01     .000000


 EXIT    6.612          4          16
>@XQT TOPO
 DATA SPACE=     16000
 E21  COMPLETED

 EXIT    8.902          3           6
>@XQT K
 DATA SPACE=     20000
 NO. OF   2-NODE ELEMENTS=     13

 TOTAL NO. OF ELEMENTS=      13
 TIME       .005       .080

 MAXCON, MAXSUB, ILMAX=     157   1400      52
 TIME       .000       .080

 KSIZE,NR5,LR5=           3          1       896

 MAXCON, MAXSUB, ILMAX=     149   1400      52
 TIME       .000       .080

 SIZE INDEX=       3,  IC1, IC2=     40     27, NR4=     1

 EXIT   12.506          5           6
>@XQT INV
 DATA SPACE=     16000

 EXIT   15.354          3          19
>@FSET CON=1
 CON =          1
>@XQT AUS
 DATA SPACE=     24500

 NSING,NNEG=       0       0

 EXIT   17.491          3           6
>SYSVEC:APPL FORC 1
 DATA SPACE=     20000
>CASE 1
>I=1 2
>J=2,14,1
>-.031 -.270
>-.162 -.2655
>-.343 -.253\32
>-.3196 -.234
>-.3914 -.2115
>-.4635 -.1845
>-.5266 -.1575
>-.594 -.1305
>-.6571 -.099
>-.711 -.063
>-.7695 -.0315
```

SHAPING BEAM DEFORMATIONS

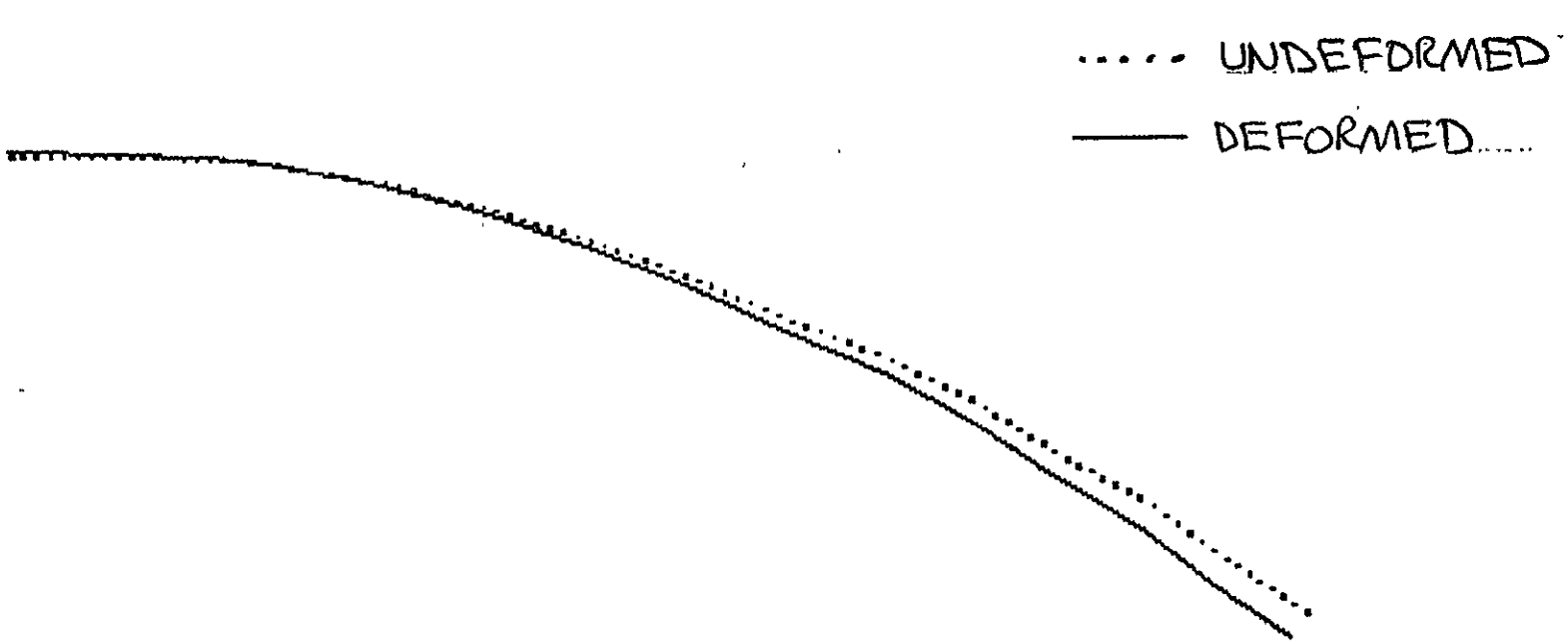

104

SPEC
1.1

0 37
SCALE

SHAPING BEAM MODEL
NODAL POINTS

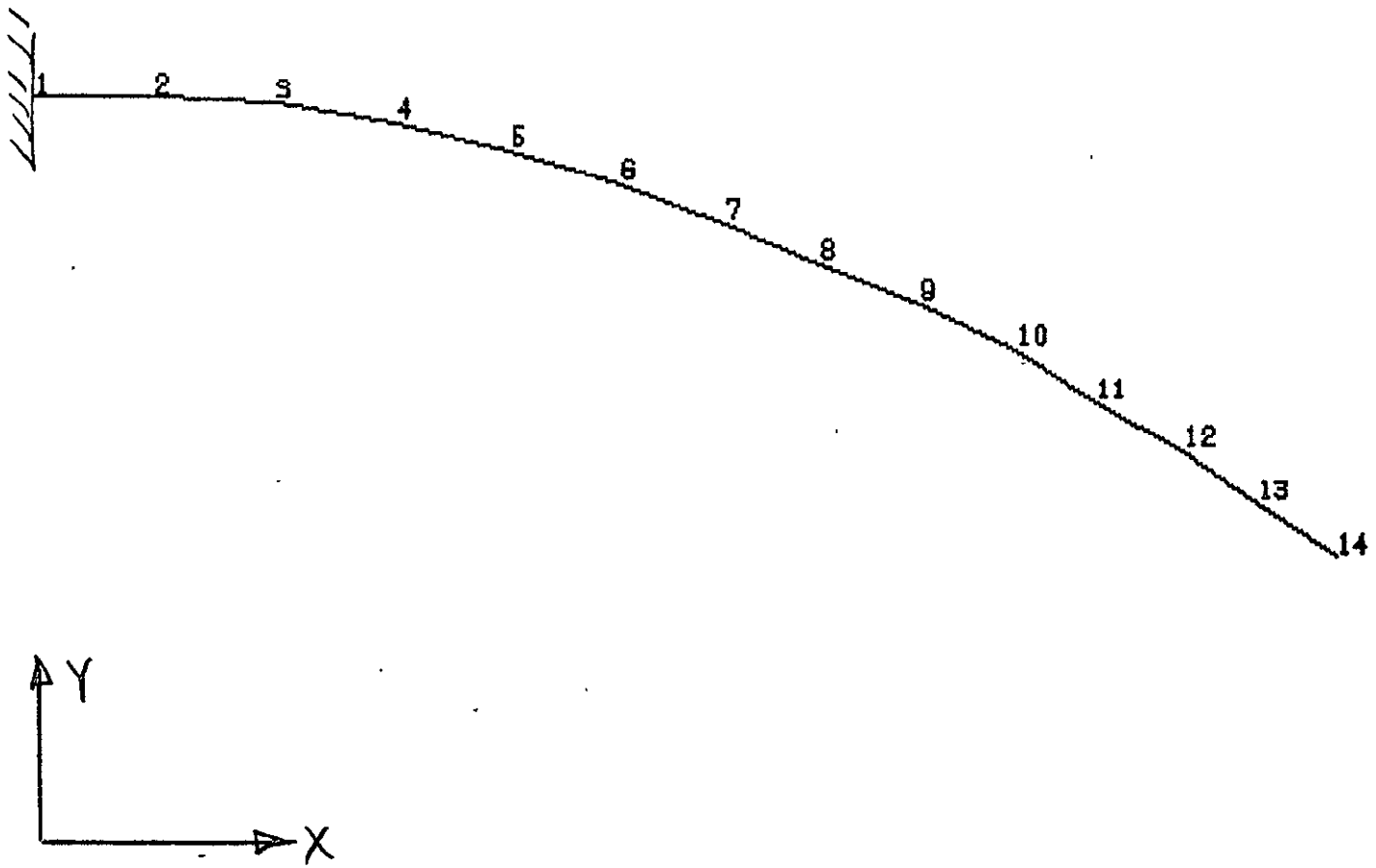

0 36
SCALE

ANALYSIS RESULTS

FROM SPAR FINITE ELEMENT MODEL

DEFLECTION — NODE 14

$\Delta_x = -5.36$ IN.

$\Delta_y = -12.0$ IN.

TOTAL $= \sqrt{5.36^2 + 12^2} = 13.14$ IN.

STRESS — BEAM 1, NODES 1 TO 2

$P = 6.59$ LB, $V = 1.84$ LB, $M = 473$ IN-LB

$$f = \frac{P}{A} + \frac{Mc}{I}$$

FOR 1.5 OD x .028 WALL TUBE

$$A = \left(1.5^2 - 1.44^2\right)\frac{\pi}{4} = .139 \text{ IN}^2$$

$$I = \left(1.5^4 - 1.44^4\right)\frac{\pi}{64} = .037 \text{ IN}^4$$

$$f_{max} = \frac{6.59}{.139} + \frac{473(.75)}{.037} = 47.4 + 9587.8$$

$f_{max} = 9635$ psi

$F_{ALLOW} > 60{,}000$ psi

$$M.S. = \frac{60}{9.6} - 1 = \text{HIGH}$$

APPENDIX B

DRAWINGS

APPENDIX C

CALCULATION FOR ESTIMATED TORSIONAL NATURAL FREQUENCY

APPENDIX C.

CALCULATION FOR ESTIMATED TORSIONAL NATURAL FREQUENCY

$$f_N = \frac{1}{2\pi}\sqrt{\frac{K_\theta}{I}}$$

$$K_\theta = \frac{GJ}{L}$$

$$f_N = \frac{1}{2\pi}\sqrt{\frac{GJ}{LI}}$$ WHERE UNITS ARE: GJ = LB-IN^2, L = IN, I = LB-IN-SEC^2

$I = MR^2$ WHERE R = RADIUS OF GYRATION (IN) OF END MASS
M = EFFECTIVE MASS AT END OF ASTRO MAST (LB-$\frac{1}{IN}$-SEC^2)

R = 15 FT = 180 IN. (ESTIMATED FROM END BEAM GEOMETRY)

$M = \frac{45.4}{386}\ \frac{LB\ SEC^2}{IN}$ ($\frac{1}{2}$ THE MASS OF 1 WING ASSUMED LUMPED AT EACH END BEAM)

$$I = \frac{45.4}{386} \times (180)^2 = 3.8 \times 10^3\ IN\text{-}LB\text{-}SEC^2$$

$L = 66 \times 12 = 792$ IN

$GJ = .02\,EI$ AEC-ABLE DESIGN PARAMETER

$EI = \frac{L^2 P}{\pi^2}$ WHERE P = ASTRO MAST END LOAD BASED ON SELECTED CABLE TENSION

$$= \frac{(792)^2 \times 14}{\pi^2} = 8.9 \times 10^5\ LB\text{-}IN^2$$

$$GJ = .02(8.9) \times 10^5 = 1.78 \times 10^4\ LB\text{-}IN^2$$

$$f_N = \frac{1}{2\pi}\sqrt{\frac{1.78 \times 10^4}{792 \times 3.8 \times 10^3}} = \underline{0.012\ Hz.}$$